Direct gamete interactions and Egg Cell1-mediated sperm cell activation in *Arabidopsis thaliana*

Dissertation zur Erlangung des
Doktorgrades der Naturwissenschaften (Dr. rer. nat.)
der Fakultät für Biologie und Vorklinische Medizin
der Universität Regensburg

vorgelegt von
MARIA ENGLHART

aus
Bad Aibling

im Jahr
2017

Das Promotionsgesuch wurde eingereicht am:
11. September 2017

Die Arbeit wurde angeleitet von:
PD. Dr. Stefanie Sprunck

Unterschrift:

Zeit bringt alles - wer warten kann.

TABLE OF CONTENTS

1. SUMMARY

Double fertilisation is a highly regulated and complex process that involves four gametes and is unique to flowering plants. Two female gametes, the egg cell and the central cell, fuse with one sperm cell each. This double fertilisation event results in a diploid zygote, which develops into the embryo, and the triploid endosperm, a nutrient-storing and embryo-nourishing tissue.

In this thesis, the focus was primarily placed on the egg-sperm fertilisation mechanism of *Arabidopsis thaliana*. This particularly included the investigation of the activation, attachment and fusion of the gametes as well as the characterization of sperm-activating EC1 proteins.

In cytological observations on *in vivo* double fertilisation, the individual phases of egg and sperm cell interactions were characterized using fluorescent marker-lines labelling the gamete plasma membranes. It was shown that the sperm cell membrane is integrated into the egg cell membrane at the sperm-egg fusion site and that the membrane projection, connecting the sperm cell pair with the pollen vegetative cell nucleus, remains outside of the egg and central cell. Furthermore, it could be shown that sperm cell pairs do neither separate from each other nor attach to the female gametes in the *ec1-RNAi* knockdown mutant lacking egg cell-secreted EC1.

Although the EC1.1-GFP fusion protein can be expressed by all cells of the female gametophyte, the phenotype of undeveloped seeds in the *ec1-RNAi* knockdown mutant could not be complemented by expression of EC1.1-GFP either in the central cell, the synergid cells or the antipodal cells.

Investigations of the role of EC1 proteins in sperm cell activation revealed that synthetic EC1.1 peptides associate with the sperm cell plasma membrane and trigger both exo- and endocytosis. In particular, endocytosis of membrane associated TET9-GFP is stimulated and the fusogen HAP2-YFP is relocated from the endomembrane system to the plasma membrane. Furthermore, the unpairing of sperm cells seems to be stimulated by the EC1.1 peptide S2. It could be shown that the sperm cell activation, in terms of HAP2-YFP relocalisation to the sperm cell plasma membrane, can be mimicked by a cyclic guanosine monophosphate (cGMP) derivative. This suggests that the second messenger cGMP is involved in the intracellular signal transduction responsible for sperm cell activation. The proposed role for cGMP as a second messenger is furthermore supported by the evidenced expression of two cyclic nucleotide gated channels in *A. thaliana* sperm cells. Physiological studies on egg cell activation suggest that the secretion of EC1 is not triggered by Ca^{2+}.

The optimization of the purification of EC1.2 fusion proteins, recombinantly expressed in *Pichia pastoris* cells, will facilitate future studies on EC1 protein structure. Diffusion ordered spectroscopy measurements and size exclusion chromatography suggest that EC1.2 is present as a tetramer at the physiological pH of 7.5. Total correlation spectroscopy indicates that the secondary structure of EC1.2 primary consists of α-helices and turns. Furthermore, it was shown that EC1.2 is able to bind the hydrophobic compound lysoPC, like it has been shown for the related non-specific lipid transfer proteins (nsLTPs). Homology modelling of EC1.2 with the nsLTP DIR1 as a template underpins the structural relationship of EC1 with nsLTPs, as EC1.2 is a globular protein of five α-helices, forming a hydrophobic cavity in the centre that may bind hydrophobic compounds.

Taken together, it could be shown that the EC1 proteins are necessary for sperm cell attachment, sperm cell activation and very likely for the separation of sperm cell pairs in *A. thaliana*. The results of this thesis suggest that egg cell-secreted EC1 proteins activate sperm cells by interacting with an unknown receptor protein at the sperm cell plasma membrane or by local modulation of the sperm cell plasma membrane lipid composition.

2. ZUSAMMENFASSUNG

Die doppelte Befruchtung ist einzigartig für Blütenpflanzen und ist ein hoch regulierter und komplexer Prozess, an welchem vier Gameten beteiligt sind. Zwei weibliche Gameten, die Eizelle und die Zentralzelle, fusionieren je mit einer Spermazelle, wobei sowohl eine diploide Zygote entsteht, die sich zu einem Embryo entwickelt, als auch das triploide Endosperm, ein Nährstoff speicherndes und Embryo versorgendes Gewebe.

Der Fokus der vorliegenden Arbeit lag auf den Befruchtungsmechanismen von Ei- und Spermazelle in *Arabidopsis thaliana*. Das beinhaltete sowohl die Untersuchung der Aktivierung, Adhesion und Fusion der Gameten, als auch die Charakterisierung des Spermazellen aktivierenden EC1-Proteins.

In zytologischen Untersuchungen der doppelten Befruchung im lebenden Organismus wurden die einzelnen Phasen der Eizell- und Spermazellinteraktionen mit Hilfe von transgenen Pflanzenlinien untersucht, welche die Plasmamembranen der Gameten fluoreszent markieren. Es wurde gezeigt, dass die Plasmamembran der Spermazelle an der Fusionsstelle in die Eizelle integiert wird und dass die Membranverlängerung, welche die beiden Spermazellen mit dem Kern der vegetativen Pollenzelle verbindet, außerhalb der Eizelle und Zentralzelle liegen bleibt. Desweiteren konnte gezeigt werden, dass das Spermazellenpaar in der *ec1-RNAi* Mutante, in der die Eizellen kein EC1 sekretieren, sich weder trennt noch sich an die weiblichen Gameten anheftet.

Der Phänotyp der *ec1-RNAi* Mutante zeigt unentwickelte Samen und obwohl das EC1.1-GFP Fusionsprotein von allen Zellen des weiblichen Gametophyten exprimiert werden kann, konnte der Phänotyp weder durch Expression von EC1.1-GFP in der Zentralzelle noch in den Synergiden oder den Antipoden komplementiert werden.

Untersuchungen der Rolle von EC1 Proteinen an der Spermazellaktivierung haben gezeigt, dass synthetische EC1.1 Peptide mit der Plasmamembran der Spermazellen assoziieren und sowohl Exo- als auch Endozytose auslösen. Genauer gesagt wird die Endozytose von Membran lokalisiertem TET9-GFP stimuliert und das Fusogen HAP2-YFP vom Endomembransystem zur Plasmamembran relokalisiert. Außerdem scheint es, als ob das EC1.1 Peptid S2 die Trennung von Spermazellen anregt. Es konnte gezeigt werden, dass die Spermazellaktivierung in Form von HAP2-YFP Relokalisierung von zyklischem Guanosinmonophosphat (cGMP) imitiert werden kann, was darauf hindeutet, dass der sekundäre Botenstoff cGMP in der intrazellullären Signaltransduktion der Spermazellaktivierung beteiligt ist. Die vorgeschlagene Rolle von cGMP als sekundärer Botenstoff wird durch die Tatsache unterstützt, dass die Expression von zwei zyklisch-Nukleotid gesteuerten Ionenkanälen (CNGCs) in den Spermazellen von *A. thaliana* nachgewiesen werden konnte. Weiterhin deuten physiologische Untersuchungen an Eizellen darauf hin, dass die Sekretion von EC1 nicht durch Ca^{2+} aktiviert wird.

Im Rahmen dieser Arbeit wurde die Aufreinigung von rekombinant in *Pichia pastoris* exprimierten EC1.2 Fusionsproteinen so weit optimiert, dass weitere Untersuchungen der Proteinstruktur von EC1.2 ermöglicht wurden. Die Ergebnisse aus DOSY-NMR Messungen und Größenausschlusschromatographie weisen darauf hin, dass die EC1 Proteine bei einem physiologischen pH von 7.5 als Tetramer vorliegen. Weiterhin zeigen zweidimensionale TOCSY-NMR Ergebnisse an, dass die Sekundärstruktur von EC1.2 fast ausschießlich aus α-Helices und Schleifen besteht. Es konnte gezeigt werden, dass EC1.2 die hydrophobe Substanz LysoPC binden kann, wie es bereits für die verwandten, nicht-spezifischen Lipidtransportproteine (nsLTPs) gezeigt wurde. Das Homologiemodell von EC1.2 mit dem nsLTP DIR1 untermauert die strukturelle Verwandtschaft zu den nsLTPs, da EC1.2 auch ein kleines, globuläres Protein ist, dass aus fünf α-Helices besteht, welche eine hydrophobe Bindetasche formen, die eine hydrophobe Substanz binden kann.

Zusammengefasst konnte gezeigt werden, dass EC1 Proteine für Spermazelladhäsion, Spermazellaktivierung und sehr wahrscheinlich auch für die Trennung der Spermazellpaare in *A. thaliana* notwendig sind. Die Ergebnisse dieser Arbeit weisen außerdem darauf hin, dass Eizell-sekretierte EC1 Proteine die Spermazellen aktivieren, indem sie entweder mit einem unbekannten Rezeptorprotein in der Plasmamembran der Spermazellen interagieren oder lokal die Lipidzusammensetzung der Spermazellplasmamembran verändern.

3. INTRODUCTION

3.1 Sexual reproduction

Sexual reproduction involves fertilisation, which is the union of two haploid gametes of opposite sexes. By the fusion of two gametes, termed syngamy, a zygote is formed that develops into an embryo. During asexual reproduction, in contrast, the offspring is formed by a single individual. A yeast cell, for example, can form a new individual via budding, aphids can give birth to living young from an unfertilised egg, which is termed parthenogenesis, and strawberries produce new plants out of stolons during vegetative propagation. However, only sexual reproduction leads to offspring which is genetically highly diverse. Sexual reproduction is thus the basis for the manifoldness of life on earth and has always fascinated mankind.

The generation of gametes occurs at different stages of development. In mammals, gametes are created in gonads: female ovaries produce egg cells, while male testicles produce sperm. The gonads are already formed prenatally and can usually not be reproduced in adults. In plants, gametes are also created in special organs. For example, in flowering plants, termed angiosperms,

female gametes develop in ovules and male gametes are formed in pollen. However, in plants, these organs are not yet formed in an embryo. They develop at later stages at multiple sites in the organism. Another big difference to animals is that plants live in alternating haploid (n) and diploid (2n) generations. There are three different life cycles that were described by Strasburger in 1894 (Figure 3.1). This means that an organism has either haploid or diploid individuals or alternates between both. In a haplontic life cycle (Figure 3.1, A), the haploid stage is multicellular since mitotic cell divisions and development occurs entirely in the haploid phase, while the diploid stage is reduced to a single cell, the zygote. After karyogamy, in which the nuclei fuse, the zygote immediately undergoes meiosis. This life cycle is typical for fungi, some green algae such as *Chlamydomonas* and protists. In a diplontic life cycle, on the other hand, mitotic cell divisions and development occur entirely in the diploid phase (Figure 3.1, B). The haploid stage is reduced to single cells, the gametes, which fuse directly to form a zygote as e.g. in animals. The most complex life cycle is the haplodiplontic life cycle (Figure 3.1, C), in which both phases form individual multicellular generations. The haploid sporophyte forms spores and the diploid gametophyte forms gametes. The most prominent representatives of this alternation of generations are spermatophytes (seed plants). The persistence of both phases allows the occupation of distinct niches to provide opportunities for species to exploit different resources (Mable and Otto 1998). This could be one of the reasons why plants are so successful in making new biotopes accessible. In bryophytes, including mosses, the dominating generation is the haploid gametophyte, while the sporophyte is a reduced structure which is completely dependent on the gametophyte (Reski and Cove 2004). In contrast, the gametophytes of angiosperms are extremely reduced to a few cells and the dominating generation is the diploid sporophyte.

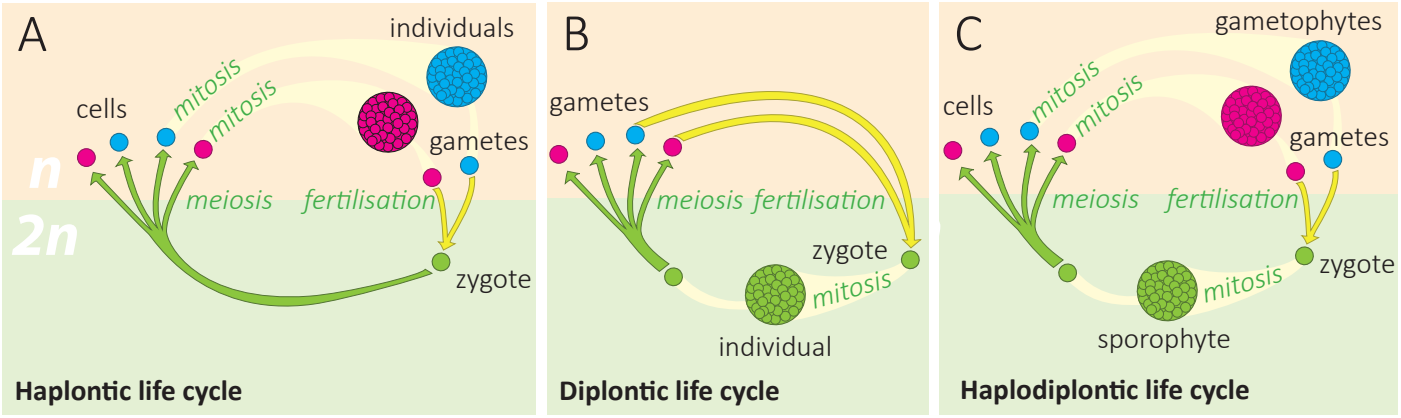

Figure 3.1 Different life cycles.
(A) During a haplontic life cycle, the zygote undergoes meiosis immediately after karyogamy. The diploid phase (2n) ends and the resulting haploid cells (n) divide mitotically to form multicellular individuals or more haploid cells. Two opposite type of gametes from these cells fuse to become a zygote. (B) During a diplontic life cycle, the zygote divides mitotically to form an individual from which single cells undergo meiosis to form gametes. Two gametes of opposite sexes fuse to form a zygote. (C) During a haplodiplontic life cycle, the zygote divides mitotically to produce a multicellular diploid sporophyte from which single cells undergo meiosis to form gametes. The haploid cells divide mitotically to form haploid multicellular gametophytes. Two gametes of opposite sexes from these cells fuse to become a zygote. Drawn after Strasburger (1894).

The sporophyte of the flowering plant *Arabidopsis thaliana* (Figure 3.2, A) has a rosette formed by leaves at the base and several simple inflorescences of about 30 cm height, with continuously developing flowers at the top. The flower (Figure 3.2, B) shows four green sepals, four white petals, six stamens and one pistil. The four long and two short stamens consist of a filament and an anther that holds the pollen. The pistil is located at the centre with the stigma at the top and 50-60 enclosed ovules that are each connected to the septum via a prolongation termed funiculus. The ovules embed the embryo sac, which is the female gametophyte. Upon pollination, the pollen grains stick to the stigma, rehydrate and germinate. The pollen tube (Figure 3.2, C) grows through the pistil to target the ovules, while transporting two sperm cells. Then, the pollen tube grows into the ovule (Figure 3.2, D) and one sperm cell fuses with the egg cell, while the other fuses with the central cell. This is called double fertilisation and is unique to flowering plants. The fertilised egg cell develops into an embryo and the fertilised central cell becomes a multinuclear syncytium termed endosperm (Figure 3.2, E).

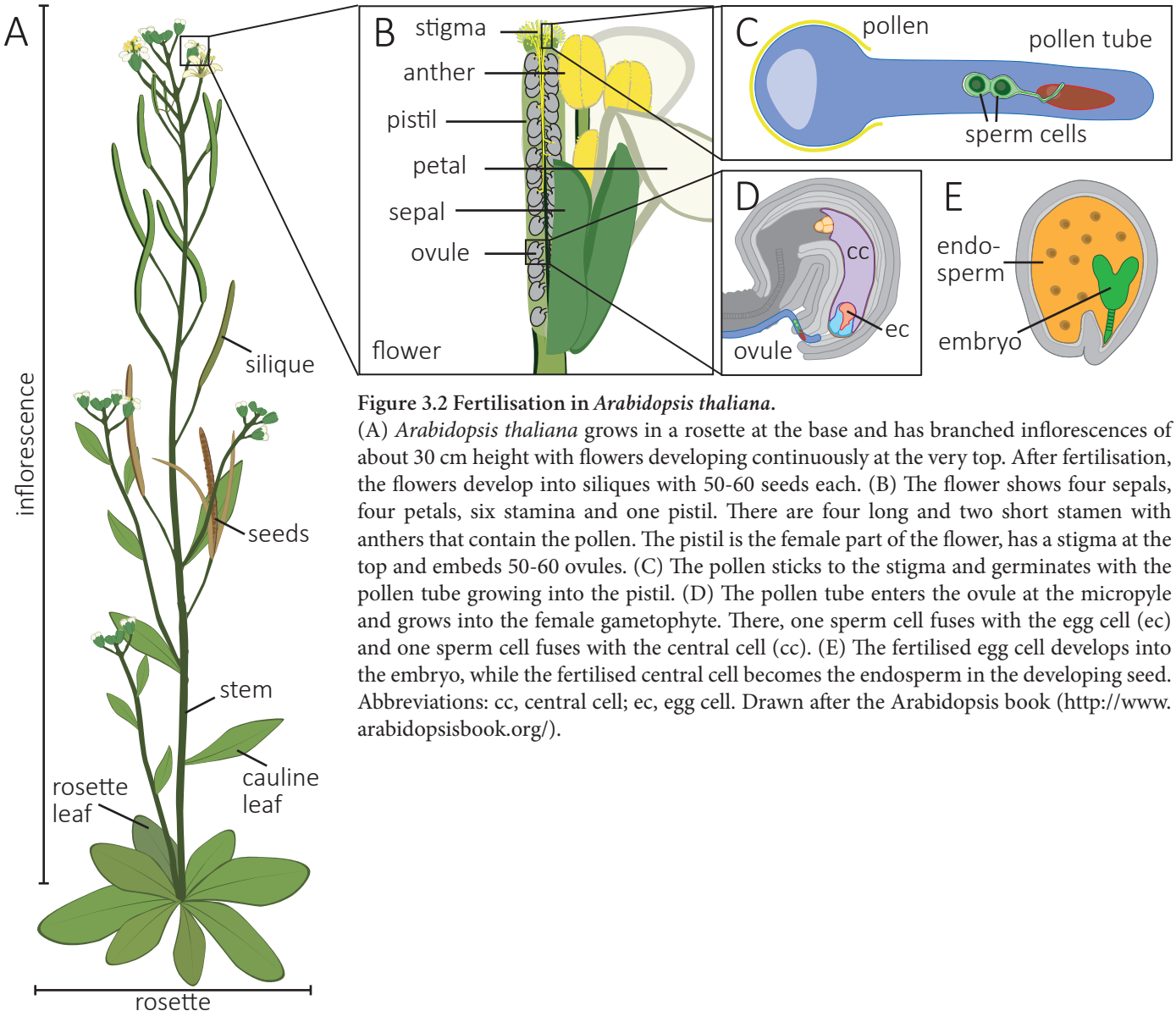

Figure 3.2 Fertilisation in *Arabidopsis thaliana*.
(A) *Arabidopsis thaliana* grows in a rosette at the base and has branched inflorescences of about 30 cm height with flowers developing continuously at the very top. After fertilisation, the flowers develop into siliques with 50-60 seeds each. (B) The flower shows four sepals, four petals, six stamina and one pistil. There are four long and two short stamen with anthers that contain the pollen. The pistil is the female part of the flower, has a stigma at the top and embeds 50-60 ovules. (C) The pollen sticks to the stigma and germinates with the pollen tube growing into the pistil. (D) The pollen tube enters the ovule at the micropyle and grows into the female gametophyte. There, one sperm cell fuses with the egg cell (ec) and one sperm cell fuses with the central cell (cc). (E) The fertilised egg cell develops into the embryo, while the fertilised central cell becomes the endosperm in the developing seed. Abbreviations: cc, central cell; ec, egg cell. Drawn after the Arabidopsis book (http://www.arabidopsisbook.org/).

3.2 Male gametophyte development

The development of the male gametophyte is divided into two distinct phases, termed microsporogenesis and microgametogenesis and takes place in the pollen sac, the microsporangium of the developing anther (Figure 3.2). Microsporogenesis in *Arabidopsis* starts with a diploid pollen mother cell, termed meiocyte, which undergoes meiosis to form a tetrad of microspores enclosed by a callose wall (Figure 3.3). A specialised microsporangium layer, the tapetum, produces an enzyme (callase) that digests the callose wall of the tetrads to release the microspores as free individual cells (McCormick 1993). After their release, the microspores develop into unicellular pollen with multiple small vacuoles, which fuse to a single large vacuole and thereby polarize the cell (Bedinger 1992). An asymmetric mitotic cell division marks the beginning of microgametogenesis and results in a large vegetative cell and a small generative cell. The latter enters the vegetative cell and becomes totally enclosed by the pollen (Russell 2017). They form a bicellular pollen with very few vacuoles and with the generative cell connected to the vegetative nucleus via a membrane projection (McCue *et al.,* 2011). The vegetative nucleus and the sperm cell are termed the male germ unit (MGU). In about 70% of flowering plants as, for example, *Nicotiana benthamiana* or *Amborella trichipoda*, the mature pollen is bicellular. In species such as *A. thaliana* and maize, however, the

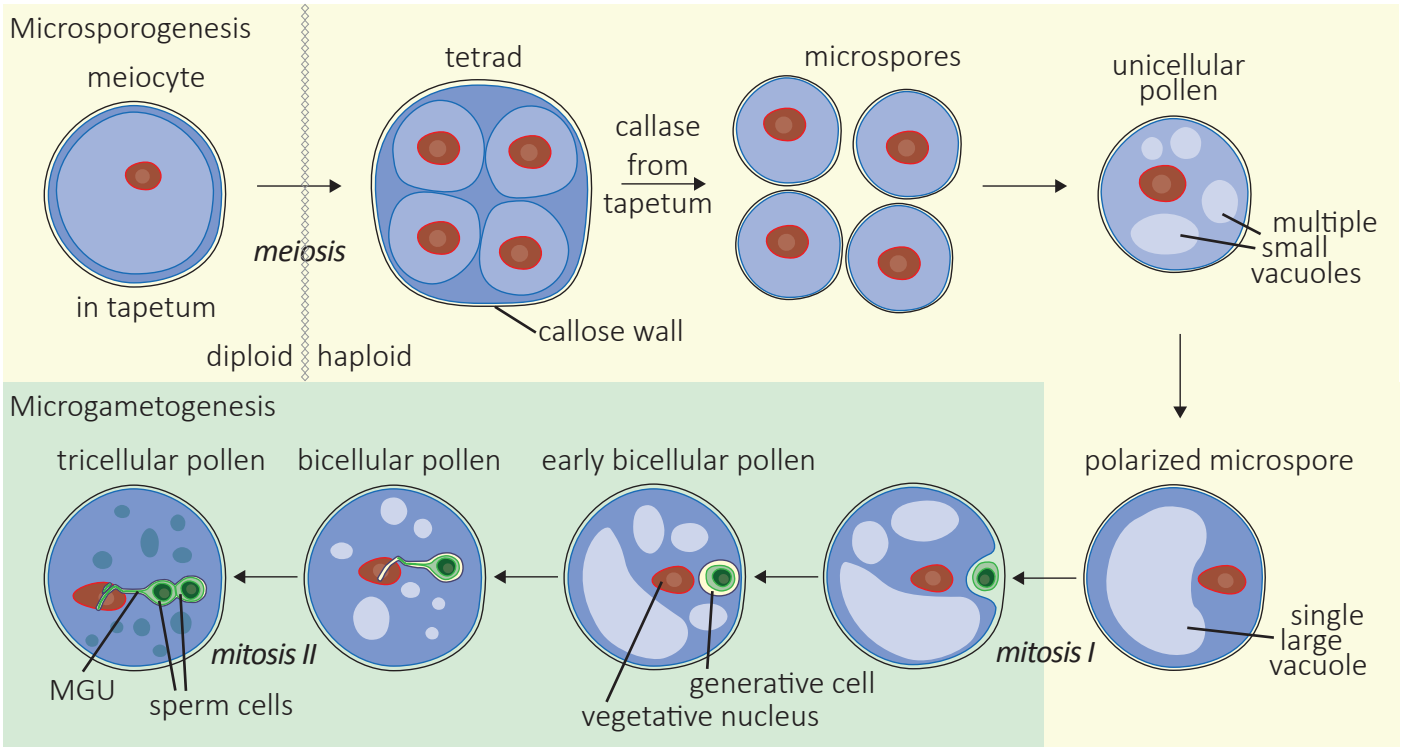

Figure 3.3 Male gametophyte development in *Arabidopsis thaliana*.
During microsporogenesis, a diploid pollen mother cell (meiocyte) in the tapetum of anthers undergoes meiosis and forms a tetrad of haploid microspores. The callose wall of the tetrad is digested by callase, produced by the tapetum. The released microspores develop into unicellular pollen with multiple small vacuoles that fuse to a single large vacuole in the polarized microspore. The first mitotic division of microgametogenesis is an asymmetric cell division, producing a small generative cell and a larger vegetative cell. The generative cell subsequently becomes engulfed by the vegetative cell in the early bicellular pollen. A membrane projection is formed that connects the generative cell with the vegetative nucleus in the bicellular pollen. After vacuole degeneration, a second mitotic division of the generative cell the mature tricellular pollen is formed that appears to have storage vacuoles. The vegetative nucleus and the two sperm cells are termed the male germ unit (MGU). Drawn after Bedinger (1992), Yamamoto, Nishimura et al. (2003) and Russell (2017).

generative cell undergoes another mitotic division in which two identical sperm cells are formed, resulting in a tricellular pollen grain.

In 1967, Brewbaker showed that tricellular pollen had many parallel and irreversible origins during evolution which suggests the tricellular pollen to be of some advantage compared to bicellular pollen. Soon after completed meiosis, the pollen cell wall is synthesized and is composed of two layers, an outer exine and an inner intine. The mature *Arabidopsis* pollen has multiple small storage vesicles (Yamamoto *et al.,* 2003) and is dehydrated (Van Aelst *et al.,* 1993). The male germ unit of the mature *Arabidopsis* pollen consists of a vegetative nucleus and two sperm cells and all three cells are physically connected.

The two sperm cells are tightly connected. It has been first shown in *Plumbago zeylanica* through electron microscopy that the cell wall between both sperm cells is thicker than the cell wall of the generative cell and irregular in form, containing numerous vesicular inclusions (Russell *et al.,* 1996). So far, only little is known about the membrane projection that connects the sperm cells with the vegetative nucleus and also contains cytoplasm. In *Plumbago zeylanica* and *Nicotiana tabacum*, its growth and expansion is provoked by microtubule elongation and formed by vesicle formation at the tip (Russell *et al.*, 1996; Yu *et al.,* 1992). Interestingly, until today, it is neither known how the membrane projection between the sperm cells and the vegetative nucleus is formed nor how it is separated again during the fertilisation process in *Arabidopsis*.

However, on a molecular basis it was shown that Germ Unit Malformed (GUM) and Male Germ Unit Displaced (MUD) are essential for correct formation and positioning of the male germ unit, as it was misplaced in both mutants (Lalanne and Twell 2002). Furthermore, it is known that Duo Pollen1 (DUO1) is a male sperm line specific transcription factor that plays a role in the processes of cell division and differentiation during gamete development (Borg *et al.,* 2014). The authors also have shown that Duo1-Activated Zinc Finger1 (DAZ1) and DAZ2 have redundant functions and are required for generative cell division in mutant analysis, as *daz1 daz2* mutant *A. thaliana* pollen is bicellular and not tricellular. It has been suggested that DUO1 acts as a network trigger in male germline development and that the DUO1-DAZ1/2 module is an ancient developmental feature, as all three proteins are highly conserved in angiosperms (Lockhart 2014). Other genes, such as *Quartet* and *Tetraspore,* function earlier during development and are responsible for successful separation of the tetrad (Preuss *et al.,* 1994).

3.3 Female gametophyte development

The female gametophyte is also termed embryo sac and is embedded in the ovule, which develops in parallel. The ovule develops from the ovule primordium, which is a finger-like protuberance from the inner ovary wall that bends during growth, while layers of inner and outer integuments grow from the basis, termed chalaza, around the nucellus and the developing embryo sac enclosing them both (Figure 3.4). Opposite to the chalaza is the micropyle, an opening in the ovule where the surrounding integuments touch again. As in male gametophytes, the development of female gametophytes is divided into two parts, the megasporogenesis and the megagametogenesis, and was subdivided into different phases (FG0-FG8; Christensen *et al.,* 1997).

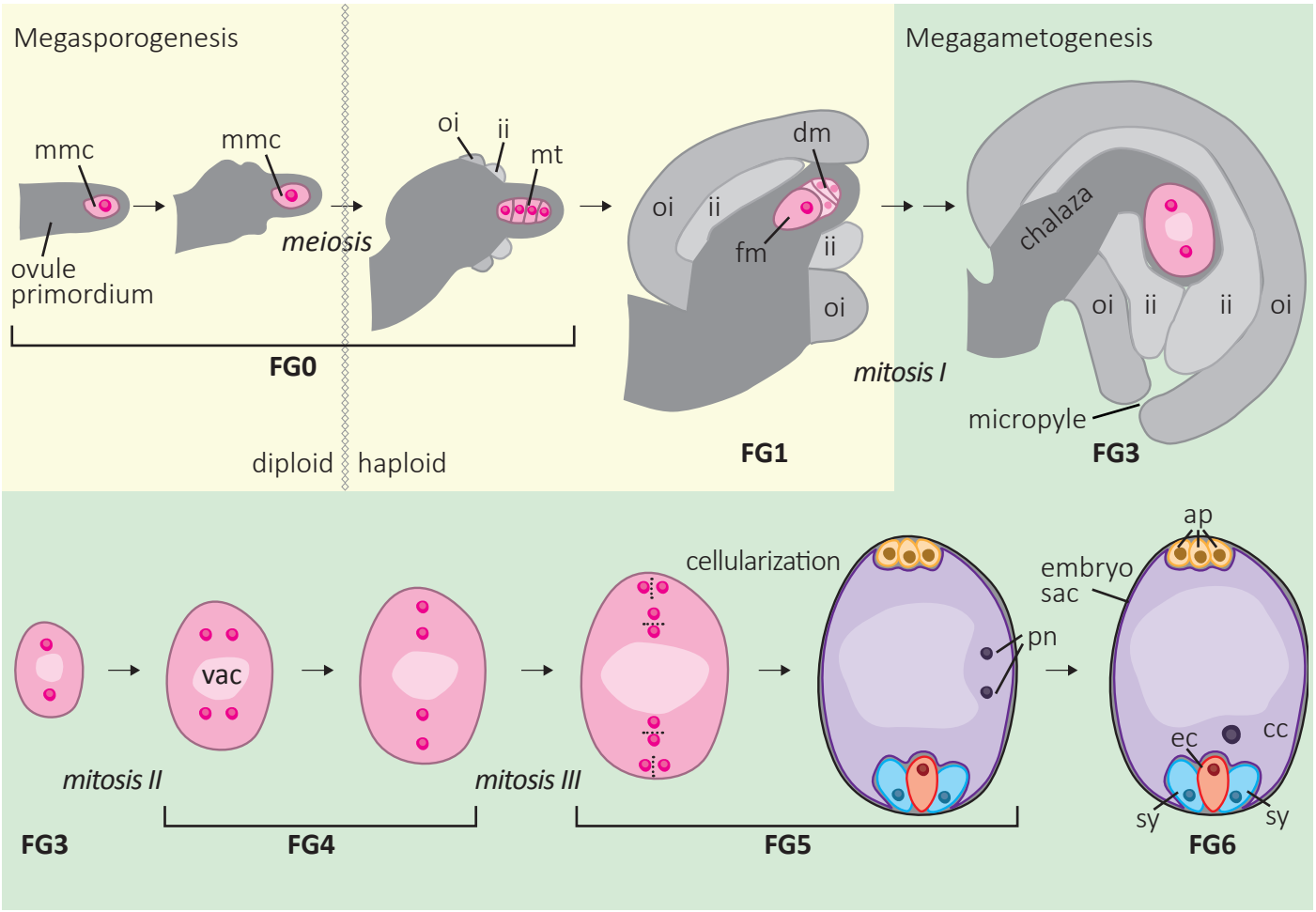

Figure 3.4 Female gametophyte development in *Arabidopsis thaliana*.
During megasporogenesis (FG0), a megaspore mother cell (mmc) forms from a sub-epidermal cell at the distal end of the ovule promordium. The diploid megaspore mother cell undergoes meiosis and forms four haploid megaspores known as the meiotic tetrad (mt). Three megaspores degenerate (dm) leaving one functinal megaspore (fm). The functional megaspore with a single nucleus (FG1) undergoes megagametogenesis. This nucleus undergoes two mitotic divisions, producing a four-nucleate coenocyte with two nuclei at each pole, the chalazal and the micropylar pole, separated by a large central vacuole (FG4). During a third mitosis, phragmoplasts and cell plates form between sister and non-sister nuclei and the nuclei become completely surrounded by cell walls (FG5). During cellularization, the two polar nuclei (pn) migrate from the poles toward the center of the female gametophyte and fuse (FG6). The mature seven-celled female gametophyte, also termed embryo sac, consists of three antipodal cells, one central cell, two synergids and one egg cell. Sporophytic tissues are drawn in grey and gametophytic cells in color. Abbreviations: ap, antipodal cell; cc, central cell; dm, degenerated megaspore; ec, egg cell; fm, functional megaspore; ii, inner integument; mmc, megaspore mother cell; mt, meiotic tetrad; oi, outer integument; pn, polar nuclei; sy, synergid cell; vac, vacuole. Drawn after Christensen *et al.* (1997).

Megasporogenesis (FG0) starts with a megaspore mother cell in the ovule primordium, which undergoes meiosis and forms a meiotic tetrad. Three of these cells undergo programmed cell death, while one cell becomes the functional megaspore (FG1; Yadegari and Drews 2004). Typically, the cell closest to the chalaza becomes the functional megaspore, recognizable by size and the large nucleus (Schneitz *et al.,* 1995). During megagametogenesis, this cell develops into the female gametophyte by three highly coordinated mitotic divisions, followed by cellularization and cell specification (Sprunck and Gross-Hardt 2011). After the nucleus of the functional megaspore has divided during mitosis I (FG2), a vacuole is formed between the two nuclei (FG3; Schneitz *et al.*, 1995) and the polarity of the female gametophyte is determined. Both nuclei divide again and form a four-nucleate coenocyte with two nuclei at each pole (FG4). During a third mitosis, phragmoplasts and cell plates form between sister and non-sister nuclei; this is the beginning of the cellularization process and the female gametophyte cells quickly become completely surrounded by cell walls (FG5; Drews and Koltunow 2011). During and after cytokinesis, two nuclei migrate from the poles, the chalazal pole and the micropylar pole, towards one another, therefore termed polar nuclei. They fuse within approximately 36 hours to form the homodiploid central cell (Jensen 1964). These events result in a seven-celled structure consisting of three antipodal cells, one central cell, two synergid cells and one egg cell, with the last four cells forming the female germ unit (FG6).

The process of female gametophyte development is highly regulated and several genes have been found to be involved in mutant analyses. The nuclear divisions and migrations, for example, are regulated by γ-tubulin and γ-tubulin-containing complex encoding genes (*TUBG1*, *TUBG2* (Pastuglia *et al.,* 2006) and *GCP2* (Nakamura and Hashimoto 2009)). Furthermore, the positioning of the nuclei is important for the cell fates during cellularization. Female gametophytes of *atnack1/ atnack2* double mutants are defective in nuclei positioning and fail to form typical cross walls between nuclei (Tanaka *et al.,* 2004). Misexpression of BEL1-like homeodomain1 (BHL1) in the embryo sac causes the *eostre* phenotype (Pagnussat *et al.,* 2007). In *eostre* female gametophytes, a single and in *lachesis* female gametophytes, multiple supernumerary egg cells are formed from nuclei determined to be synergid cells or central cells, respectively (Groß-Hardt *et al.,* 2007). Also, *clotho* and *atropos* female gametes contain more than one egg cell. In both mutants, synergid cells and the central cell can adopt egg cell identity and additionally, antipodal cells can adopt central cell fate (Moll *et al.,* 2008). As, compared to *eostre*, the central cell differentiates egg cell fate and the antipodal cells show characteristics of central cells in *lachesis*, *clotho* and *atropos* mutants, it has been emphasized that all cells of the female gametophyte can differentiate into gametes (Sprunck and Gross-Hardt 2011).

3.4 The cells of the female gametophyte

3.4.1 The egg cell

The egg cell is the true female gamete, as it produces the embryo after fertilisation and passes on genetic information to the progeny (Sprunck and Gross-Hardt 2011). In *Arabidopsis,* egg cells are located at the micropylar end of embryo sacs and have the shape of an inverted drop (Figure 3.5). The nucleus with its large nucleolus is located to the chalazal pole, while a single large vacuole fills the micropylar pole of the cell. The egg cell shares a common cell wall surface with the synergid cells on two sides and with the central cell towards the chalazal end (Huang and Russell 1992). Interestingly, the common cell wall of the egg and central cell shows dense bodies that have been suggested to function as stabilisers of the egg-central cell boundary during fertilisation due to their proximity

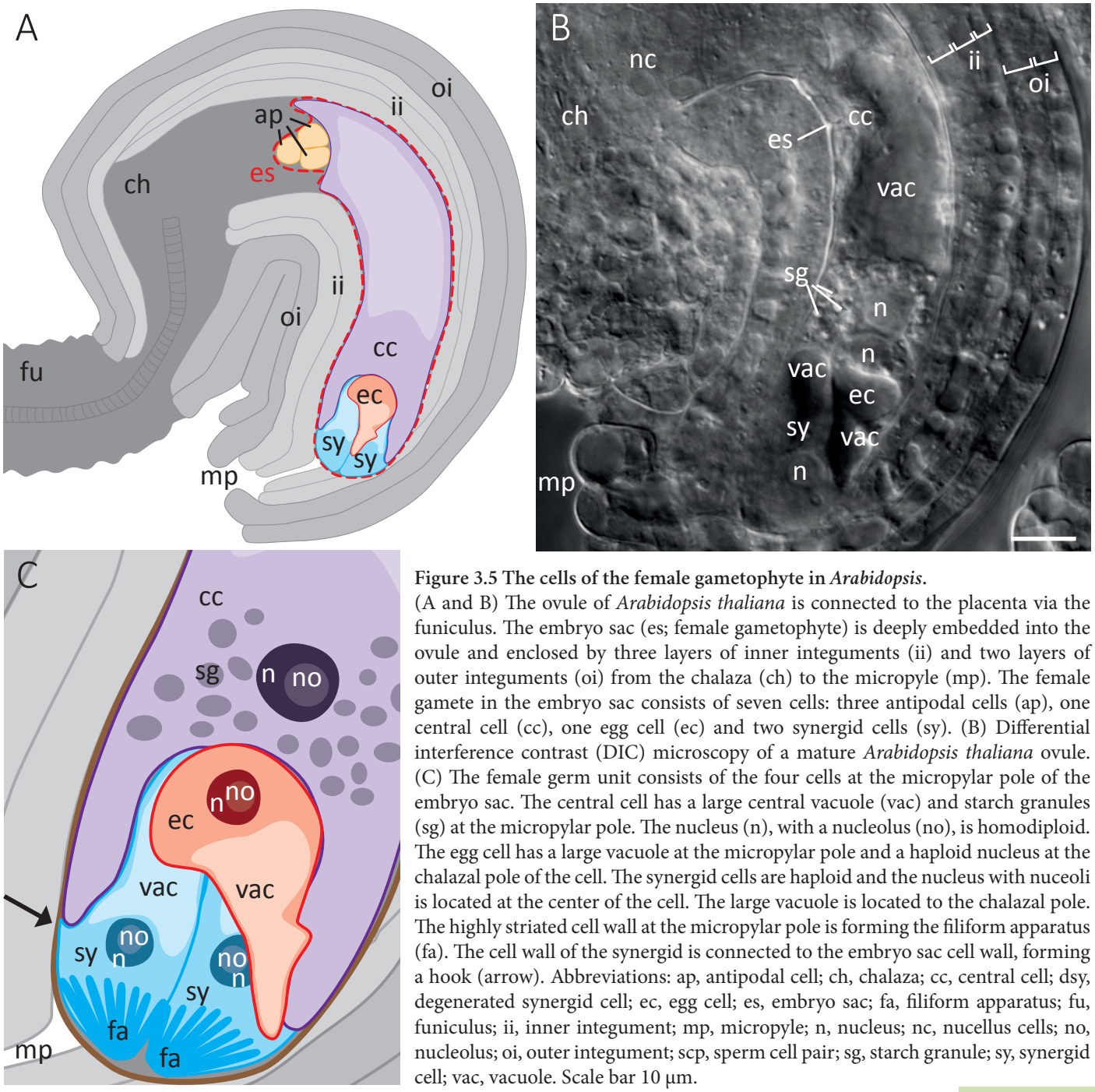

Figure 3.5 The cells of the female gametophyte in *Arabidopsis*.
(A and B) The ovule of *Arabidopsis thaliana* is connected to the placenta via the funiculus. The embryo sac (es; female gametophyte) is deeply embedded into the ovule and enclosed by three layers of inner integuments (ii) and two layers of outer integuments (oi) from the chalaza (ch) to the micropyle (mp). The female gamete in the embryo sac consists of seven cells: three antipodal cells (ap), one central cell (cc), one egg cell (ec) and two synergid cells (sy). (B) Differential interference contrast (DIC) microscopy of a mature *Arabidopsis thaliana* ovule. (C) The female germ unit consists of the four cells at the micropylar pole of the embryo sac. The central cell has a large central vacuole (vac) and starch granules (sg) at the micropylar pole. The nucleus (n), with a nucleolus (no), is homodiploid. The egg cell has a large vacuole at the micropylar pole and a haploid nucleus at the chalazal pole of the cell. The synergid cells are haploid and the nucleus with nuceoli is located at the center of the cell. The large vacuole is located to the chalazal pole. The highly striated cell wall at the micropylar pole is forming the filiform apparatus (fa). The cell wall of the synergid is connected to the embryo sac cell wall, forming a hook (arrow). Abbreviations: ap, antipodal cell; ch, chalaza; cc, central cell; dsy, degenerated synergid cell; ec, egg cell; es, embryo sac; fa, filiform apparatus; fu, funiculus; ii, inner integument; mp, micropyle; n, nucleus; nc, nucellus cells; no, nucleolus; oi, outer integument; scp, sperm cell pair; sg, starch granule; sy, synergid cell; vac, vacuole. Scale bar 10 µm.

to the site of sperm cell deposition (Russell 1983). Based on ultrastructural characteristics, the unfertilised egg cell is thought to be secretory quiescent due to the infrequency of dictyosomes and dictyosome vesicles (Huang and Russell 1992).

RWP-PK domain (RKD) genes were found to induce an egg cell like transcriptome in *A. thaliana* (Kőszegi *et al.,* 2011) and the RKD transcription factor Minus Dominance (MID) determines the *minus* gamete mating type of the green algae *Chlamydomonas reinhardtii* (Lin and Goodenough 2007). Interestingly, in *MpRKD* knockdown lines of the liverwort *Marchantia polymorpha*, the gametophyte-sporophyte transition is disturbed, resulting in non-quiescent egg cells that proliferate in the absence of fertilisation (Rövekamp *et al.,* 2016). It is therefore likely that egg cell needs to be activated upon fertilisation to leave this quiescent state. It is not yet known how egg cells are activated, but there is evidence that Ca^{2+} might play a role. In *semi-in vivo* fertilisation assays, *A. thaliana* ovules, with egg cells expressing a cytosolic Ca^{2+} sensor, were targeted by pollen tubes. As the egg cells showed Ca^{2+} spiking upon sperm cell release and at the start of sperm cell movement towards the egg cell prior to fusion, is was proposed that the second Ca^{2+} spike occurred upon start of gamete fusion (Denninger *et al.,* 2014). This is in line with the finding that in similar experiments, using fusion deficient sperm cells, egg cells showed the first Ca^{2+} spike upon sperm cell release, but no second spike was detected (Hamamura *et al.,* 2014). This indeed suggests that the second Ca^{2+} spike occurs as soon as the fusion begins and leaves the question whether the activation of egg cells is initiated by this spike or occurred at an earlier point during the fertilisation process.

3.4.2 The synergid cells

The shape and size of the two synergid cells are quite similar to the egg cell (Figure 3.5), but they are positioned a little further towards the micropyle. They are located nearest to the entry point of the pollen tube and show an inverted polarity. Their nuclei are usually located to the centre of the cell and a large vacuole is visible at the chalazal end that becomes fragmented during the fertilisation process (Wang *et al.,* 2017). Synergid cells are highly specialised secretory cells and can be divided into three sub-zones: the chalazal end, the "neck"-like shape and the "head"-like shape at the micropylar end (Leshem *et al.,* 2013). The cell wall of the synergid cells becomes thinner towards the chalazal pole and typically becomes discontinuous or even disappears (Mansfield *et al.,* 1991). The chalazal part (Zone I) of the synergid cell is engulfed by a cytoplasmic protrusion and the region where this protrusion ends is visible as the synergid hook or the central cell apical pocket (Figure 3.5, C, arrow; Cass *et al.,* 1986). The "neck"-like shape describes the middle part where the synergid cell has the smallest perimeter (Zone II) and the "head"-like shape describes the micropylar part that is most accessible to the arriving pollen tube (Zone III; Leshem *et al.,* 2012). The micropylar end of the mature synergid cell is typically occupied by a variably thick area of

cell wall invaginations known as the filiform apparatus (FA), which was first described in 1856 by Schacht. The surface of the FA is extremely enlarged, which facilitates high secretion rates. Although the size and shape of the FA varies among species, the essentially universal occurrence of the FA and its restriction to the synergid cells has suggested numerous functions, including specialisations for pollen tube reception and chemotropic attraction of the pollen tube. However, it was shown for *A. thaliana* that pollen tube reception does very likely not take place at the FA but between zone II and III (Leshem *et al.*, 2012). As one synergid cell degenerates during pollen tube reception, the second synergid cell can function as a backup for a second pollen tube if fertilisation fails. By default, polytubey is blocked to decrease the risk of multiple fertilisations, as in the first 10 hours after pollination most ovules are targeted by only one pollen tube (Kasahara *et al.,* 2012).

3.4.3 The central cell

While the egg cell develops into the embryo, the central cell is the second female gamete and develops into the endosperm after fertilisation. It clearly is the largest cell of the female gametophyte (Figure 3.5) that occupies about 75% of the volume in some species (Russell 1987). It shares cell walls with the antipodal cells at the chalazal end and with the synergid cells and the egg cell at the micropylar end and has a prominent vacuole (Huang and Russell 1992). In *Arabidopsis,* the central cell is the only cell of the female gametophyte that is homodiploid, as the two polar nuclei fuse during cellularization. At female gametophyte stage FG5, two polar nuclei migrate towards one another and fuse. In cotton (*Gossypium hirsutum*) it has been observed that the endoplasmic reticuli at the nuclei fuse at several points before the inner membranes of the nuclei merge (Jensen 1964). The nucleus of the mature *Arabidopsis* central cell has a nucleolus that is larger than in the surrounding cells (Christensen *et al.*, 1997). In *Torenia fournieri,* it has been shown that the central cell is symplastically connected to the egg cell and the synergid cells and that after fertilisation, the symplastic permeability decreases continuously (Han *et al.,* 2000). The central cell starts to accumulate starch when the two polar nuclei lie next to each other (stage FG5) and the starch deposit continues to increase through fertilisation and development of the endosperm (Hedhly *et al.,* 2016). The endosperm (Figure 3.2, E) is the product of the second fertilisation in the female gametophyte and is a triploid coenocyte, a cell with multiple nuclei in the same cytoplasm. During seed development, the endosperm and the embryo develop in parallel with the endosperm surrounding the embryo. Interestingly, the central cell is able to produce endosperm without being fertilised. When fertilisation is prevented in the *Arabidopsis thaliana* mutant *f644*, lacking the polycomb protein MEDEA (Grossniklaus *et al.,* 1998), seed-like structures were formed containing endosperm (Kiyosue *et al.,* 1999). The importance of endosperm is evident as it constitutes the edible part of the cereal seed and as such sustains directly or indirectly (via animal food) > 60% of human nutrition (Li and Berger 2012). But compared to cereals, the endosperm of *Arabidopsis* is nonpersistent, as it is depleted gradually as the embryo

grows. Therefore, it is generally assumed that the purpose of the nonpersistent endosperm is to support the developing and growing embryo, while the cotyledons support the germinating embryo (Olsen 2004).

3.4.4 The antipodal cells

The antipodal cells in *Arabidopsis* are located towards the chalazal pole of the embryo sac (Figure 3.5). Compared to cells of the female germ unit, they do not develop large vacuoles and exhibit condensed nuclei without nucleoli (Song *et al.,* 2014). However, antipodal cells have variable destinies among species. In maize, for example, antipodal cells proliferate and form a cluster of about 40-100 polyploid cells in the mature female gametophyte (Diboll and Larson 1966; Vollbrecht and Hake 1995). A mature egg apparatus of wheat includes a mass of 20-30 antipodal cells (An and You 2004). Although it has been repeatedly reported that antipodal cells in *A. thaliana* degenerate at stage FG6 (Poliakova 1964; Schneitz *et al.*, 1995; Christensen *et al.*, 1997), other researchers showed that the antipodal cells persist during fertilisation when transgenic plants expressing fluorescent reporter constructs for this cell type were investigated (Song *et al.*, 2014). Interestingly, it has been suggested that the lifespan of antipodal cells is determined by the central cell, as in *fiona* mutants antipodal cells showed an extended lifespan although FIONA is not expressed in antipodal cells but in central cells (Kägi *et al.,* 2010). Additionally, cell fate of antipodal cells may be amended since, for example, in *cytokinin independent 1* (*cki1)* mutants, antipodal cells show egg cell identity (Yuan *et al.,* 2016), while in *lachesis* (*lis*) mutants antipodal cells adopt central cell fate (Groß-Hardt *et al.*, 2007). Also, in *Zea mays,* the antipodal cells can adopt a central cell fate, but controlled by the egg cell secreted protein EA1-LIKE1 (EAL1). In *eal1* knockout mutants, antipodal cells have been shown to have central cell specificity (Krohn *et al.,* 2012). The antipodal cells might serve as a backup for other cells of the female gametophyte. Now, an efficient technique for *Arabidopsis* antipodal cell isolation is at hand (Yu *et al.,* 2016). With the help of transcriptomic and proteomic data, new insights to the function of antipodal cells are to be expected soon.

3.5 Key players during double fertilisation in *Arabidopsis*

After the pollen germinates on the papillae of the pistil, pollen tubes grow through the stigma, the style and the transmitting tract to transport male germ units to the female gametes. Pollen tubes get redirected to grow out of the transmitting tract and along the funiculus through the micropyle of the ovule.

3.5.1 Micropylar pollen tube attraction

Micropylar pollen tube attraction starts when the pollen tube emerges from the transmitting tract (Higashiyama and Yang 2017). As shown by laser ablation experiments in *Torenia fournieri*, synergid cells are necessary to attract pollen tubes to the female gametophyte and both synergid cells secrete pollen tube attraction signals (Figure 3.6, A; Higashiyama *et al.,* 2001). The MYB98 transcription factor, which is expressed exclusively in the synergid cells, is essential for micropylar guidance of pollen tubes and is additionally required for development of the filiform apparatus. In *myb98* mutant ovules, the pollen tubes grew to the funiculus, but failed to grow into the micropyle (Kasahara *et al.,* 2005). However, the authors stated that MYB98 very likely plays only an indirect role and controls the expression of downstream genes that are required for attraction.

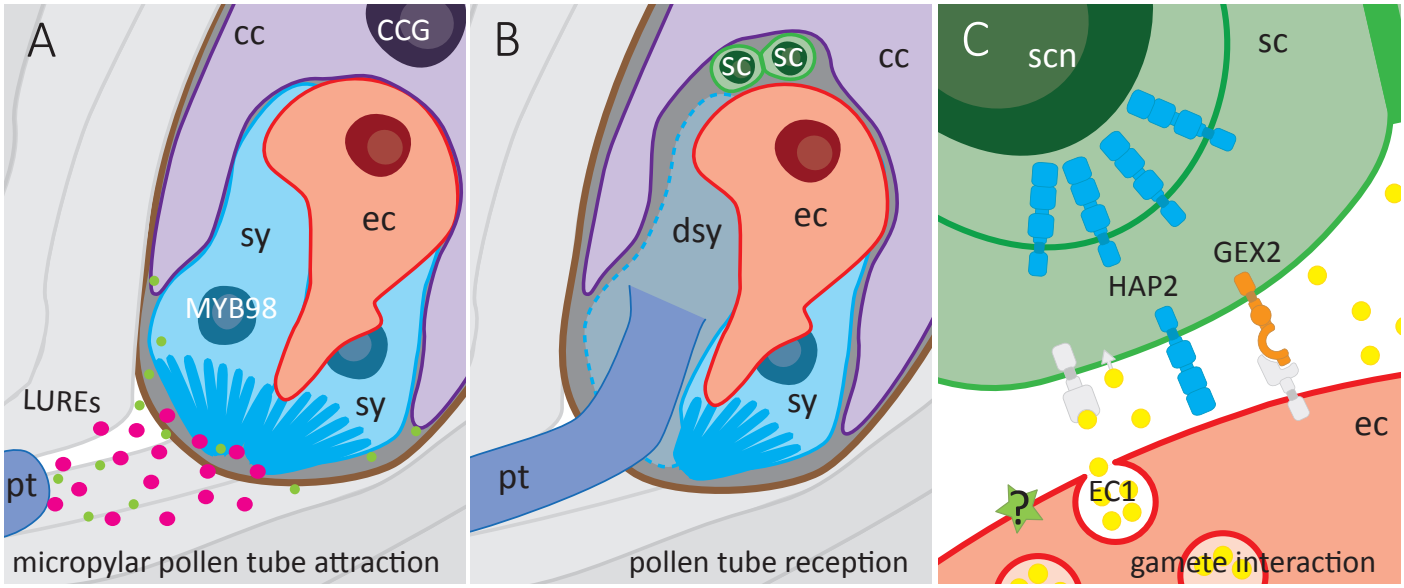

Figure 3.6 Mechanisms for double fertilisation in *Arabidopsis thaliana*.
(A) Pollen tube attraction to the female gametophyte is mediated via diffusable peptides. LUREs are secreted from the synergid cell (sy). MYB98 and CCG are transcription factors important for pollen tube guidance. (B) During pollen tube reception one synergid cell becomes the receptive synergid cell and undergoes programmed cell death (PCD). The pollen tube bursts and releases the sperm cells to the female gametophyte. (C) Prior to and during fertilisation, the gametes interact through various proteins. The egg cell (ec) is activated via an unknown mechanism (question mark) and secretes EC1 from storage vesicles. EC1 activates the sperm cells through an unknown mechanism, which leads to a shift of the fusion protein HAP2 from the endomembrane system to the plasma membrane of the sperm cells (sc). The protein GEX2 is important for gamete attachment, but its interaction partner on the egg cell plasma membrane is still unknown. Abbreviations: cc, central cell; ec, egg cell; dsy, degenerated synergid cell; pt, pollen tube; sc, sperm cell; scn, sperm cell nucleus. Drawn after Dresselhaus *et al.* (2016).

Some well-known pollen tube attractants are the LURE peptides, which are defensin-like CRPs (cysteine rich peptides) with 60-70 amino acids length. The LURE peptides induce reorientation of pollen tube tip growth (Okuda *et al.,* 2009; Takeuchi and Higashiyama 2016). In *Zea mays,* Egg Apparatus1 (ZmEA1), a highly hydrophobic small protein of 94 amino acids expressed in the egg apparatus, is required for pollen tube attraction (Marton *et al.,* 2005). *A. thaliana* LURE1 peptides diffuse passively along the path of the pollen tube without active transport (Takeuchi and Higashiyama 2012). Interestingly, the LURE1 peptides do not diffuse towards other parts of the ovule surface. Therefore, it has been suggested that special surface properties along the pollen tube path guarantee directed diffusion (Higashiyama and Yang 2017). It should also be mentioned that LURE peptides of different species preferentially attracted pollen tubes from their own species in *semi-in vivo* assays (Okuda *et al.*, 2009). However, *Torenia fournieri* synergid cells expressing AtLURE1.2 and *A. thaliana* synergid cells expressing ZmEA1 allowed pollen tubes of *A. thaliana* and *Zea mays* to be attracted, respectively (Takeuchi and Higashiyama 2012; Márton *et al.,* 2012). Despite the recently found pollen tube receptors for LUREs in *A. thaliana* (Wang *et al.,* 2016; Cheung and Wu 2016), not much is known for the recognition mechanisms and downstream signalling. Last but not least, the central cell has also been found to play a role in micropylar pollen tube guidance. In *central cell guidance* (*ccg*) mutants lacking CCG, a nuclear protein expressed in the central cell, pollen tubes grow to the ovule, but do not find the micropyle (Chen *et al.,* 2007). The authors suggested that CCG acts as a transcription regulator for pollen tube guidance, but its function is still unclear. However, an interaction partner of CCG was found quite recently. The Ccg Binding Protein1 (CBP1) has been demonstrated to bind CCG and in *cbp1* mutants, micropylar pollen tube guidance was disturbed, because more than one pollen tube entered the micropyle simultaneously (Li *et al.,* 2015).

3.5.2 Pollen tube reception

Once the pollen tube has grown through the micropyle to the female gametophyte, it needs to be received by one of the synergid cells. This requires complex bilateral cell signalling via multiple factors, including receptor-like kinase activation steps, intricate Ca^{2+} oscillations and programmed cell death (PCD) in both of the participating gametophytes (Thomas *et al.,* 2016). Several studies have uncovered synergid cell receptors that very likely operate in the same genetic pathway and whose functional loss causes the failure of pollen tube discharge (Wang *et al.*, 2017). These include early nodulin-like proteins (ENODLs), which accumulate at the filiform apparatus and interact with the extracellular domain of the receptor-like kinase Feronia (FER). Wild type pollen tubes failed to arrest growth in *enodl11-15* quintuple and *feronia* mutants (Escobar-Restrepo *et al.,* 2007; Hou *et al.,* 2016). Another important factor is Lorelei (LRE), which is a putative glycosylphosphatidylinositol (GPI)-anchored protein, as *lre-5* female gametophytes do

not allow pollen tube reception (Tsukamoto *et al.,* 2010). Furthermore, it was suggested that LRE plays a role at the interface of the pollen tube and synergid cell (Lockhart 2016). Additionally, *nortia* (*nta*) mutants show reduced fertility and pollen tube overgrowth, similar to the *feronia* mutant, with NTA being expressed in synergid cells (Kessler *et al.,* 2010).

Successful pollen tube reception includes PCD of the male gametophyte, meaning the pollen tube bursts and releases its content including the male germ unit. Simultaneously, one of the synergid cells randomly becomes the receptive synergid cell (Christensen *et al.,* 1997). The receptive synergid cell undergoes PCD as well and gives way to the pollen tube (Figure 3.6, B). It has been suggested that PCD is triggered by physical contact between the synergid cell and the pollen tube (Higashiyama *et al.,* 2000). If the followed fertilisation fails, the non-receptive synergid can attract and receive a second pollen tube (Kasahara *et al.,* 2012; Beale *et al.,* 2012).

3.5.3 Direct gamete interactions and gamete activation

After sperm cells have been released from the pollen tube, they need to get in close contact with the female gametes for successful double fertilisation. Through pollen tube burst, the sperm cells become located at the fusion site, the space between the central cell and the egg cell that is given by the degenerated synergid cell (Figure 3.6, B). During fertilisation, the gametes get activated, the sperm cells attach to the central cell and the egg cell, respectively and they fuse. To prevent polytubey after successful fertilisation, the remaining synergid cells are inactivated via a cell fusion mechanism with the endosperm, where the synergid cytoplasm, containing pollen tube attractants, becomes diluted with the endosperm cytoplasm (Maruyama *et al.,* 2015).

A few key proteins for gamete interactions are known in *A. thaliana* (Figure 3.6, C). A protein essential for attachment is Gamete Expressed2 (GEX2), which is localised to the sperm cell membrane and contains extracellular immunoglobulin-like domains, similar to gamete interaction factors in mammals (Mori *et al.,* 2014). One of the best studied fusion-essential proteins is the sperm cell specific protein Generative Cell Specific1/Hapless2 (GCS1/HAP2; further referred to as HAP2; Mori *et al.,* 2006; von Besser *et al.,* 2006). HAP2 is highly conserved in many species from prokaryotes (*Plasmodium* and *Paramecium*) to animals (*Hydra* and *Apis*) and plants (*Chlamydomonas*, *Zea* and *Arabidopsis*; Wong and Johnson 2010). In *Chlamydomonas* and *Plasmodium,* HAP2 functions after gamete activation and is essential for fusion of gametes (Liu *et al.,* 2008). Quite recently, the 3D structure of HAP2 was calculated via homology modelling and the 3D structure indicates that HAP2 has structural similarities with class II viral fusogen (Fédry *et al.,* 2017; Valansi *et al.,* 2017). Further, the authors showed evidences that HAP2-mediated fusion occurs through hemifusion intermediates, where the fusion of outer leaflets of two membranes are already merged but the inner leaflets remain distinct (Chernomordik and Kozlov 2005). Notably, in *A. thaliana* the

HAP2-YFP fusion protein mainly localises to the endomembrane system of sperm cells and it has been shown to be relocated from the endomembrane system to the plasma membrane upon sperm cell activation by Egg Cell1 (EC1) in *semi-in vivo* studies (Sprunck *et al.,* 2012). The EC1 proteins are a small family of five proteins in *A. thaliana.* Transcripts encoding EC1 proteins were initially found in isolated egg cells from wheat (Sprunck *et al.,* 2005). In *A. thaliana*, they were found to be secreted from egg cells during fertilisation and to be essential for double fertilisation. In a quintuple *ec1-RNAi* mutant, the sperm cells were arrested in fusion with the central cell or the egg cell (Sprunck *et al.*, 2012). It has been shown that some sperm cells are able to fuse with a delay of about 30-40 hours (compared to 6-8 hours after pollination (hap) in wild type) and it has been suggested that secreted EC1 proteins promote rapid sperm activation to accelerate gamete fusion and to prevent polytubey (Rademacher and Sprunck 2013). However, so far nothing is known about how EC1 proteins contribute to sperm cell activation on a molecular level. The structure of EC1 could give hints about molecular functions, but no structural information is available up to now.

3.6 Similarities between EC1 and non-specific lipid transfer proteins

Interestingly, 53% of female gametophyte-specific genes encode small cysteine rich proteins (CRPs), suggesting their important roles in male-female interactions (Huang *et al.,* 2015). EC1 is a CRP and belongs to the large and unexplored group of Early Culture Abundant1 (ECA1) gametogenesis-related proteins that are characterized by their conserved cysteine signature (Sprunck *et al.*, 2012). The ECA1 gametogenesis-related proteins have six cysteine residues forming three disulfide bridges and have probably been evolved from non-specific lipid transfer proteins (nsLTP), which are part of the prolamin superfamily. Figure 3.7 (modified from Zhang 2009) shows the suggested gain and loss of cysteine bridges during the evolution of the prolamin superfamily with the nsLTPs as a starting point, which show two conserved patterns of four cysteine pairs. It has been hypothesized that proteins with the domains of unknown function 784 (DUF784) and 1278 (DUF1278) form a structural fold similar to the prolamin superfamily despite their loss of two cysteine residues (Zhang 2009). Therefore, it has been suggested that EC1 proteins might also show a structure similar to that of nsLTPs (Sprunck *et al.,* 2014). Notably, from the more than 745 CRPs encoded in the *A. thaliana* genome, 127 genes encode for nsLTPs and 124 genes encode ECA1 gametogenesis-related proteins (Zhou *et al.,* 2013). Aside from EC1, many ECA1 gametogenesis-related and nsLTPs have been proposed to play vital roles in different aspects of reproduction in angiosperms (Sprunck *et al.*, 2014).

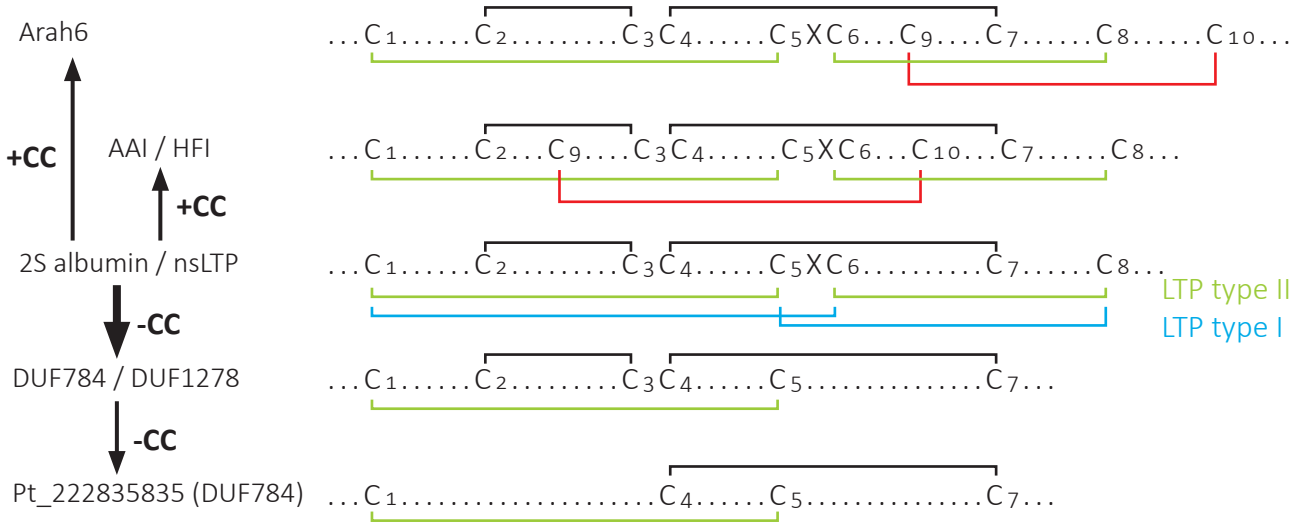

Figure 3.7 Gain and loss of cysteine pairs during evolution of the prolamin superfamily.
Cys residues in DUF784 and DUF1278 domains are numbered based on the positions of the Cys counterparts in the prolamin superfamily. Thin arrows indicate changes of disulfide bond patterns among domains, while thick arrow show the major transition from the prolamin superfamily to DUF784 and DUF1278 domains. The two different cysteine pair patterns of LTP type I and II are shown in blue and green. Abbreviations: AAI, alpha-amylase inhibitor; Arah6, *Arachis hypogaea* 6 allergen; HFI, Hageman factor inhibitor; nsLTP, non-specific lipid transfer protein. Modified from Zhang (2009).

Non-specific lipid transfer proteins are small, soluble, cysteine-rich proteins, usually with an alkaline isoelectric point and a molecular size below 10 kDa (Kader 1996). For a long time, there were only two big families of plant specific nsLTPs classified, type I and type II. They share the same cysteine residue pattern, but have different disulfide patterns and therefore different protein folding (Kader 1996). Many other classification systems were suggested over time in various species (Liu *et al.,* 2015). Quite recently, Salminen et al. (2016) introduced a new classification system and suggested a consistent nomenclature for all plant nsLTPs, considering sequence identity, spacing between cysteine residues and post-translational modifications. These classes are termed LTP1, LTP2, LTPc, LTPd, LTPe, LTPf, LTPg, LTPh, LTPj, LTPk and LTPx.

Initially, a nsLTP protein was purified and characterized as a spinach-leaf protein that was capable of transferring phospholipids between membranes in vitro (Kader *et al.,* 1984). Since then, nsLTPs have been found to play roles in synthesis of lipid barrier polymers, such as cuticular waxes, suberin and sporopollenin (Edstam *et al.,* 2013; Deeken *et al.,* 2016), but also in sexual reproduction, seed development and germination (Liu *et al.,* 2015). The LiLTP1.1 (SCA) from *Lilium longiflorum* (lily) was the first LTP suggested to have a role in the sexual reproduction of plants (Park *et al.,* 2000). SCA is involved in pollen tube adhesion-mediated guidance during pollen tube growth through the transmitting tract. It seems that SCA forms an adhesive matrix with pectin that guides the pollen tubes to the ovules (Park *et al.*, 2000). On the basis of sequence similarity, seven SCA-like LTPs were identified in *A. thaliana* (Chae *et al.,* 2010). When T-DNA insertion mutants for those seven genes were investigated, only AtLTP1.8 (LTP5) showed a phenotype. Furthermore, the root-specific nsLTP N5 of *Medicago truncatula* has been found to be important in signalling during symbiotic

interactions (Pii *et al.,* 2009) and *A. thaliana* Defective Induced Resistance1 (DIR1) plays a role in systemic required resistance (SAR) signalling (Maldonado *et al.,* 2002). Consequently, a new subfamily of LTPs was suggested, the signalling LTPs (Pii *et al.,* 2010). Interestingly, DIR1 is not alkaline as most of the nsLTPs, but acidic (pI=4.25), like the EC1 proteins.

However, nsLTPs have not only been shown to be capable of lipid transfer, but the 3D structure of several nsLTPs could be solved with and without bound lipids using X-ray crystallography and NMR (Heinemann *et al.,* 1996; Samuel *et al.,* 2002; Lascombe *et al.,* 2008). These studies revealed that nsLTPs are globular proteins with a long hydrophobic cavity, which incorporates the lipids. This example illustrates that knowledge of the folding of a protein gives important hints on the molecular function of the same.

3.7 Aims of this work

The five genetically redundant *A. thaliana EC1* genes (*EC1.1* to *EC1.5)* are characterized by two highly conserved signature motifs, a predicted signal peptide at the N-terminus and six cysteine residues. Secreted EC1 proteins are essential for double fertilisation in flowering plants and synthetic EC1 peptides induce the relocation of the fusion protein HAP2-YFP from the endomembrane system to the plasma membrane of released sperm cells, which is an indication of sperm cell activation. Nevertheless, little is known about gamete fusion on the cellular level and about the structure and the molecular action of EC1 proteins on sperm cells.

This work sought to give deeper insights into direct gamete interactions during double fertilisation and the role EC1 plays during this process. One research focus was to explore the process of gamete fusion through *in vivo* studies with suitable *A. thaliana* marker lines. Using confocal microscopy, the membrane dynamics of the sperm cells and the egg cell were monitored during fertilisation, providing information about interactions between the two gamete membranes.

A second focus was to investigate the role of secreted EC1 during double fertilisation, using *ec1* quintuple knockdown ovules and sperm cell marker lines in *in vivo* studies. In *semi-in vivo* experiments, the direct effect of EC1 peptides and second messengers on sperm cell activation was analysed and the trigger for EC1 secretion by the egg cells was investigated. Subcellular localisation studies for EC1.1-GFP in different cell types of *A. thaliana* and in epidermal leaf cells of *Nicotiana benthamiana* were performed and functional complementation studies of the quintuple *ec1-RNAi* knockdown line was done.

As a third, it was aimed to purify recombinant EC1 proteins for functional and structural studies. Therefore, an efficient method for EC1.2 protein purification was established using the *Pichia pastoris* expression system. With purified protein, several approaches were made to elucidate the structure of EC1.2. This included chromatography methods, nuclear magnetic resonance spectroscopy (NMR) and homology modelling. Moreover, the ability for lipid binding of EC1 was tested.

4. RESULTS

4.1 Cytological observations of the double fertilisation process

4.1.1 Membrane dynamics during double fertilisation

To investigate the plasma membrane dynamics of the egg cell and the sperm cell during fertilisation, gamete membrane marker lines were utilised. To visualise the membrane of gametes in the ovule, homozygous transgenic lines with strong fluorescence within the membranes were needed. The gene *Medicago truncatula* symbiotic remorin 1 (*MtSYMREM1*) encodes a protein almost exclusively localised to the plasma membrane (Lefebvre *et al.,* 2010) in *Arabidopsis thaliana*. The C-terminal remorin anchor of MtSYMREM1 was C-terminally fused to the fluorescence marker protein tagRFP-T and expressed in the egg cell by the *EC1.1* promoter (*EC1.1p:tagRFP-T-REM*). *A. thaliana* wild type plants were transformed with the construct and homozygous plants were selected for further studies.

In the homozygous *EC1.1p:tagRFP-T-REM*-expressing plant line #2_Q the tagRFP-T-derived red fluorescence was exclusively and strongly detected at the plasma membrane of the egg cell (Figure 4.1, A). For pollination experiments, the double marker line *HTR10p:HTR10-mRFP; HTR10p:TET9-GFP* (further referred to as H33T9; Sprunck *et al.*, 2012) with red fluorescent sperm cell nuclei and green fluorescent sperm cell membrane was used. The Tetraspanin9 (TET9) protein fused to GFP was shown to be expressed in the egg cell, the central cell and the synergid cells and to be uniformly distributed to the plasma membrane (T. Hackenberg, unpublished; Boavida *et al.*, 2013). As shown in Figure 4.1, B and C, sperm cells are connected to each other via the sperm cell plasma

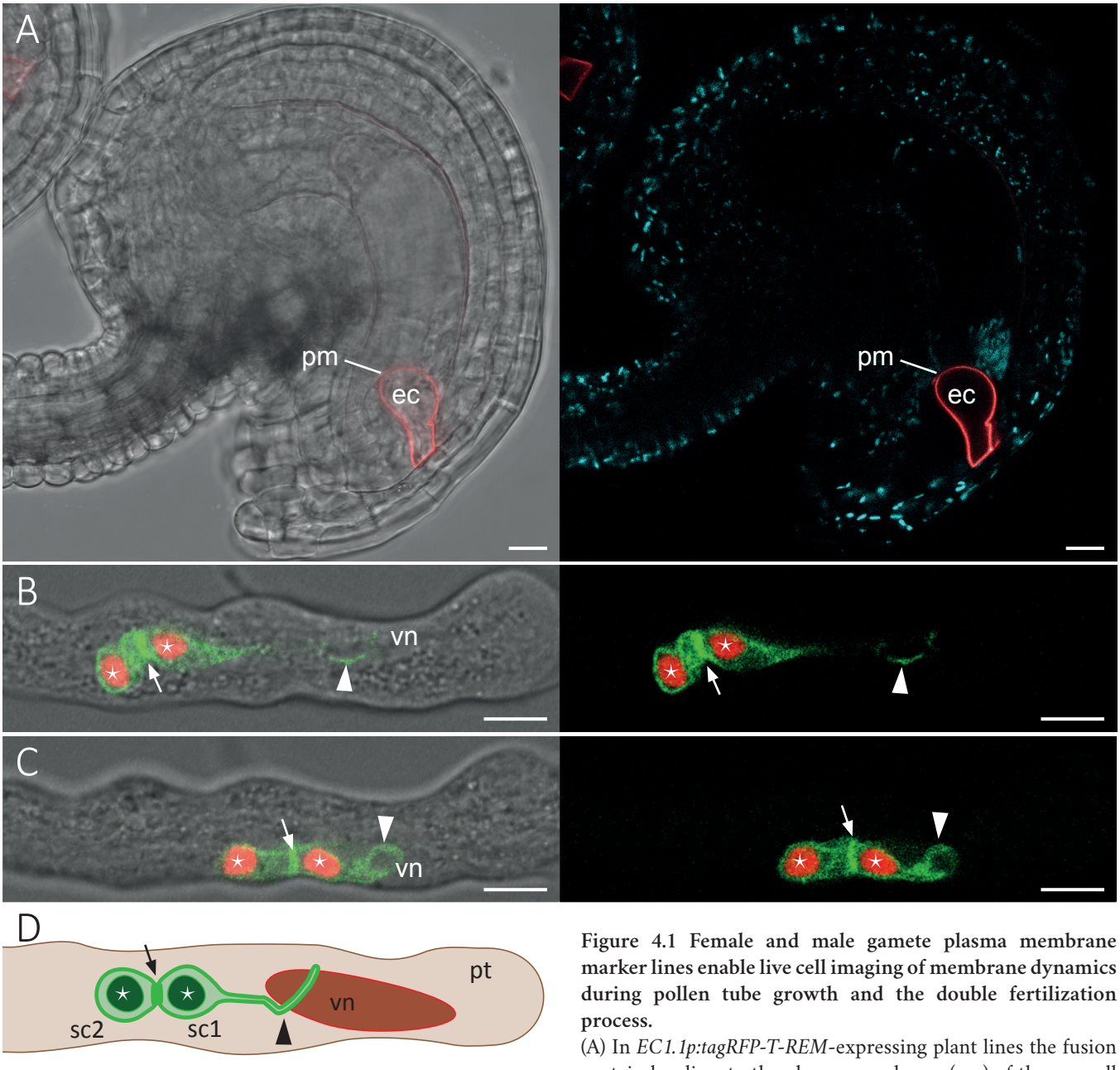

Figure 4.1 Female and male gamete plasma membrane marker lines enable live cell imaging of membrane dynamics during pollen tube growth and the double fertilization process.
(A) In *EC1.1p:tagRFP-T-REM*-expressing plant lines the fusion protein localises to the plasma membrane (pm) of the egg cell (ec), shown in red. Autofluorescence of the plastids in the ovule is shown in cyan. (B and C) In the double marker line H33T9 the sperm cell nuclei (asterisks) are shown in red and the sperm cell plasma membrane is shown in green. The sperm cells are connected to each other (arrow) and the leading sperm cell is connected to the pollen vegetative cell nucleus (vn) via a plasma membrane projection (arrowhead). (B) and (C) show different time points of the same pollen tube grown *in vitro*. (D) Drawing of a pollen tube with the male germ unit. Images are maximum projections of confocal images. Asterisk, sperm cell nucleus; arrow, sperm cell plasma membrane; arrow head, membrane projection. Abbreviations: ec, egg cell; pm, plasma membrane; pt, pollen tube; sc1, sperm cell 1; sc2, sperm cell2; vn, pollen vegetative cell nucleus. Scale bars 10 µm in (A) and 5 µm in (B and C).

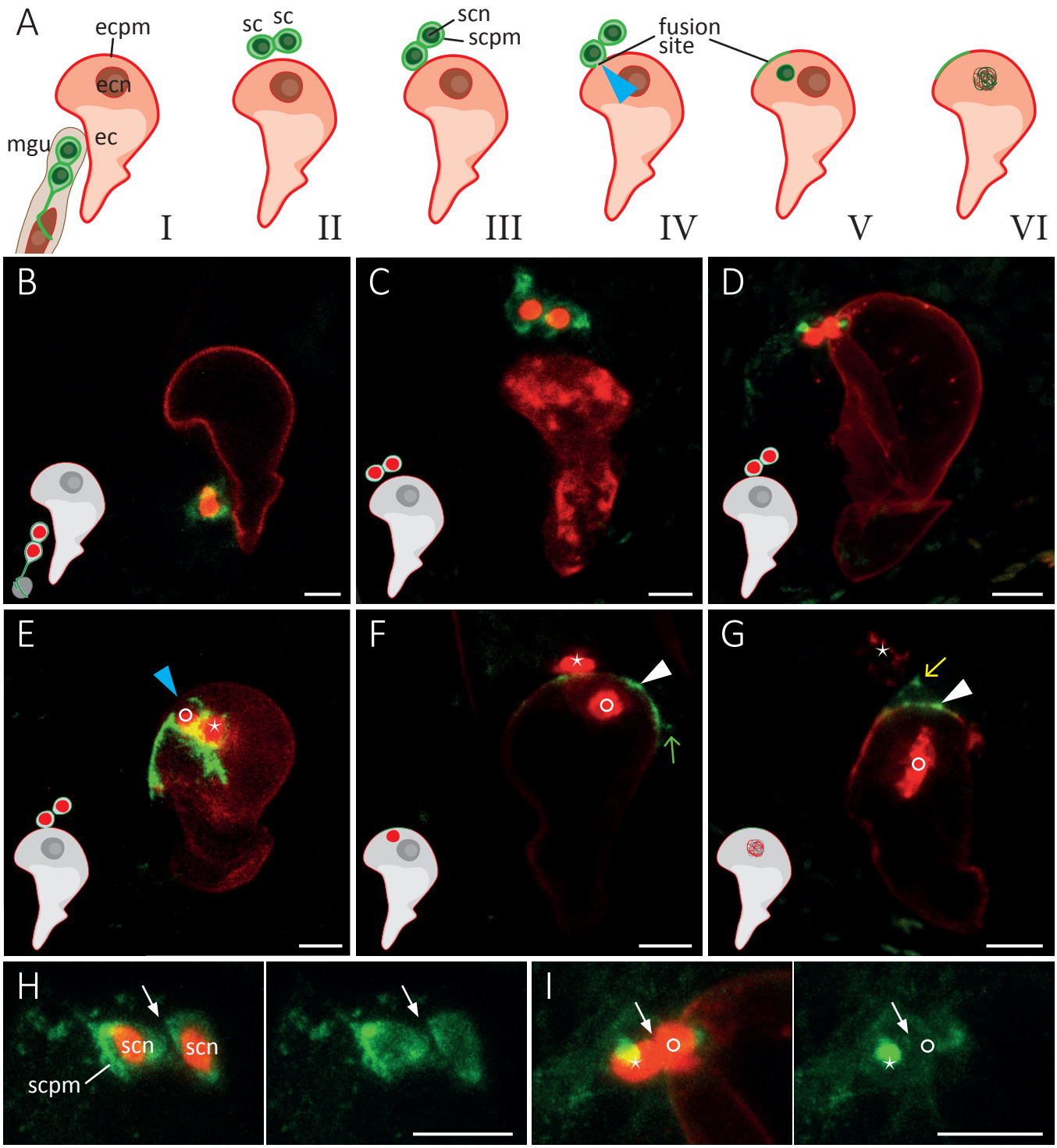

Figure 4.2 Sperm cell membrane dynamics during fertilization of the egg cell.
Egg cells of *EC1.1p:tagRFP-T-REM*-expressing plant lines are fertilized by the sperm cells of the double marker line H33T9, 6-8 hap. (A) CLSM studies revealed that the fertilization of the egg cell can be described by 6 phases, also shown as schematic representations in the insets of (B-G). (B) Phase I: the male germ unit is delivered by the pollen tube. (C) Phase II: after pollen tube burst the sperm cell pair is repositioned at the fusion site. (D) Phase III: the sperm cells are in close proximity to the egg and central cell (attachment). (E) Phase IV: the sperm cell fuses with the egg cell at the fusion site (blue arrowhead). (F) Phase V: the sperm cell nucleus moves towards the egg cell nucleus. (G) Phase VI: During karyogamy one sperm cell nuclus fuses with the egg cell nucleus. The second sperm cell nucleus already fused with the central cell nucleus (asterisk). The sperm cell plasma membrane is integrated into the egg cell (arrowhead) and the central cell plasma membrane (yellow arrow). (H and I) The TET9-GFP labelled connection of sperm cells is lost in phase III (arrow). Fluorescence of tagRFP-T and mRFP are depicted in red and GFP in green. Images are maxima projections of confocal images. Arrowhead, scpm integrated into ecpm; asterisk, sperm cell nucleus fusing with central cell nucleus; blue arrowhead, fusion site; green arrow, GFP signal outside the egg cell after fusion; circle, sperm cell nucleus fusing with egg cell nucleus; yellow arrow, scpm integrated into central cell plasma membrane. Abbreviations: ec, egg cell; ecn, egg cell nucleus; ecpm, egg cell plasma membrane; mgu, male germ unit; sc, sperm cell; scn, sperm cell nucleus; scpm, sperm cell plasma membrane. Scale bars 5 μm.

membrane and are also connected to the nucleus of the vegetative cell (the pollen tube cell) via a plasma membrane projection (arrow head). The fluorescence signal of TET9-GFP is not evenly distributed, but shows strong accumulations at the area between the two sperm cells (arrow).

To follow gamete-membrane dynamics during fertilisation of the egg cell, hand pollination experiments using the above described plasma membrane marker lines were performed. Representative images and a scheme summarizing the microscopic observations are shown in Figure 4.2. The process of egg-sperm fusion can be described in six phases (Figure 4.2, A). Prior to pollen tube burst, the sperm cell pair is still connected to the nucleus of the vegetative cell and is detected at the micropylar pole of the female gametophyte (Phase I, Figure 4.2, B). Upon pollen tube burst, the sperm cell pair is discharged towards the fusion site between the central cell and the egg cell (Phase II, Figure 4.2, C). Next, it can be assumed that one sperm cell attaches to the egg cell, while the other attaches to the central cell. Thus, the plasma membranes of egg cell and sperm cell get into close contact (Phase III, Figure 4.2, D). This is followed by the membrane merger of the sperm cell and the egg cell (Phase IV, Figure 4.2, E). The sperm cell plasma membrane is integrated into the egg cell plasma membrane, while parts of the membrane projection that connects the sperm cell pair with the vegetative cell nucleus stays extracellularly. The sperm cell nucleus migrates to the egg cell nucleus (Phase V, Figure. 4.2, F), followed by karyogamy (Phase VI, Figure 4.2, G). The central cell meanwhile fuses with the second sperm cell and the fading fluorescence signal of the sperm cell nucleus marker (asterisk) indicates karyogamy of sperm and central cell nucleus, while the sperm cell plasma membrane marks the central cell plasma membrane (arrow). The strong TET9-GFP signal between the two sperm cells vanishes during phases III and IV, as it is pointed to with an arrow in Figure 4.2, H.

The detailed examination of single optical sections of a fusion event between a sperm cell (circle) and an egg cell (Figure 4.3, A) showed no fluorescence signal of TET9-GFP at the fusion site (triangle). This indicates that the sperm cell plasma membrane is not incorporated into the egg cell but integrated to the egg cell plasma membrane. To proof this, plot profiles of red and green fluorescence channels of several fertilised egg cells were made. Using the software ImageJ, a line was drawn along the fluorescent labelled egg cell plasma membrane (Figure 4.3, B). The grey values of the green and red fluorescence channels along the egg cell plasma membrane were measured and are depicted in Figure 4.3, C. This representative plot profile reveals opposing trends of signal intensities with one region of preferential GFP-derived fluorescence (3-6.5 µm) flanked by two regions of preferential tagRFP-T-derived fluorescence signal (0-2 µm and 8.5-12 µm). The GFP signal at the egg cell plasma membrane is not distributed homogeneously but in patches. Furthermore, the GFP signal was still visible at the fusion site during karyogamy and was not diluted throughout the complete egg plasma membrane. Interestingly, the GFP signal at the central cell membrane was not visible as strong as at the egg cell. In summary, it could be shown that

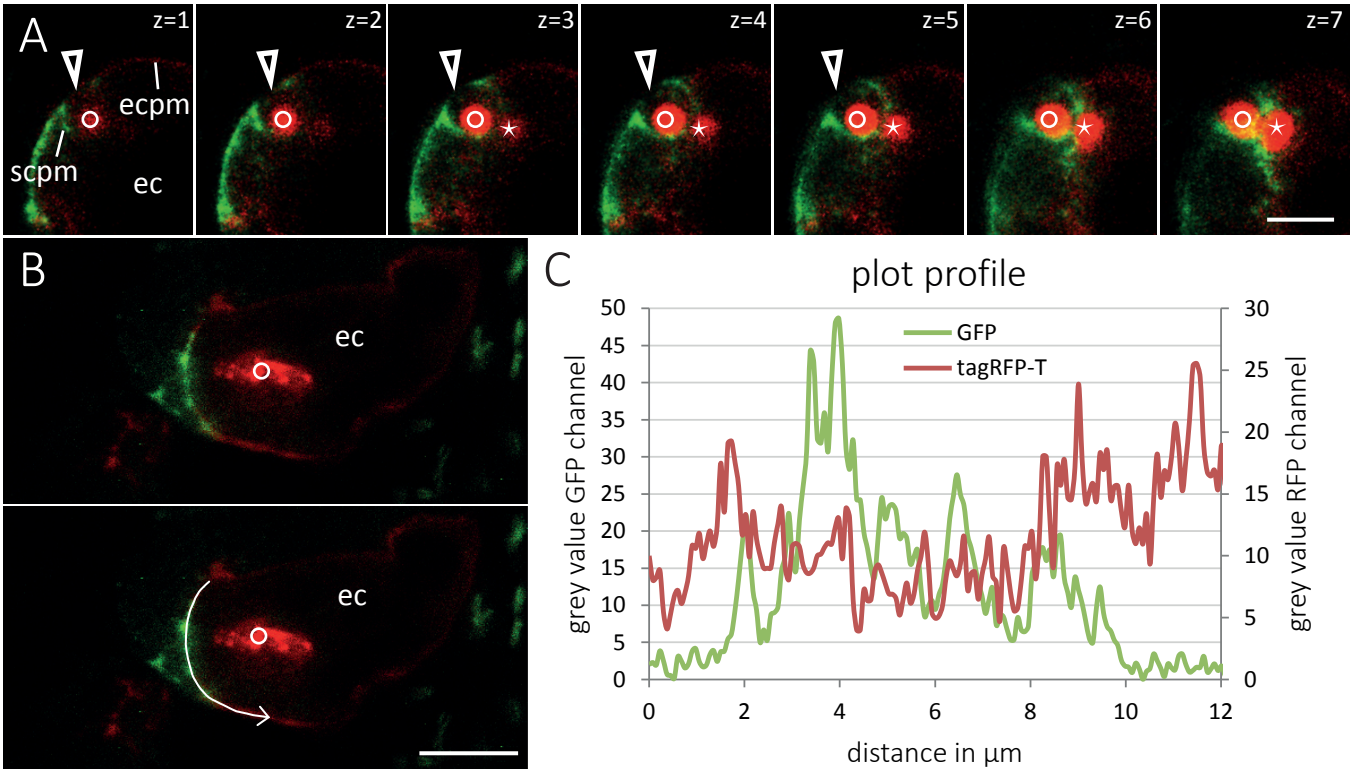

Figure 4.3 The egg-sperm fusion site during and after plasmogamy.
An egg cell of a *EC1.1p:tagRFP-T-REM*-expressing plant line is fertilized by a H33T9 sperm cell, 6-8 hap. (A) The sperm cell pair is located on top of the egg cell. The sperm cell plasma membrane merges with egg cell plasma membrane. No TET9-GFP signal of the sperm cell membrane is visible at the fusion pore (triangle). Images are individual z-slices of the same stack (stack size = 1.8 µm). The stack is shown as a maximum projection in Figure 4.2E. (B) A fertilized egg cell, shortly after karyogamy. Patches of TET9-GFP-derived fluorescence are visible in the membrane of the fertilized egg cell, highlighting the site of sperm cell entry (fusion site). Arrow in (B) shows the line drawn to create the plot profile in (C). (C) Plot profiles of the green and the red fluorescence channel were made of a single optical section. All images are single optical sections. Fluorescence of tagRFP-T and mRFP is depicted in red and GFP in green. Asterisk, second sperm cell; circle, sperm cell fusing with egg cell. Abbreviations: ec, egg cell; ecpm, egg cell plasma membrane; sc, sperm cell. Scale bars 5 µm.

the sperm membrane decorating TET9-GFP was visible at the egg cell plasma membrane after fertilisation and that no TET9-GFP signal was visible inside the egg cell. This suggests that the sperm cell plasma membrane is integrated into the egg cell plasma membrane during fertilisation.

4.1.2 Sperm cell attachment

4.1.2.1 Localisation of delivered sperm cells in the ec1-RNAi *mutant*

It is known that the EC1 protein is essential for successful fertilisation and that recombinant EC1 peptides activate endo- and exocytosis in sperm cells released from the pollen tube (Sprunck *et al.*, 2012). Whether EC1 is also necessary for the attachment of sperm cells to the female gametes and/or the physical separation of a sperm cell pair was not known. To elucidate the attachment of sperm cells, a heterozygous quintuple knockdown mutant of *EC1* (*ec1-RNAi*) was hand-pollinated with the sperm cell double marker H33T9, as no homozygous progeny can be obtained for the *ec1* triple mutant (*ec1.1/ec1.4/ec1.5*) expressing the *EC1.2/EC1.3 RNAi* construct.

50% of the egg cells in the heterozygous line *ec1-RNAi_16* are wild type for *EC1.2* and *EC1.3*, while 50% carry the *RNAi* construct and can be used in these experiments. As 6-8 hours after pollination (hap) most of the ovules are fertilised in a wild type plant, the ovules were imaged 14-16 hap to ensure imaging only *ec1-RNAi* mutant egg cells (Figure 4.4). As expected, the sperm cells were not able to fuse with the egg cells in *ec1* knockdown ovules and the red fluorescent sperm cell nuclei remained outside the female gametes. Notably, all unfused sperm cell pairs remained paired (100%; n (pairs of sperm cells)=69). The unfused sperm cell pairs remained at the fusion site in 31% of the cases (Figure 4.4, A to C). However, the majority of sperm cell pairs (69%) localised closer to the micropylar pole of the female gametophyte, away from the fusion site (Figure 4.4, D to F) suggesting that these sperm cell pairs were not attached to the female gametes.

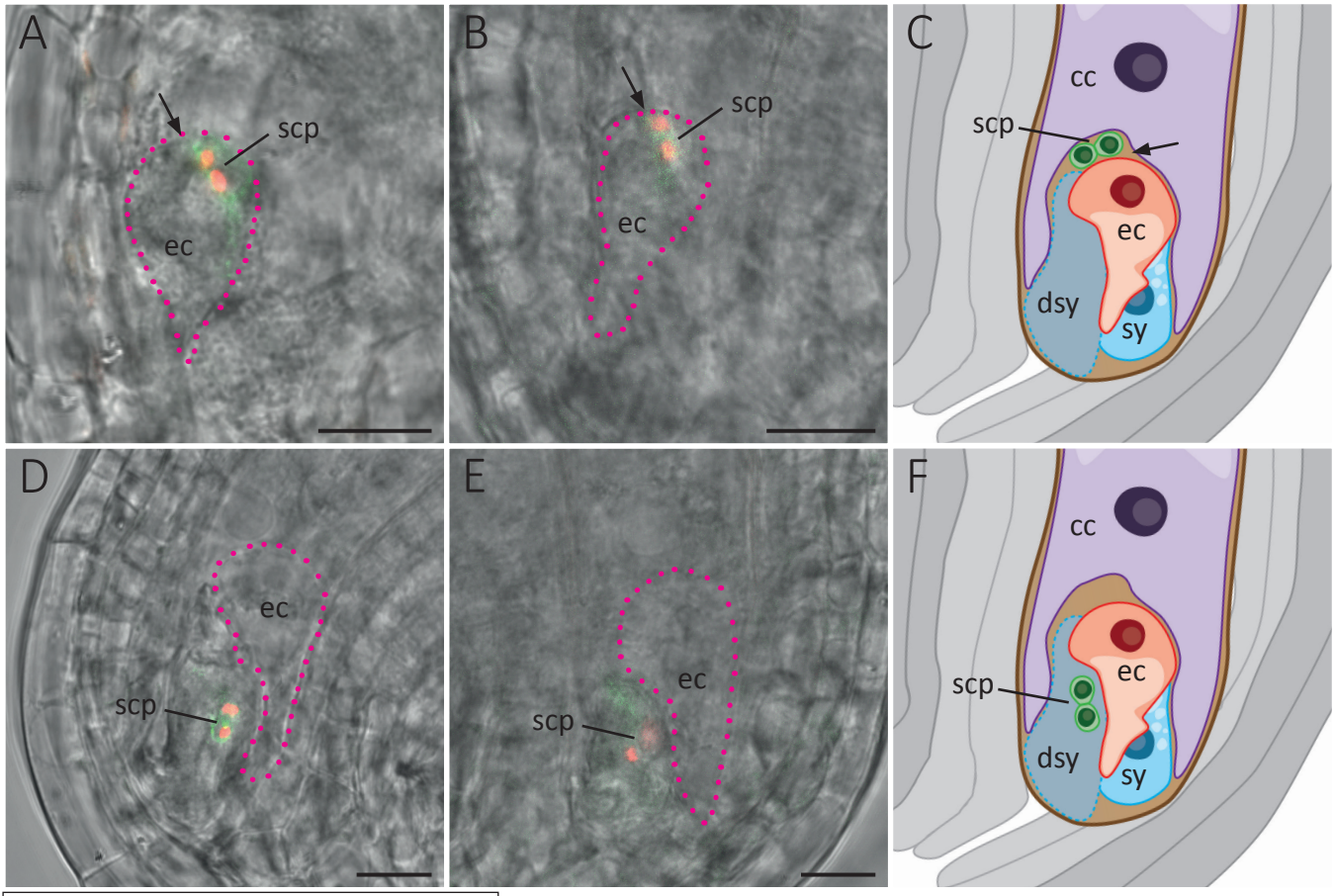

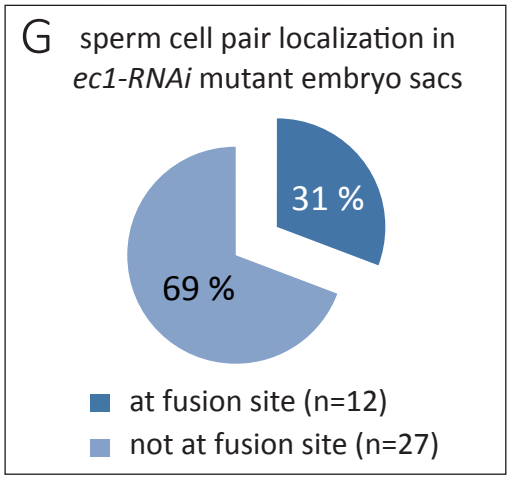

Figure 4.4 Localization of delivered H33T9 sperm cells in the female gametophytes of the *ec1-RNAi mutant*.
In CLSM studies the pistils of the quintuple knockout mutant line *ec1-RNAi*_16 were pollinated with pollen of the double marker line H33T9. Even after 14--16 hap, the sperm cell pairs are still visible, indicating that double fertilization failed. They either remain at the fusion site (arrow in A-C) or they are located closer to the micropyle (D-F). Images are optical sections with mRFP depicted in red and GFP in green. The egg cell borders are highlighted in magenta. Note that the sperm cell pairs in A and B are positioned on top of the egg cell. (G) 31% of the evaluable sperm cell pairs localised to the fusion site in *ec1-RNAi* mutant embryo sacs and 69% did not. Abbreviations: cc, central cell; dsy, degenerated synergid cell; ec, egg cell; scp, sperm cell pair; sy, synergid cell. Scale bars 10 µm.

These results suggest that the majority of sperm cells pairs fail to attach to the egg cell and the central cell when EC1 is absent. A considerable number of sperm cells (n=30) however, remained at the fusion site but with these experiments it was not possible to distinguish between attached or non-attached sperm cells.

4.1.2.2 Sperm cell pairs do not attach to the female gametes in the ec1-RNAi *knockdown line*

As it was shown in Figure 4.4, the sperm cells remained unfused and stayed paired in the embryo sac of the quintuple *ec1-RNAi* mutant knockdown. To investigate whether the sperm cell pairs are attached to the female gametes or not, a plasmolysis experiment according to Mori *et al.* (2014) was performed. In a pilot experiment, unfertilised ovules of the egg cell plasma membrane marker line *EC1.1p:tagRFP-T-REM* were plasmolysed within a solution of 1% cellulase, 0.1% pectolyase,

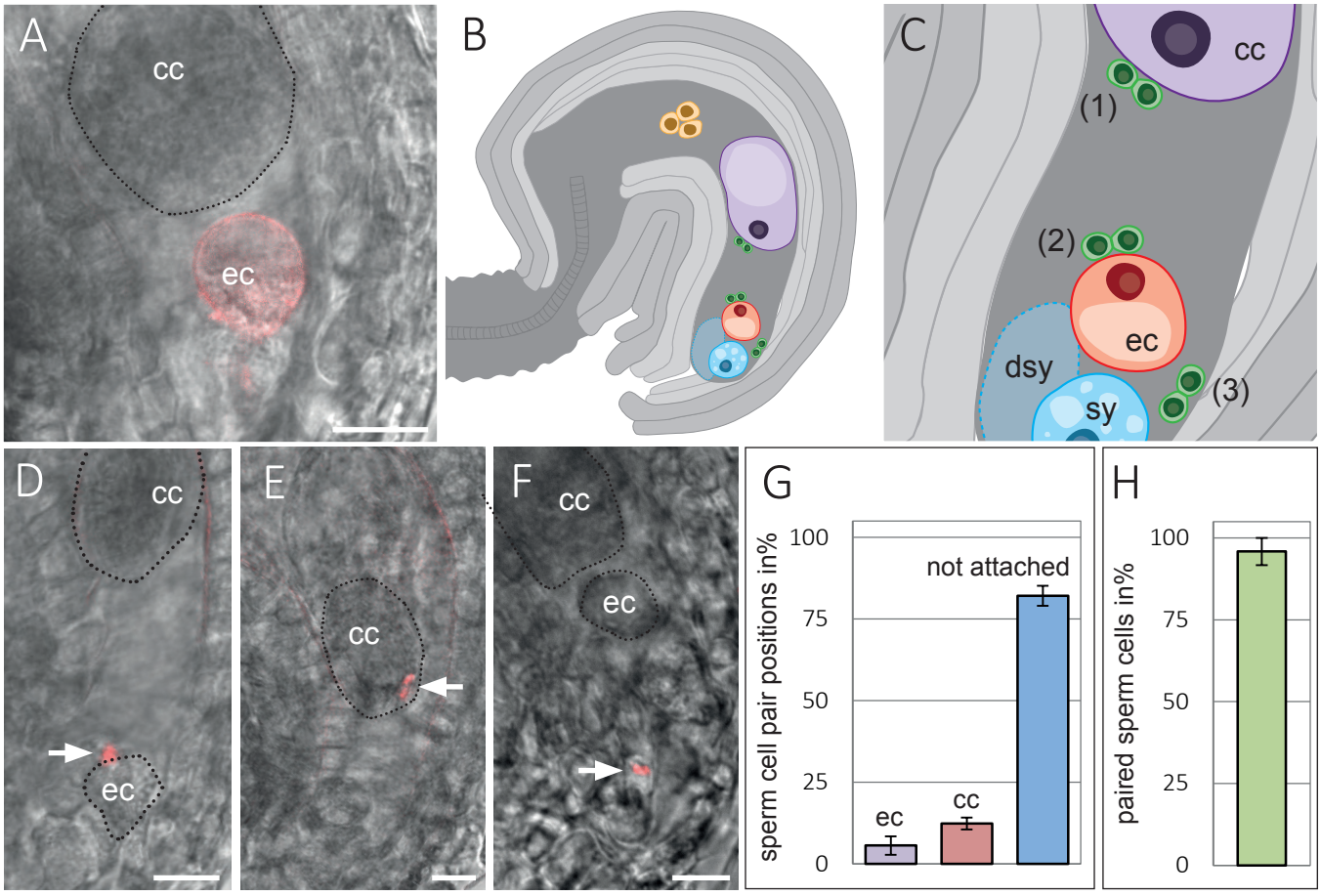

Figure 4.5 Sperm cells do neither attach to the female gametes nor do they separate in the female gametophytes of *ec1-RNAi*. Plasmolysis of wild type ovules and ovules from the *ec1-RNAi_16* line, after hand-pollination with the sperm cell nuclei marker *HTR10p:HTR10-mRFP*. (A) Plasmolysed central cell and egg cell of the marker line EC1.1p:tagRFP-T-REM, showing the egg cell plasma membrane in red and the central cell border marked with a dotted line. (B and C) Schematic representation of an ovule with plasmolysed central cell (cc), egg cell (ec) and synergid cell (sy). Possible positions of unfused sperm cell pairs ((1),(2),(3)) are shown. (D to F) Plasmolysed ovules of pollinated *ec1-RNAi_16* 14-20 hap with a pair of unfused sperm cells with red fluorescent nuclei (arrows) close to the plasmolysed egg cell (D), the central cell (E) and a pair of non-attached sperm cells (F). Positions of the sperm cell pairs (n=32) in the female gametophyte of *ec1-RNAi* 14-16 hap (G) and their percentage of paired sperm cells (H). Mean values (±SEM) of three experiments with ≥ 8 sperm cell pairs each are shown. Images are single confocal planes with mRFP depicted in red. Arrows label sperm cell pairs. Abbreviations: cc, central cell; dsy, degenerated synergid cell; ec, egg cell; sy, synergid cell. Scale bars 10 µm.

1 M sucrose and 50 mM MES, pH 5.8. After 60 min, the ovules were transferred to phosphate buffer and were imaged. The cells of the embryo sac did undergo sufficient plasmolysis to be clearly distinguishable from each other as single cells and they exhibited the typical round shape of protoplasts (Figure 4.5, A).

Then, mature emasculated pistils (flower stage 12 according to Smyth *et al.* (1990)) of the quintuple knockdown line *ec1-RNAi_16* were hand-pollinated with the sperm cell double marker H33T9 and plasmolysed for 60 min 14-20 hap. The sperm cell pairs (n=32) were detected at three distinct positions in the embryo sac (Figure 4.5, B to F). 18% of the sperm cell pairs were attached to the central cell (1) or the egg cell (2) whereas 82% (SEM±3.1) were non-attached but could be detected at different positions in the micropylar region of the embryo sac (3). Furthermore, the sperm cells appeared as a pair in 96% (SEM±4.2) of all analysed ovules of the *ec1-RNAi* mutant, as the red fluorescence marking both sperm cell nuclei was visible in close proximity.

Taken together, the unfused sperm cells stayed as a pair in the *ec1-RNAi* mutant and the vast majority of sperm cells were attached to neither the egg cell nor the central cell. Therefore, the results shown so far indicate that EC1 proteins are responsible for both sperm cell adhesion and sperm cell activation.

4.2 Egg and sperm cell activation

4.2.1 EC1 induces changes in TET9-GFP labelled sperm cell membranes

EC1 genes and especially the two EC1 signature motifs S1 and S2 (Figure 4.6, A) are conserved in the genomes of angiosperms and synthetic peptides, covering the signature motifs, promote sperm cell activation in *A. thaliana* (Sprunck *et al.*, 2012). In these analyses, the fusogen HAP2-YFP was relocated from the endomembrane system to the plasma membrane in released sperm cells treated with the synthetic S1 and S2 peptides.

As shown in chapter 4.1.2 the sperm cells stayed unpaired in the female gametophyte of the *ec1-RNAi* mutant. Therefore, possible effects of the synthetic EC1.1 signature motif peptides were tested according to their capability to unpair sperm cells. Released sperm cells were treated with synthetic carboxytetramethylrhodamine (TAMRA) labelled EC1.1 peptides. A pilot experiment indicated that the synthetic TAMRA-S2 peptide is more active than the synthetic TAMRA-S1 peptide (data not shown). Therefore only TAMRA-S2 was used in the following experiments.

The stigma of wild type pistils was hand-pollinated with pollen expressing *HTR10p:TET9-GFP* and put on solid pollen germination media (PGM) for 2 h at RT for the pollen to germinate. They were transferred to liquid PGM for the pollen tubes to grow through the stigma (*semi-in vivo*) into the liquid for 2 h and then transferred to a microscopy slide with 100 mM sodium phosphate buffer, pH 7.5 containing the TAMRA-labelled EC1 peptide S2 or DMSO control. The pollen tubes were sliced crosswise releasing the sperm cells into the buffer. The sperm cell pairs were then imaged with a confocal fluorescence microscope. Figure 4.6, B shows a released sperm cell pair with the highest signal intensity of TET9-GFP, depicted in intensity false colour image in red, at the connection of the two sperm cells (arrow) after control treatment with DMSO. After treatment with TAMRA-S2, the GFP signal was more evenly distributed all over the sperm cell plasma membrane and a clear separation of the two sperm cells was visible (Figure 4.6, C). In at least three independent experiments with ≥10 released sperm cell pairs each, the TET9-GFP-derived signal intensities at the membrane connection of the sperm cell pairs were quantified. When the highest intensity of the GFP-signal was detected continuously between the two sperm cells, this situation was defined as “connected” membranes (Figure 4.6, D). The released sperm cell pairs treated with TAMRA-S2 showed a highly significant ($p \leq 0.001$, independent t-test) lower percentage of connected membranes (46%, ±2.6) than the released sperm cell pairs with the control treatment (86%, ±4.0). For comparison, 100% (n=16) of the sperm cells in *in vitro* growing pollen tubes did show high signal intensities of TET9-GFP at the sperm cell connection (Figure 4.6, E).

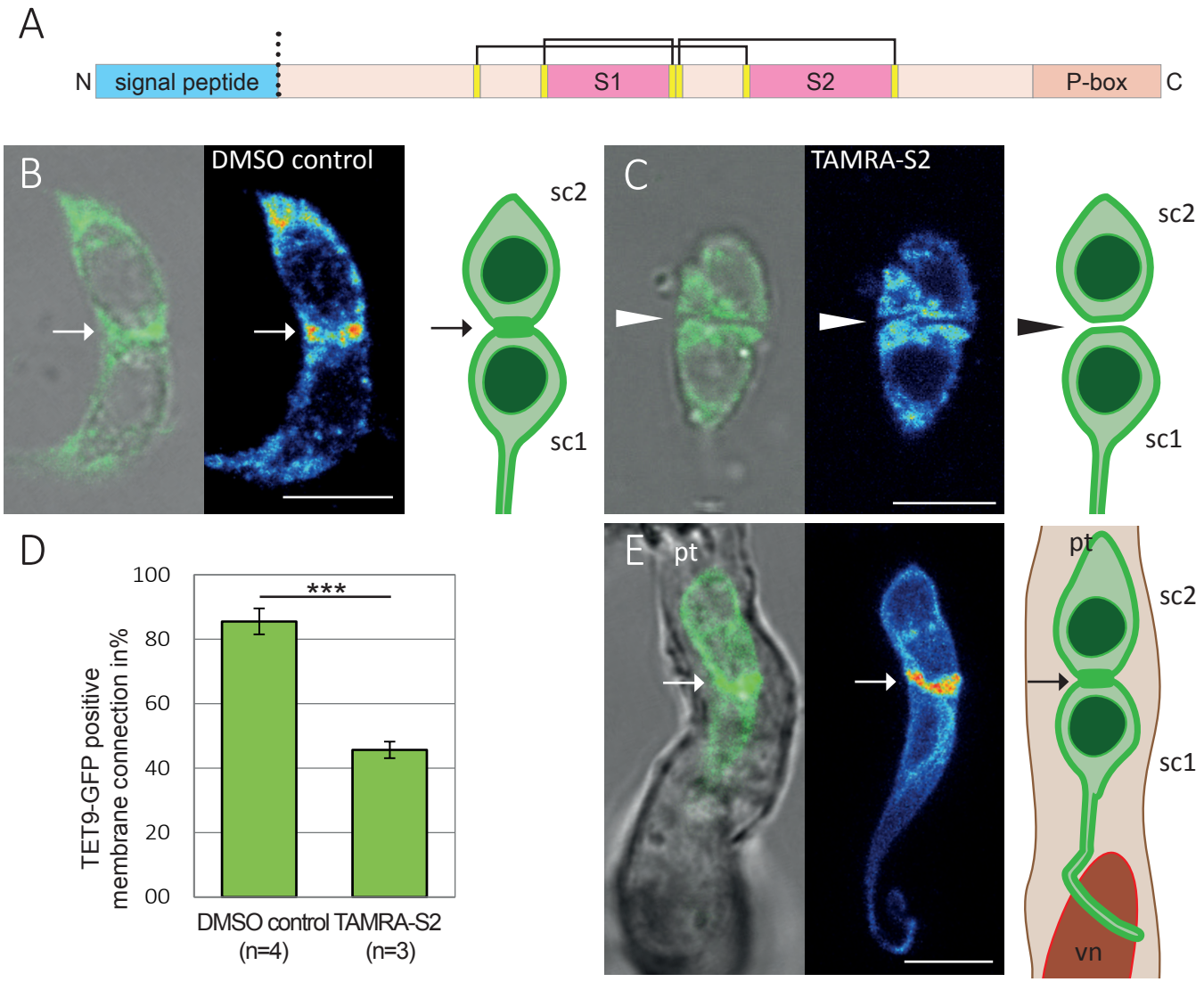

Figure 4.6 EC1 induces changes in TET9-GFP labelled sperm cell membranes.
(A) Predicted structure of the EC1.1 protein from *A. thaliana* with an N-terminal secretion signal, cleavage site (dotted line), six cysteines (yellow) forming three disulfide bonds, two highly conserved signature motifs (S1 and S2) and an C-terminal prolin rich domain (P-box) (Sprunck *et al.*, 2014). (B and C) Sperm cells of *HTR10p:TET9-GFP,* released from the pollen tube, shown as bright field image merged with GFP signal in green, maximum projection intensity false color image (blue to red) and a schematic representation. (B) Released sperm cell pair with the highest signal intensity at the membrane connection (arrow) of sperm cells after control treatment with DMSO. (C) Released sperm cell pair with a gap lacking TET9-GFP fluorescence in the sperm cell plasma membranes (arrowhead) after the treatment with the EC1.1 peptide TAMRA-S2, a TAMRA labelled version of a synthetic S2 peptide, covering the conserved S2 signature motif of EC1.1. (D) Quantitative assessment of TET9-GFP-positive membrane connections in sperm cell pairs treated with TAMRA-S2 and the control (DMSO). Mean values (±SEM) of independent experiments with ≥10 sperm cell pairs each are shown, $p<0.001$. (E) Sperm cells in in-vitro germinated pollen tube with the highest TET9-GFP signal intensity at the membrane connection (arrow) between the two sperm cells. Abbreviations: sc1, sperm cell 1; sc2, sperm cell 2; pt, pollen tube; vn, pollen vegetative cell nucleus of the pt. Scale bars 5 μm.

In summary, the released sperm cell pairs of *semi-in vivo* grown pollen tubes show a high accumulation of TET9-GFP derived fluorescence where the two sperm cells are connected to each other and this fluorescent signal was significantly reduced after treatment with the synthetic EC1.1 peptide S2. The lack of TET9-GFP signal between the sperm cell pair was considered as an indication that the sperm cell pair started to physically separate. The results therefore suggest that EC1 is also necessary to unpair the sperm cells.

4.2.2 Physiological studies on the plasma membranes of the male germ unit to find the target membrane for EC1

It was suggested that regulated secretion of EC1 by the egg cell upon sperm-egg interaction ensures the appropriate localisation of the cell-fusion machinery in distinct sperm membrane domains (Sprunck *et al.*, 2012). Released sperm cells from *semi-in vivo* grown pollen tubes expressing the fusogen HAP2-YFP fusion protein were treated with an EC1 peptide mix containing synthetized peptides of the conserved signature motifs S1 and S2. Compared to the control treatments with either a mixture of two scrambled peptides, based on the same amino acids, or a peptide-free solution, the HAP2-YFP derived fluorescence signal shifted significantly from the endomembrane system towards the sperm plasma membrane. However, it remained to be investigated whether the sperm cell plasma membrane is the direct target of EC1 proteins or whether EC1 proteins act on the vegetative membrane enclosing the two sperm cells.

The male germ unit consists of the two sperm cells that are connected to each other and the vegetative cell nucleus. The male germ unit is formed by a membrane extension linking one sperm cell with the vegetative cell nucleus (Figure 4.7, A). Furthermore, the sperm cells are enclosed by a membrane of the vegetative cell, the pollen tube. To visualise both types of membranes, the sperm cell membranes and the vegetative cell membrane, the styryl dye FM™ 4-64 was added at a concentration of 5 µg/ml after sperm cell release from the growing pollen tube. As shown in

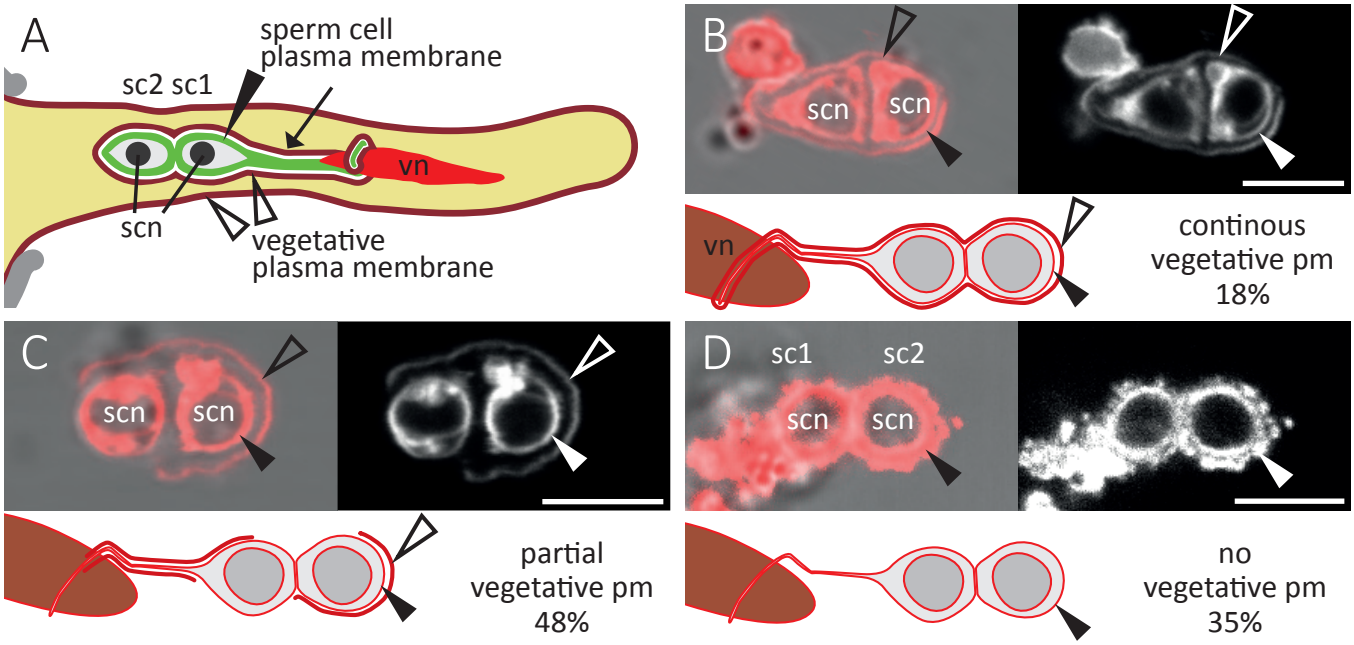

Figure 4.7 The pollen vegetative cell membrane of the male germ unit is ruptured after sperm cell release.
(A) Schematic diagram of a growing PT with the male germ unit (MGU) consisting of two sperm cells (sc1 and sc2) and the pollen vegetative cell nucleus (vn). The sperm cells are enclosed by the membrane of the pollen vegetative cell and the leading sperm cell is physically associated with the pollen vegetative cell nucleus by a membrane projection (arrow). (B-D) Membranes of released sperm cell pairs stained with FM4-64 (n=124). 18% of the sperm cell pairs showed a continous pollen vegetative cell membrane (B), 47% showed a partial pollen vegetative cell membrane (C) and 37% of released sperm cell pairs showed no pollen vegetative cell membrane (D). Arrow, membrane projection; open triangle, vegetative plasma membrane; triangle, sperm cell plasma membrane. Abbreviations: sc1, sperm cell 1; sc2, sperm cell 2; scn, sperm cell nucleus; vn, pollen vegetative cell nucleus. Scale bars 5 µm.

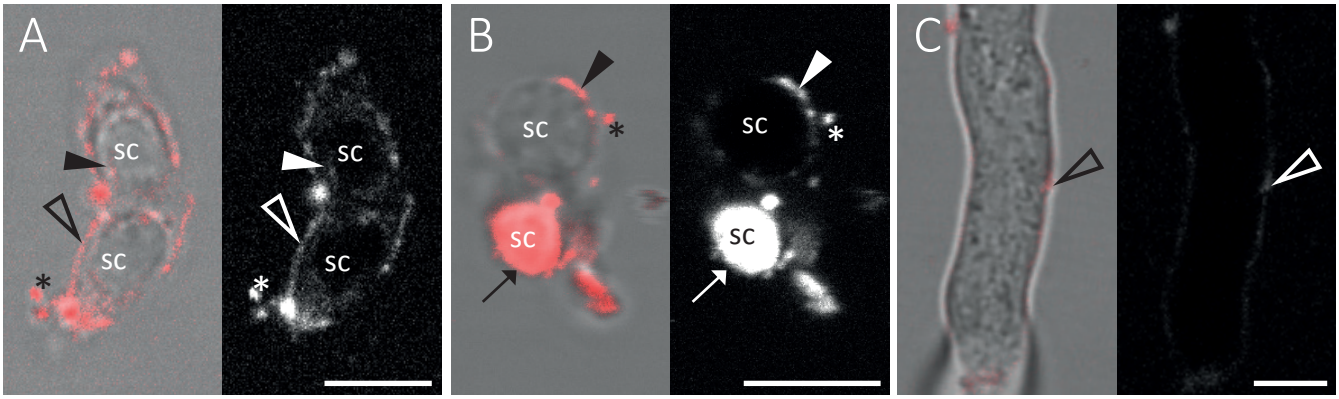

Figure 4.8 TAMRA-S2 peptide associates to membranes of male germ unit.
Single confocal plains of released sperm cells incubated in PGM with TAMRA-S2 peptide. (A) Released sperm cell pair with TAMRA-S2 peptide, which associats with the pollen vegetative cell plasma membrane (open triangle) and the sperm cell plasma membrane (triangle). (B) Released sperm cell pair with TAMRA-S2 peptide associated with the sperm cell plasma membrane (triangle) and strongly sticking to a degenerated sperm cell (arrow). (C) In-vitro germinated pollen tube with traces of TAMRA-S2 associated to the pollen tube cell wall. Arrow, degenerated sperm cell; asterisk, membrane fractions outside of the sperm cells; open triangle, vegetative cell plasma membrane; triangle, sperm cell plasma membrane. Abbreviation: sc, sperm cell. Scale bars 5 µm.

Figure 4.7, both plasma membranes and the endomembrane system of the sperm cell pairs were stained with FM™ 4-64 and analysed 10-60 min after sperm cell release. Out of 124 sperm cell pairs, 18% had a continuous and intact vegetative membrane enclosing the sperm cell pair (open triangle) and 48% had a ruptured or only partial visible vegetative membrane. In 35%, the vegetative cell membrane was not detectable by FM™ 4-64, suggesting the membrane got completely stripped off. Assuming that *in vivo*, a large part of sperm cell pairs do not have a continuous vegetative membrane at pollen tube burst and sperm cell release, the main target membrane for EC1 proteins is very likely the sperm cell membrane. Further, the sperm cell connection was not stained by FM™ 4-64 and a gap was visible between the sperm cells.

To visualise a possible direct interaction of EC1 peptides with the sperm cell membrane, a TAMRA-labelled version of the S2 peptide was added to released sperm cells. The TAMRA-S2 peptide associated not only with the sperm cell membrane, but also with the vegetative membrane of the male germ unit (Figure 4.8, A and B). Additionally, it decorated degenerated sperm cells (B) and the cell wall of pollen tubes (C). This suggests the sperm cell plasma membrane to be a direct target or to host an interaction partner for the EC1 protein.

4.2.3 Cyclic nucleotides may play a role in sperm cell activation

Cyclic nucleotide-gated channels (CNGCs) play several roles in plant signalling and mediate Ca^{2+} signalling in response to diverse stimuli (DeFalco *et al.,* 2016). The *A. thaliana* genome encodes for 20 CNGCs, but little is known about their function during reproduction. Array-based expression data showed that in sperm cells *CNGC9* and *CNGC10* are the most highly expressed *CNGCs* (Borges *et al.,* 2008).

To verify *CNGC9* and *CNGC10* expression in *Arabidopsis* sperm cells, the promoter activity of both genes was investigated by generating transgenic plants expressing a reporter under control of 995 bp 5' upstream of *CNGC9* and1449 bp 5' upstream of *CNGC10*, respectively. Promoter reporter constructs were cloned using a fusion protein of three GFP molecules with an N-terminal nuclear localisation sequence (NLS) as a reporter. Plants expressing CNGC9p:NLS3xGFP or CNGC10p:NLS3xGFP showed GFP signals in the sperm cell nuclei (Figure 4.9). The promoters of both *CNGCs* are thus active in sperm cells. Taken together with published expression data, it can be assumed that cyclic nucleotides may play a role in signalling during sperm cell activation.

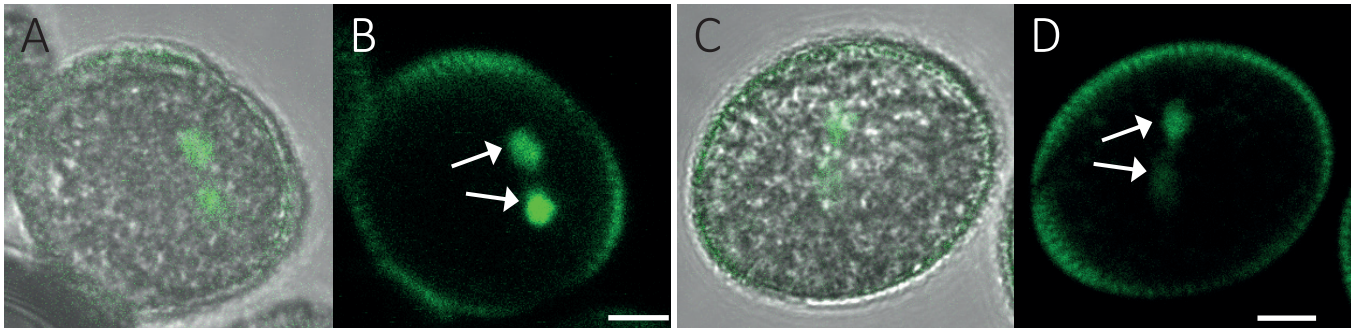

Figure 4.9 *CNGC9* and *CNGC10* promoters are active in the sperm cells.
(A and B) Pollen grains from the promoter reporter line CNGC9p:NLS3xGFP_1 show GFP signals in the sperm cell nuclei (arrows). (C and D) Pollen grains from the promoter reporter line CNGC10p:NLS3xGFP_10 show GFP signals in the sperm cell nuclei (arrows). (A and C) show single confocal plains and (B and D) show average intensity projections. Scale bars 5 µm.

The second messenger cyclic guanosine monophosphate (cGMP) is a key signalling molecule that mediates many physiological and developmental processes in plants (Marondedze *et al.,* 2016). Therefore, the effects of cGMP on released sperm cells were tested under identical conditions as described for the EC1.1 peptides S1 and S2 in Sprunck *et al.* (2012). As cGMP hardly crosses membranes, two derivatives were used. According to manufacturer's technical specifications, cGMP has a lipophilicity of 0.77, which is relatively low compared to the high membrane-permeable 8-Br-cGMP that has a lipophilicity of 1.77 and to 8-pCPT-cGMP with a lipophilicity of 2.52 and excellent membrane permeability (Figure 4.10, A). Released sperm cells were incubated in PGM containing or lacking cGMP derivates and imaged under a confocal microscope. Then, the proportion of sperm cells showing HAP2-YFP signal in the sperm cell plasma membrane was calculated. When 8-Br-cGMP was added to released sperm cells at a concentration of 50 mM,

45% (85 sperm cells analysed; n=2) of sperm cells showed HAP2-YFP localisation at the plasma membrane (Figure 4.10, B and C). The effect of 8-pCPT-cGMP was stronger: 69% of all sperm cells showed HAP2-YFP in the sperm cell plasma membrane at a concentration of 100 µM (89 sperm cells analysed; n=2) and 55% at a concentration of 1 mM (107 sperm cells analysed, n=2). When a control solution without cGMP was used, HAP2-YFP was detected at the plasma membrane in 32% of all sperm cells (167 sperm cells analysed; n=5; Figure 4.10, D), which is close to 28% sperm cells with HAP2-YFP signals at their plasma membrane in *in vitro* grown pollen tubes (193 sperm cells analysed; n=6; Figure 4.10, E).

These results suggest that the cGMP signalling pathway is involved in sperm cell activation as the detection of the fusogen HAP2-YFP in the plasma membrane of the sperm cells increases, compared with the controls, when treated with 100 µM 8-pCPT-cGMP. However, more experiments should be performed and different concentration of 8-pCPT-cGMP should be applied to be able to verify the sperm cell activation effect by statistical analysis.

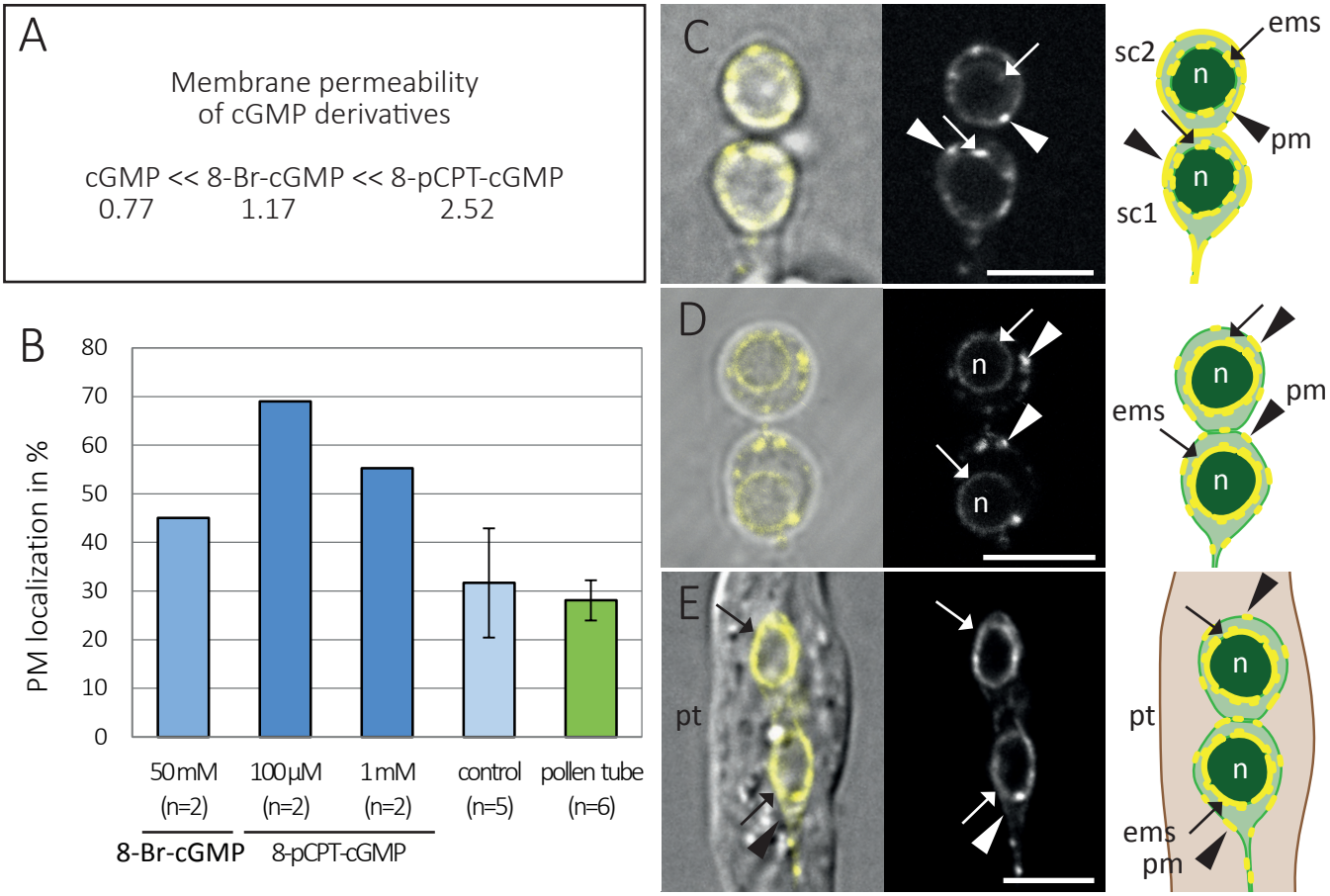

Figure 4.10 8-pCPT-cGMP activates sperm cells.
(A) Membrane permeability of cGMP derivatives displayed as lipophilicity according to manufacturers (BIOLOG) information. (B) Quantitative assessment of HAP2-YFP localization at plasma membranes of 8-Br-cGMP and 8–pCPT–cGMP-treated sperm cells compared to a cGMP-free solution and sperm cells in in-vitro grown pollen tubes. Each independent experiment included ≥20 sperm cells. Mean values (±SEM) of at least three independent experiments are shown. (C-E) Single confocal planes of HAP2-YFP expressing sperm cells and corresponding drawings. (C) HAP2-YFP localization at the plasma membrane (pm, arrowhead) of a released sperm cell pair in PGM with 25 mM 8-Br-cGMP. (D) HAP2-YFP localization in the endomembrane system (ems, arrow) of a released sperm cell pair in PGM control. (E) HAP2-YFP localization in the endomembrane system of an *in-vitro* growing pollen tube (pt). Arrow, endomembrane sytem of sperm cells; arrowhead, sperm cell plasma membrane. Abbreviations: ems, endomembrane system; n, sperm cells nucleus, pm, plasma membrane; sc1, sperm cell 1; sc2, sperm cell 2; pt, pollen tube. Scale bars 5 µm.

4.2.4 Physiological studies on egg cell activation

4.2.4.1 Subcellular localisation of EC1 in Nicotiana benthamiana *leaf epidermis cells*

In *A. thaliana* wild type plants, EC1 is exclusively expressed in egg cells and localised to vesicle-like structures. To further determine the shape and localisation of these structures, the EC1.1-GFP fusion protein was transiently expressed in leaf epidermis cells of *Nicotiana benthamiana* under the ubiquitously active *Cauliflower Mosaic Virus 35S* (*35S*) promoter (*35Sp:EC1.1-GFP*). EC1.1-GFP was localised in vesicle-like structures, further referred to as EC1-labelled bodies, in the cytoplasm. In a previous study it was shown that these EC1-labelled bodies neither co-localised with fluorescent markers for peroxisomes nor with the endoplasmic reticulum (ER; Kraus 2015). However, indications for a co-occurrence of these bodies with the ER were given and co-expression studies with markers of Golgi bodies (*cis*-Golgi) revealed partial co-localisation. Figure 4.11 shows confocal images (imaged by Michael Kraus) of tobacco leaf epidermis cells with fluorescent *cis*-Golgi bodies marked in magenta (magenta arrow; G-rb, *CD3-968*; Nelson *et al.*, 2007) co-expressing with EC1.1-GFP marked in cyan. The CLSM images were analysed in more detail and revealed that EC1-labelled bodies appear not only as single dots (cyan arrow in A), but are in most of the cases

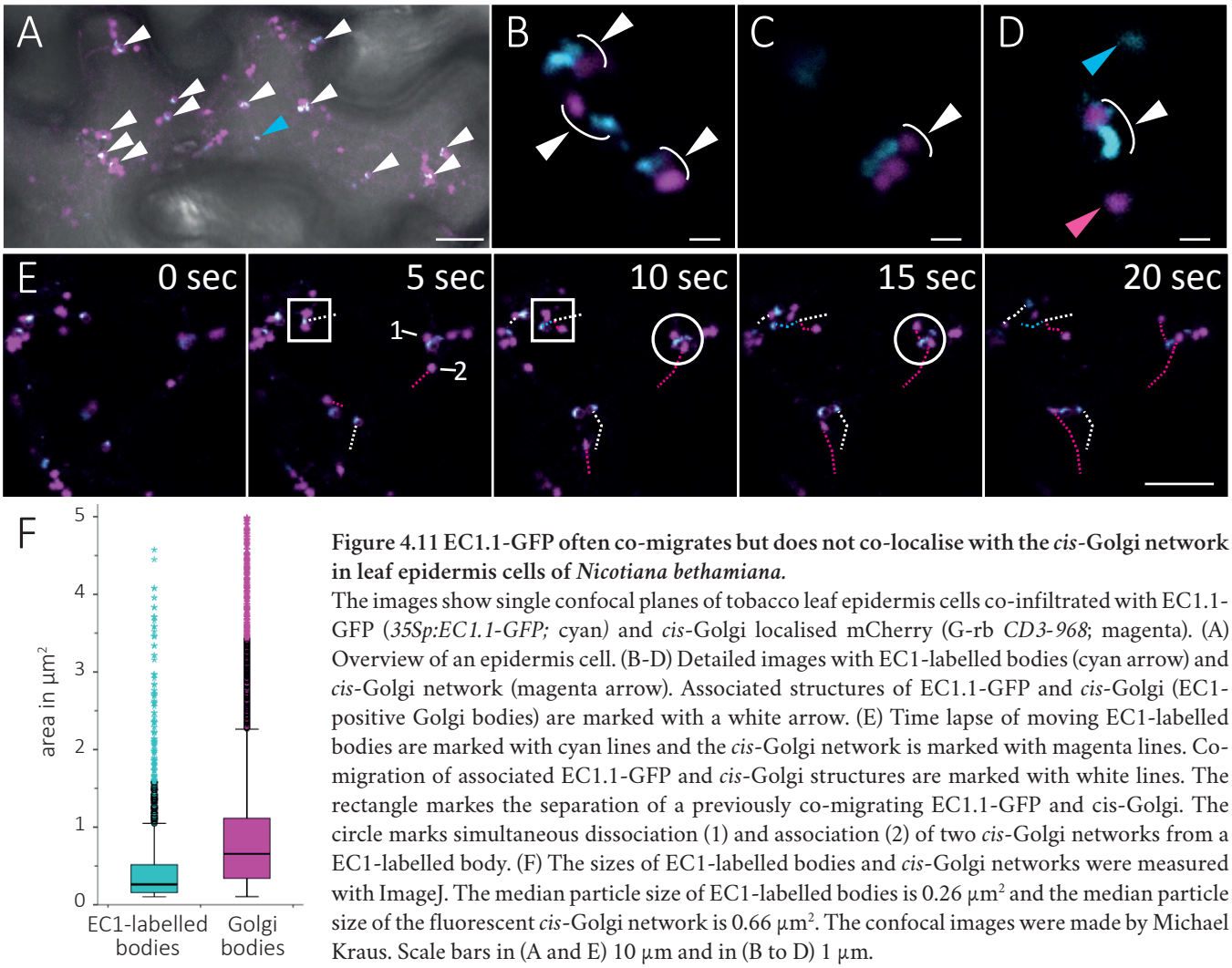

Figure 4.11 EC1.1-GFP often co-migrates but does not co-localise with the *cis*-Golgi network in leaf epidermis cells of *Nicotiana bethamiana*.
The images show single confocal planes of tobacco leaf epidermis cells co-infiltrated with EC1.1-GFP (*35Sp:EC1.1-GFP;* cyan) and *cis*-Golgi localised mCherry (G-rb *CD3-968*; magenta). (A) Overview of an epidermis cell. (B-D) Detailed images with EC1-labelled bodies (cyan arrow) and *cis*-Golgi network (magenta arrow). Associated structures of EC1.1-GFP and *cis*-Golgi (EC1-positive Golgi bodies) are marked with a white arrow. (E) Time lapse of moving EC1-labelled bodies are marked with cyan lines and the *cis*-Golgi network is marked with magenta lines. Co-migration of associated EC1.1-GFP and *cis*-Golgi structures are marked with white lines. The rectangle markes the separation of a previously co-migrating EC1.1-GFP and cis-Golgi. The circle marks simultaneous dissociation (1) and association (2) of two *cis*-Golgi networks from a EC1-labelled body. (F) The sizes of EC1-labelled bodies and *cis*-Golgi networks were measured with ImageJ. The median particle size of EC1-labelled bodies is 0.26 µm² and the median particle size of the fluorescent *cis*-Golgi network is 0.66 µm². The confocal images were made by Michael Kraus. Scale bars in (A and E) 10 µm and in (B to D) 1 µm.

associated to, but not overlapping with, the *cis*-Golgi (white arrows). These composite structures were referred to as EC1-positive Golgi-bodies.

In time lapse images (Figure 4.11, E), the parallel movement of EC1.1-GFP-labelled bodies and Golgi-bodies could be followed (white lines). Manual tracking of EC1-positive Golgi-bodies with ImageJ revealed a velocity of about 0.15 µm/sec (SEM=0.062; n=15). Furthermore, the image 4.11E also shows the separation of an EC1-positive Golgi-body between the time points 5 and 10 seconds (rectangle), where an EC1.1-GFP-labelled body moved into a different direction (cyan line) than the *cis*-Golgi (magenta line). Additionally, an EC1.1-GFP-labelled body, associated to one *cis*-Golgi body, was transferred to become associated to another *cis*-Golgi. Between the time points 5 and 15 seconds (circle), a *cis*-Golgi body (Number 1) dissociated from, while another *cis*-Golgi body (number 2) associated with the EC1.1-GFP-labelled body.

For particle analysis with ImageJ, fluorescence images of both fluorescence channels (GFP and mCherry) were processed separately to binary images using the RenyiEntropy method followed by a watershed algorithm to separate touching particles. In the analysis, it was not distinguished between single or associated EC1.1-GFP-labelled bodies and *cis*-Golgi bodies. EC1.1-GFP-labelled bodies with a median area of 0.26 μm^2 were comparably smaller than *cis*-Golgi bodies with a median area of 0.66 μm^2 (Figure 4.11). As EC1-labelled bodies showed no direct overlay with the *cis*-Golgi, it is hypothesized that EC1.1-GFP proteins accumulate at the *trans*-face of the Golgi stack or at the *trans*-Golgi network, the organelle responsible for sorting secretory pathway proteins to their final destinations.

4.2.4.2 Calcium ionophores cannot stimulate EC1 secretion in Arabidopsis thaliana

In *A. thaliana,* EC1 is secreted during double fertilisation (Sprunck *et al.*, 2012), but the trigger for this secretion is not known yet. As intracellular Ca^{2+} spiking was found to play an important role during double fertilisation, it was suggested that Ca^{2+} may be involved in egg cell activation (Denninger *et al.*, 2014). Therefore, several different Ca^{2+} ionophores were tested upon their effect on egg cell activation.

Ovules from homozygous plants expressing *EC1.1p:EC1.1-GFP* were used to monitor EC1-GFP secretion from egg cells. In mature egg cells, the fusion protein EC1.1-GFP is localised to vesicle-like structures in the cytoplasm (Figure 4.12, A and B, arrows). As shown in Figure 4.12, C and D, the fluorescence of the fusion protein EC1.1-GFP was visible extracellularly (arrowheads) after gamete fusion. The sperm cell nuclei (asterisks), marked with HTR10-mRFP, were incorporated by the egg cell. The activated egg cells expressing EC1.1-GFP can be recognized by extracellular GFP signal. Therefore, ovules were dissected and incubated in 100 mM phosphate buffer pH 7.5 containing 1% DMSO as a control and additional 100 µM ionomycin calcium salt, 100 µM A23187

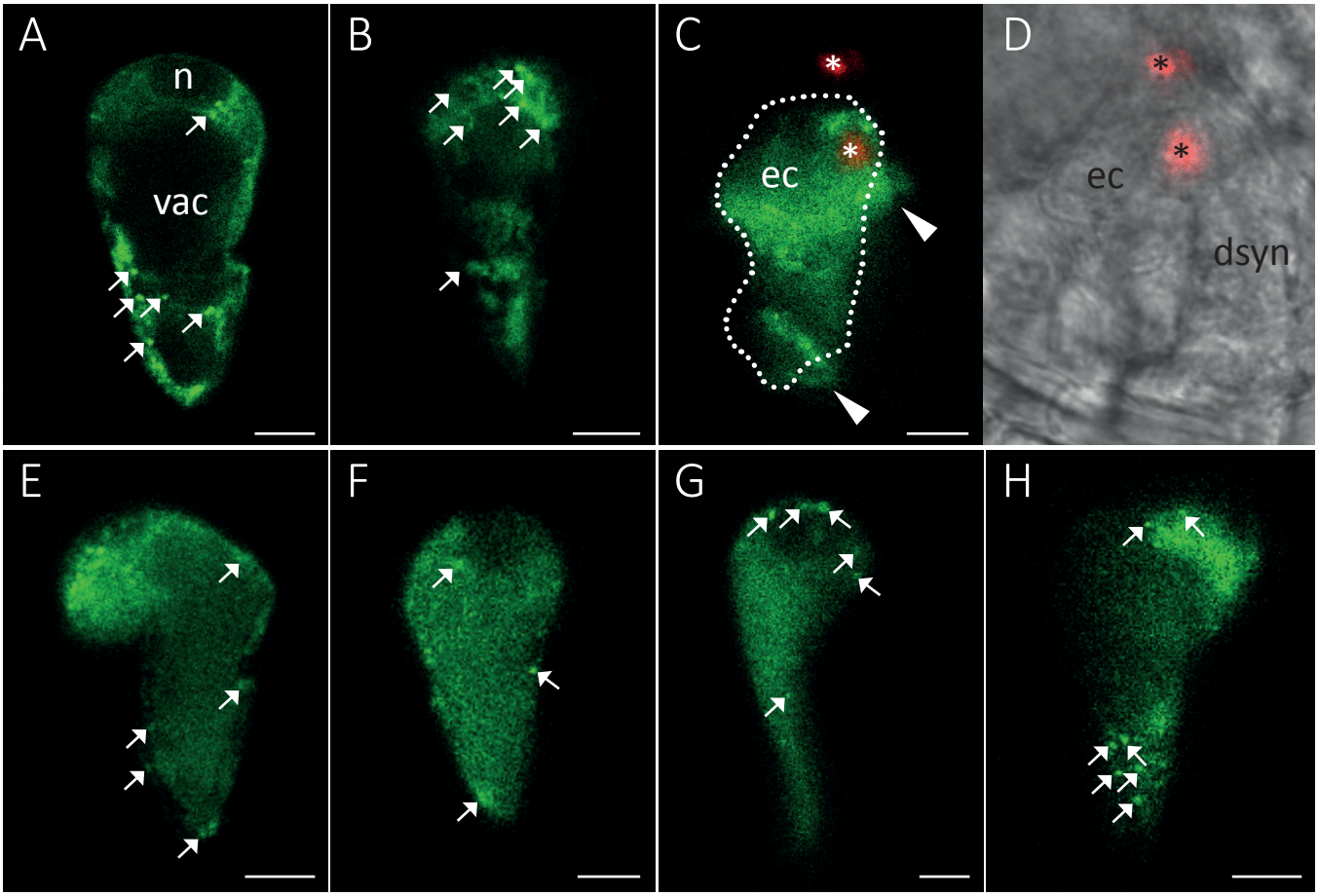

Figure 4.12 EC1.1-GFP protein localization in ionophore treated ovules.
The images show single confocal planes of ovules from *EC1.1p:EC1.1-GFP*-expressing plants. The fluorescence of the fusion protein EC1.1-GFP in egg cells is depicted in green. The preprarations were made in 100 mM sodium phosphate buffer pH 7.5. (A and B) EC1.1-GFP is expressed in egg cells and localised in vesicle like structures (arrows). (C and D) Pistils were hand-pollinated with *HTR10p:HTR10-mRFP*-expressing pollen. 6-8 hap sperm cells, sperm cell nuclei depicted in red, fuse with the egg cells. The EC1.1-GFP fusion protein is more evenly distributed in the egg cell and additionally localised outside the egg cell. (E-H) Ovules incubated in 1% DMSO (E), 1% DMSO + 100 µM ionomycin calcium salt (F), 1% DMSO + 100 µM A23187 (G), 1% DMSO + 100 µM A23187 hemicalcium salt (H) for 30-60 min. The EC1.1-GFP derived signal was only detected inside the egg cells. Abbreviations: n, egg cell nucleus; vac, egg cell vacuole; ec, egg cell; dsyn, degenerated synergid cell. Scale bars 5 µm.

or 100 µM A23187 hemi-calcium salt for 30-60 min before imaging (Figure 4.12, E to H). The egg cells showed neither a secretion of EC1.1-GFP nor obvious differences in protein localisation (n=41), suggesting that the application of calcium ionophores does not trigger EC1 secretion.

In summary, egg cell activation of *A. thaliana* could not be stimulated by calcium ionophores, while the sperm cells were activated by application of cGMP derivates. Furthermore, the synthetic EC1.1 peptide S2 induced endocytosis in TET9-GFP labelled sperm cell plasma membranes. Moreover, ectopic expression of EC1.1-GFP in tobacco leaf epidermis cells suggests that the fusion protein mainly accumulates at the *trans*-Golgi network in these cells.

4.3 Ectopic expression of EC1 in the female gametophyte

4.3.1 EC1.1-GFP is ectopically expressed in all cells of the female gametophyte

Rademacher (2011) described that transgenic *A. thaliana* plants with the expression construct *35Sp:EC1.1-GFP* do not show detectable fluorescence expression of the fusion protein despite the presence of transcript. As seedlings grown on solid MS media containing the proteasome inhibitor MG132 did show EC1.1-GFP expression, it was hypothesized that the misexpressed EC1.1-GFP fusion protein is immediately degraded after translation. Hence, compared to *Nicotiana benthamiana, A. thaliana* is not able to express functional EC1.1 in vegetative tissues.

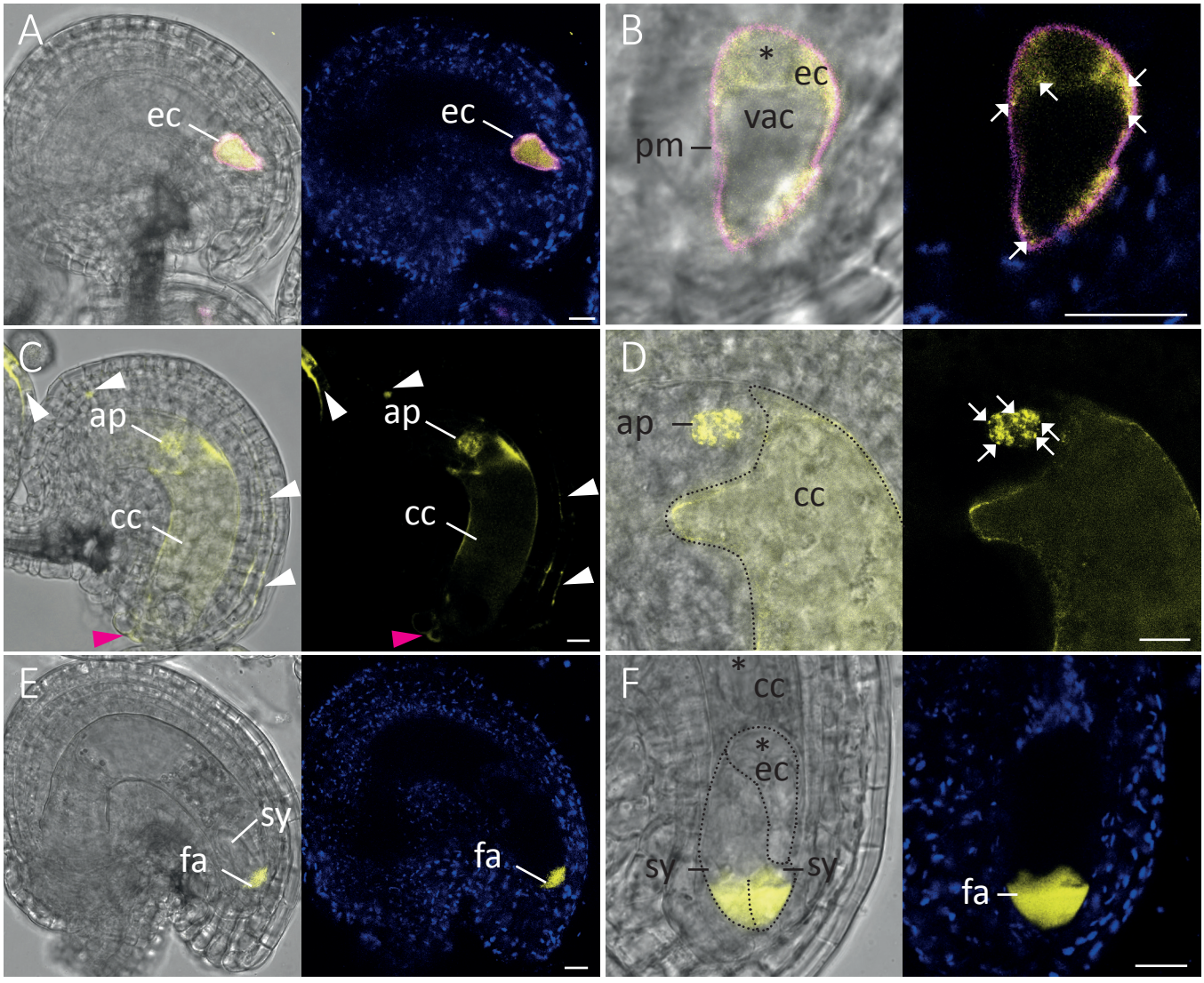

Figure 4.13 Ectopic expression of EC1.1-GFP in the cells of the female gametophyte.
(A and B) Ovules from the double homozygous line *EC1.1p:EC1.1-GFP*; *EC1.1p:tagRFP-T-REM,* showing fluorescence of the fusion protein EC1.1-GFP in yellow and the egg cell plasma membrane (pm) in magenta. EC1.1-GFP is expressed in egg cells (ec) and localised in vesicle-like structures (arrows) to the cytoplasm. (C and D) Ovules from the homozygous line *DD65p:EC1.1-GFP* showing fluorescence of the fusion protein EC1.1-GFP in yellow. (C) EC1.1-GFP is expressed in central cells (cc), where it localises strongest at the chalazal cell border of the central cell. EC1-GFP is also secreted to the integuments (white arrowheads) and the micropyle (magenta arrowhead). (D) EC1.1-GFP signals are also detected in antipodal cells (aps), localizing in vesicle-like structures (white arrows). (E and F) Ovules from the homozygous line *DD31p:EC1.1-GFP,* showing fluorescence of the fusion protein EC1.1-GFP in yellow. EC1.1-GFP is expressed in synergids (syn) and localised to the filiform apparatus (fa). Images are single confocal planes. Autofluorescence in blue. Asterisk, nucleus; arrowheads, secreted EC1.1-GFP; arrows, vesicle-like structures. Abbreviations: ap, antipodal cells; cc, central cell; ec, egg cell; fa, filiform apparatus; sy, synergid cell; pm, plasma membrane; vac, vacuole. Scale bars 10 µm.

As egg cells are generative and haploid cells, this inevitably leads to the question whether the other cells of the female gametophyte can express EC1. In egg cells, EC1.1-GFP fusion protein (Figure 4.13, A and B; yellow) is localised in vesicle-like structures and is evenly distributed to the cytoplasm. The plasma membrane marker (magenta) showed no colocalisation and there was neither a signal in the nucleus nor in the vacuole nor extracellular prior to fertilisation.

To express EC1.1-GFP in central cells, the fusion protein construct was driven by the *DD65* promoter, which is specific for the central cell (Steffen *et al.,* 2007). In homozygous *DD65p:EC1.1-GFP* plants, fluorescence signals were detected in the central cell (Figure 4.13, C and D). It was evenly distributed in the cytoplasm, but showed no accumulation in vesicle-like structures. The EC1.1-GFP fusion protein was also expressed in antipodal cells, indicating a leaky *DD65* promoter. In antipodal cells, the fluorescence signal derived from EC1.1-GFP was located in similar vesicle-like structures as in the egg cell. In terms of EC1 expression competence, antipodal cells therefore seem to be more similar to egg cells than to central cells. However, GFP signal was additionally visible extracellularly at the micropyle (magenta arrowhead) and between the layers of the outer integuments (white arrowheads). This indicates that the central cell continuously secretes EC1 prior to fertilisation.

In synergid cells, the localisation of EC1.1-GFP driven by the *DD31* promoter showed a complete different picture (Figure 4.13, E and F). The fluorescence signal was detected in the filiform apparatus (fa) and not within the cytoplasm, as it had been the case with all other cells of the embryo sac. Furthermore, no extracellular fluorescence signal was detected.

4.3.1 Functional complementation study of the *ec1-RNAi* mutant

The quintuple knockdown lines *ec1-RNAi_16* and _18 are homozygous triple knockout plant lines for *ec1.1/4/5* and are heterozygous for the *RNAi* construct against *EC1.2/3.* They show a reduced seed set due to loss of fertility in the quintuple knockdown ovules and therefore no quintuple homozygous plants can be generated (Sprunck *et al.*, 2012). The loss of fertility in the quintuple *ec1-RNAi_18* line was tried to be rescued by expression of At*EC1.1, AtEC1.5* and *NtEC1.1L1* (Ec1 Like1 of *Nicotiana benthamiana*) genes in the egg cell, but RNAi inhibited the expression of the newly introduced genes as well (Hackenberg, unpublished data).

Therefore, a functional complementation study was performed by ectopic expression of *EC1.1-GFP* in the other cells of the female gametophyte of the *ec1-RNAi* mutant. To express the fusion protein in synergid cells EC1.1-GFP was cloned under transcriptional control of the DD31 promoter and to express it in central cells under the control of the DD65 promoter. For expression in antipodal cells, EC1.1-GFP was cloned under transcriptional control of the Pumilio14 (PUM14) promoter that was shown to be active in antipodal cells (Šoljić 2012; Englhart 2012). To select transgenic

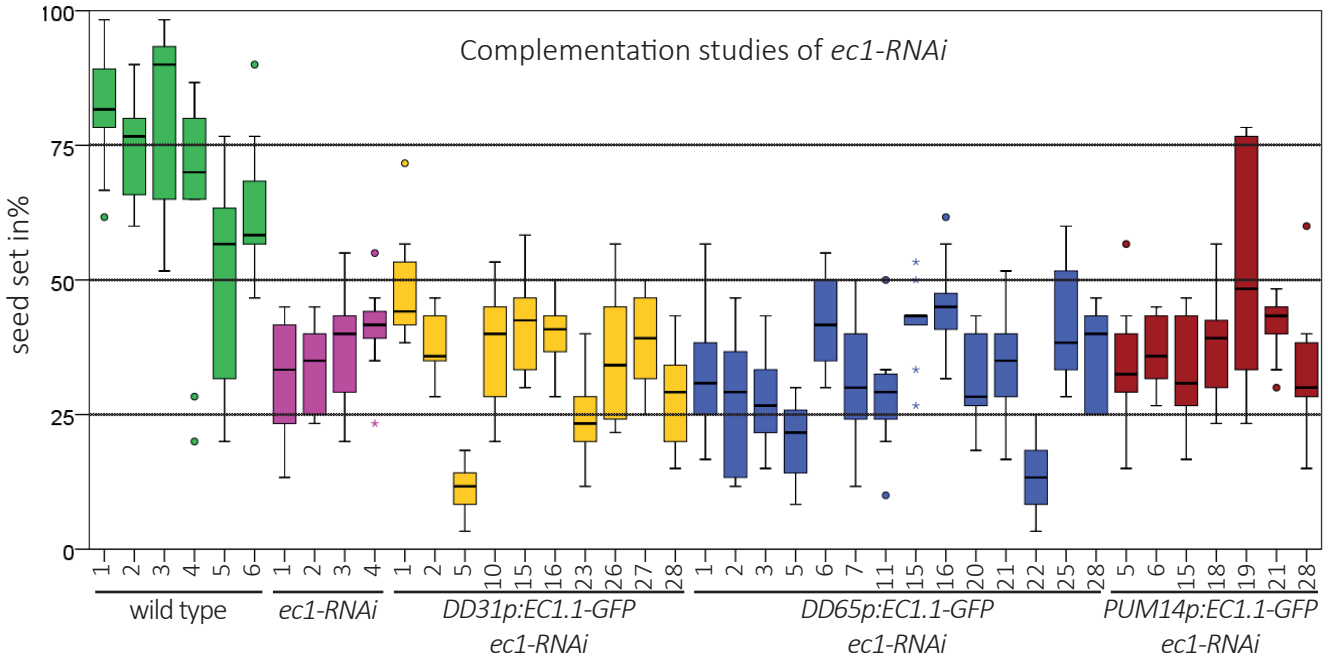

Figure 4.14 Ectopic expression of EC1.1-GFP in the other three cell types of the female gametophyte cannot rescue the *ec1-RNAi* phenotype.
The mutant *ec1-RNAi_16* plant line was transformed with three different constructs to express EC1.1-GFP in the other three cell types of the female gametophyte. Each box plot corresponds to a single wild type plant, heterozygous *ec1-RNAi* plant or plant of the T_1-generation that is heterozygous for *ec1-RNAi* and heterozygous for the complementation construct. The seed sets of at least 8 siliques of each plant were calculated, with a theoretical seed set of 100% set to 60 seeds per silique.

plants, the constructs were cloned in a plasmid containing the expression cassette *At2S3p:eGFP* to express GFP in the seed coat. After transformation of heterozygous *ec1-RNAi_16* plants, the seeds of the T_1-generation were screened for green fluorescence by exposure to UV light and positive seeds were put on soil to germinate. As the T_0-plants were heterozygous for *ec1-RNAi*, the T_1-plants needed to be genotyped. The positive plants, heterozygous for *ec1-RNAi* and heterozygous for the complementation construct, were selected for further studies.

For seed set analysis of *ec1-RNAi DD31p:EC1.1-GFP* plants, of *ec1-RNAi DD65p:EC1.1-GFP* plants, of *ec1-RNAi PUM14p:EC1.1-GFP* plants and of wild type and *ec1-RNAi_16* plants, at least 8 siliques per plant were harvested. The seeds of each silique were counted and the seed set was calculated by setting the maximal number of seeds to 60, which results in a theoretical seed set of 100%. The calculated seed sets are displayed in a box plot in Figure 4.14. The mean median seed set of wild type plants is 72.2%, while the mean median seed set of *ec1-RNAi* plants is 37.5%. With mean median seed sets of 34.1%, 32.3% and 37.1%, the seed sets of the plants with expression of functional complementation constructs show no obvious differences to the seed sets of the *ec1-RNAi* plants.

In summary, all cells of the female gametophyte could express EC1.1-GFP with varied subcellular localisation. However, expression of EC1.1-GFP in synergid cells, central cells or antipodal cells could not rescue the reduced seed set phenotype of the *ec1-RNAi_16* plant line.

4.4 Recombinant EC1 expression in *Pichia pastoris*

In previous studies, ectopic EC1 expression using the strong *Cauliflower Mosaic Virus 35S* (*CaMV35S*) promoter in *A. thaliana* and in *Nicotiana benthamiana* was not successful (Rademacher 2011) although, transcripts of EC1 constructs could be detected in these plant tissues. In *A. thaliana* wild type plants, all five EC1 proteins are exclusively expressed in egg cells. Because only 50 to 60 ovules are present in one flower, purification of EC1 proteins from plant tissue is not suitable for biochemical studies. Recombinant expression of EC1.1-EC1.5 proteins in *Escherichia coli* strains (Rosetta™, ArcticExpress™, Origami™ and Lemo21) was tested by Rademacher (2011) and even though expression of some EC1 fusion proteins was possible, no recombinant protein could be purified. In search of a different expression system, the methylotrophic yeast *Pichia pastoris* got into focus, which utilises the eukaryotic subcellular machinery needed for correct protein folding and disulfide bond formation of the recombinant EC1 proteins. Further *Pichia pastoris* is able to secrete the EC1 fusion proteins into the culture medium, which serves as a first purification step. The fusion protein EC1.1-myc-HIS was expressed, but not purified (Rademacher 2011).

To test the purification of other EC1 proteins in *Pichia pastoris*, the coding sequence of *EC1.2* excluding its signal peptide was cloned into the pPICZα vector (Invitrogen), which contains the native *Saccharomyces cerevisiae* α-factor secretion signal that allows efficient secretion, and a C-terminal *myc* epitope and polyhistidine (HIS) tag. This permitted detection of the EC1.2-myc-HIS fusion proteins through an anti-*myc* antibody and purification via the HIS tag.

4.4.1 Affinity purification of HIS tagged EC1 proteins

The polyhistidine tag is one of the most widely used affinity tags for purification of target proteins. Various immobilised metal affinity chromatography (IMAC) methods are available, in which histidine residues interact with metal ions and allow isolation of the target protein.

The Ni^{2+}-nitrilotriacetate complex (Ni-NTA) interacts with histidine residues by formation and dissociation of coordination bonds and is available on different matrices, e.g. as Ni-Sepharose (GE Healthcare) or as Ni-NTA-Agarose (Qiagen and Sigma-Aldrich). An alternative to Ni^{2+} ions based IMAC, is the Co^{2+} based metal affinity resin TALON® (Clontech Laboratories).

Because not all HIS-tagged proteins behave uniformly, one cannot predict which IMAC method would result in the highest yield and purity of the target protein. TALON® from Clontech Laboratories, Ni-Sepharose from GE Healthcare and Ni-NTA-Agarose from Qiagen and Sigma-Aldrich were tested for yield and purity in purification of HIS-tagged EC1. EC1.2-myc-HIS was expressed in the *Pichia pastoris* strain X-33 and secreted to the media. 24 h after induction (hai)

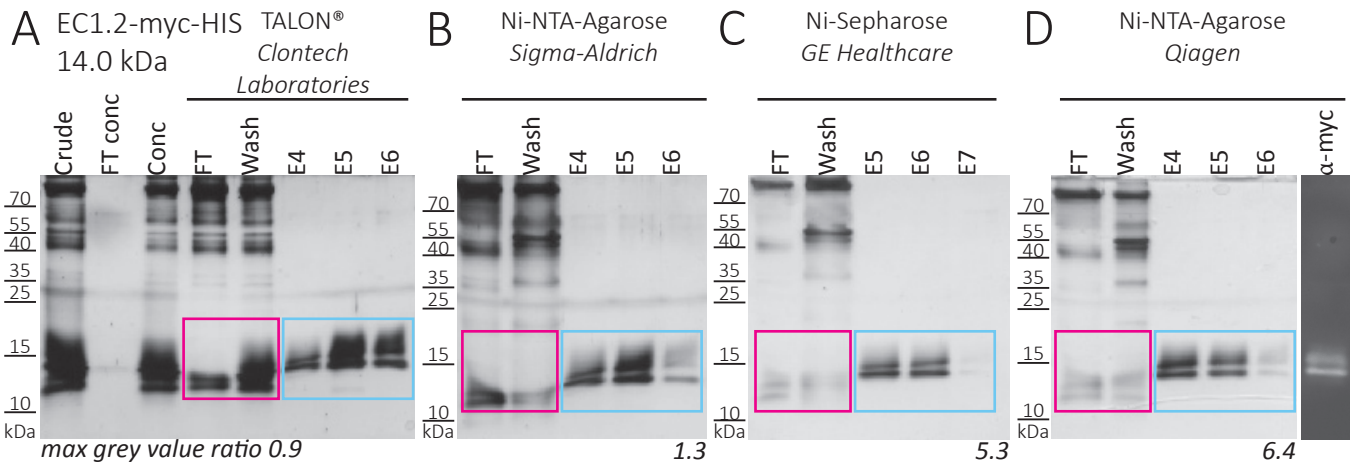

Figure 4.15 Comparison of different affinity resins for purification of HIS-tagged EC1.2 protein.
(A to D) Crude culture media of EC1.2-myc-HIS, expressed in *Pichia pastoris*, were adjusted to a pH of 8.0 and filter sterilized (Crude). They were concentrated with Amicon® stirred cells at 10 kDa cut off (Conc). Equal amounts (50 ml) of concentrate were purified with four different affinity columns. Crude, flow through of the concentrator (FT conc), Conc, flowthrough of the affinity column (FT) and washing (Wash) fractions were precipitated and separated on a Tris/Tricine gel together with the eluate fractions (E4-6). Images show protein gels that were stained simultaneously with silver nitrate. The ratio of EC1.2 protein amount in the FT and Wash fractions (magenta rectangle) to the EC1.2 protein amount in eluate fractions (E4-6; cyan rectangles) was the highest with Ni-NTA-Agarose from Qiagen (D). Right panel in (D) western blot of pooled eluate fractions of EC1.2-myc-HIS with immunodetection via the anti-myc antibody. EC1.2-myc-HIS has a calculated MW of 14.0 kDa. Two bands (apparent MW of ~15-17 kDa and 14 kDa) were visible both in the silver stained gel and upon immunostain on the western blot.

yeast cells in culture medium were centrifuged and the supernatant was filter sterilised (crude). The sterile culture medium (1000 ml) was concentrated with Amicon® stirred cells at 10 kDa cut off, while the concentrate (Conc; 200 ml) and flow through (FT conc) were collected for analysis. Equal amounts of concentrate (50 ml) were applied overnight onto affinity columns containing four different resins for binding the HIS-tagged protein. The flow through (FT) was collected and the resins were washed with the respective washing buffers (wash; 20 ml). The fusion proteins were eluted with the respective elution buffers (E1-E6).

The efficiency of purification was monitored by separation of the collected samples on a Tris/Tricine SDS-PAGE, stained with silver nitrate (Figure 4.15). The calculated size of EC1.2-myc-His is 14.0 kDa and the detected double band between the protein standard bands of 10 and 15 kDa was deemed to be the fusion protein. This was confirmed via mass spectrometry. The diffuse upper band with an apparent molecular weight (MW) of ~15-17 kDa and the lower band with an apparent MW of 14 kDa were analysed separately by Astrid Bruckmann and confirmed to contain EC1.2. No differences in the composition of the analysed peptides were detected.

The double band of EC1.2-myc-HIS was also visible on a western blot via immunodetection using the anti-myc antibody (Figure 4.15, D). Thus, both bands, which were visible on the Tris/Tricine SDS-PAGE after the purification of EC1.2-myc-HIS with Ni-NTA, contain a myc-tagged protein. To further analyse the identity of the diffuse upper band, a polyclonal peptide antibody, generated specifically against a peptide with the amino acid sequence of a C-terminal region of EC1.2 (provided by Svenja Rademacher; generated by Pineda Antikörper-Service), was used. Flow through, wash and elution fractions of an EC1.2-myc-HIS purification with Ni-NTA were separated on two

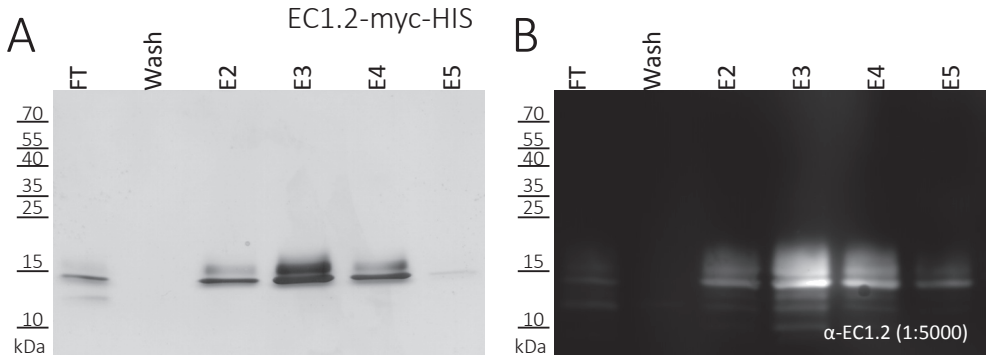

Figure 4.16 The EC1.2 peptide antibody recognizes purified EC1.2-myc-HIS.
Crude culture medium of EC1.2-myc-HIS expressed in *Pichia pastoris* was filter sterilized and purified with Ni-NTA-Agarose. Flowthrough (FT) and washing (Wash) fractions were precipitated and separated on two Tris/Tricine gels together with the eluate fractions (E2-5). One protein gel was stained with silver nitrate (A), while the other was blotted on a nitrocellulose membrane. The calculated size of EC1.2-myc-HIS is 14.0 kDa, but the fusion protein was detected in two both bands via anti-EC1.2 peptid serum (B). The diffuse upper band has an apparent MW of 15-17 kDa and the lower band has an apparent MW of 14 kDa.

identical gels by Tris/Tricine SDS-PAGE (Figure 4.16). One gel was stained with silver nitrate and the other was blotted on a nitrocellulose membrane followed by immunodetection with the anti-EC1.2 antibody. The antibody serum was used in a dilution of 1:5000 and could detect both bands of the purified EC1.2 fusion protein, confirming that both bands contain EC1.2, which is consistent with the results of the mass spectrometry.

To compare the purification efficiency of the four different affinity resins, the relative amount of EC1.2 protein in the eluate fractions to the FT and wash fractions (Figure 4.15) was estimated using ImageJ. The maximum grey values in the areas of the magenta and the cyan rectangles in Figure 4.15 were measured: the ratio of eluates to FT/Wash was lowest with the TALON® resin (0.9; Figure 4.15, A), followed by Ni-NTA-Agarose from Sigma-Aldrich (1.3; Figure 4.15, B) and Ni-Sepharose from GE Healthcare (5.3; Figure 4.15, C). The best ratio was obtained with Ni-NTA-Agarose from Qiagen (6.4; Figure 4.15, D) indicating the highest yield of purified EC1.2-myc-HIS. In terms of purity, no obvious difference was detected when comparing the four different resins. Based on these results, Ni-NTA-Agarose from Qiagen was used for all further purifications of histidine tagged EC1 proteins. Nevertheless, a lot of target protein did not bind to the affinity column, but was detected in FT and washing fractions.

4.4.2 Effects of different affinity tags on EC1.2 affinity purification

To gain a higher yield of purified recombinant EC1.2, other affinity tags and the influence on the yield by the location of the tags at the N-terminus versus the C-termius of EC1.2 were tested. The HIS tag was cloned N-terminal as well as C-terminal with an additional linker sequence. A Strep II tag and a Poly R tag were cloned N- and C-terminal, as well. In addition, different protease cleavage sites were introduced to cleave the tags after affinity purification. The different constructs for expression in *Pichia pastoris* are listed in Table 1.1.

Table 4.1 Features of the EC1 fusion proteins cloned into the pPICZα vector for expression in *Pichia pastoris*.

Fusion protein	N-term. tag	Cleavage site	EC1 protein	Cleavage site	C-term. tag	Size in kDa
StrepII-(-2)-EC1.2	Strep II	Enteropeptidase	(-2)EC1.2	*-2 aa at the N-terminus*		12.8
StrepII-EC1.2	Strep II	Enteropeptidase	EC1.2			13.1
PolyR-(-2)-EC1.2	PolyR	Enteropeptidase	(-2)EC1.2	*-2 aa at the N-terminus*		12.5
HIS-EC1.2	HIS	Enteropeptidase	EC1.2			12.8
EC1.2			EC1.2			11.3
EC1.2-StrepII			EC1.2	Thrombin	Strep II	12.7
EC1.2-PolyR			EC1.2	Thrombin	PolyR	12.4
EC1.2-Thr-myc-HIS			EC1.2	Thrombin	myc-HIS	14.6
EC1.2-PreSci-myc-HIS			EC1.2	PreScission™	myc-HIS	14.9
EC1.2-linker-myc-HIS	*long linker, 34 aa*		EC1.2	-	linker-myc-HIS	15.3
EC1.2-myc-HIS	*short linker, 18 aa*		EC1.2	-	myc-HIS	14.0
EC1.1-myc-HIS	*provided by Svenja Rademacher*		EC1.1	-	myc-HIS	17.8

The pPICZα vectors with the expression cassettes were transferred into yeast via electroporation and tested for induced expression. For all yeast clones, except for EC1.2-thrombin-myc-HIS, expression of the respective fusion protein was detected. To purify the fusion proteins, the yeast cells were cultivated in liquid media for 20-24 h, followed by methanol induction for 20-24 h. After centrifugation and filter sterilisation, the culture media containing the secreted proteins (Crude) were loaded to affinity resins. For Strep II tagged fusion proteins the *Strep*Tactin Superflow Plus and for HIS tagged fusion proteins the Ni-NTA-Agarose from Qiagen was used. The fusion proteins tagged with PolyR were loaded to a strong cation exchanger (SP Sepharose HP from GE Healthcare). The fusion proteins were eluted with the respective elution buffer (for details see chapter 6.6) and separated on Tris/Tricine SDS-PAGEs.

The purification yield of EC1.2-myc-HIS was not satisfying (Chapter 4.4.1) and it was presumed that the C-terminal HIS tag might not be accessible to the affinity resin. Therefore, a construct with a longer linker (34 vs. 18 aa) between the EC1.2 and the HIS tag was created. A purified fusion protein could be detected at the calculated MW of 15.3 kDa (Figure 4.17, A, red arrow), but the yield was very low. Moreover, a second more diffuse band with an apparent MW of ~20-25 kDa (green bracket) appeared on the silver stained Tris/Tricine SDS-PAGE. Neither of the two bands could be detected by western blot analysis with the anti-EC1.2 peptide antibody, likely due to the low amount of protein. The inclusion of a PreScission™ cleavage site between the EC1.2 and the myc-HIS tag at the C-terminus impaired the EC1.2-PreSci-myc-HIS to be expressed by *Pichia pastoris* (Figure 4.17, B). The amount of protein in the crude fraction at a MW lower than 20 kDa appears to be much lower than in the crude fraction of EC1.2-Linker-myc-HIS purification (Figure 4.17, A). The purification of EC1.2-PreSci-myc-HIS was not successful. There was no protein visible in the eluate fractions on the silver stained Tris/Tricine SDS-PAGE and only a very faint band at the calculated MW of 14.9 kDa in the western blot analysis with the anti-myc

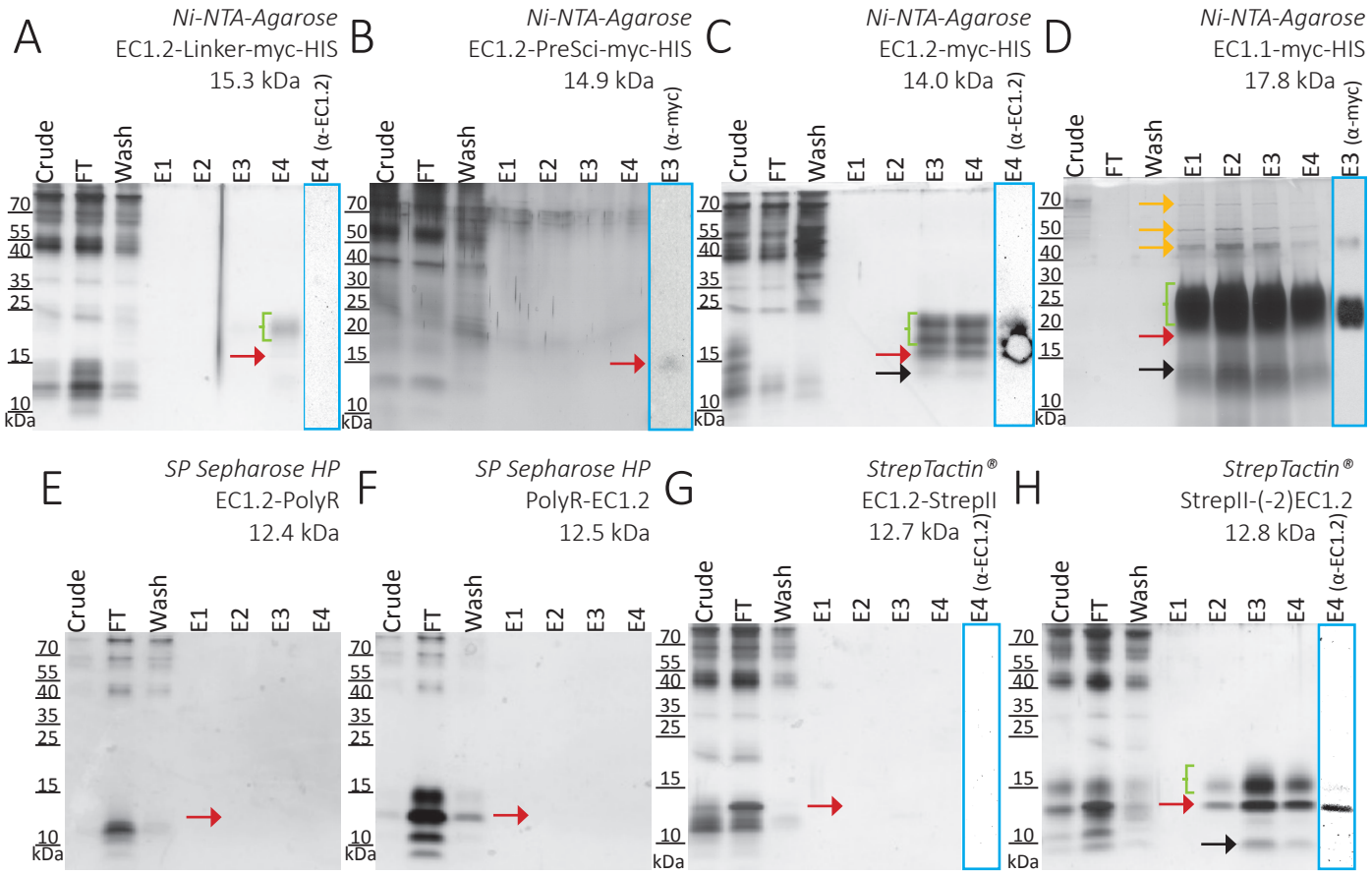

Figure 4.17 Testing various tags for EC1.2 affinity purification.
(A to H) Differently tagged EC1 proteins were expressed in *Pichia pastoris* and secreted to the culture media (BMM for EC1.2; BMMY for EC1.1). Culture media containing the tagged EC1.2 proteins were adjusted to a pH of 8.0 with 1 M NaOH, filter sterilized (Crude) and loaded to the according affinity columns over night (FT). The columns were washed with the according washing buffer (Wash). The proteins were eluted with the according elution buffer in four fractions (E1-4). Crude, FT and Wash fractions were precipitated, separated on a Tris/Tricine gel together with E1-4 and stained with silver nitrate. Protein bands matching the calculated MWs of the fusion proteins are marked with a red arrow. The corresponding immunoblots of eluate fraction E4 are labelled with a blue rectangle. (A) EC1.2 with C-terminal His tag and linker could not be purified. A diffuse band is visible at a apparent MW of ~20 kDa (green bracket). (B) EC1.2 with C-terminal His tag and PreScission cleavage site could not be purified. (C) EC1.2 with C-terminal HIS tag was purified and verified via western blot analysis (E4 (α-EC1.2)). Additional diffuse bands appeared at an apparent MW of 15-25 kDa (green bracket) and degradation products appeared at an apparent MW of 12 kDa (black arrow). (D) EC1.1 with C-terminal HIS tag was purified and verified via western blot analysis (E3 (α-myc); western blot by Ingrid Fuchs). Additional bands appeared at apparent MWs of 70 kDa, 55 kDa and 45 kDa (orange arrows) and a diffuse band was visible from ~20-30 kDa (green bracket). Degradation products were visible at an apparent MW of ~12-14 kDa (black arrow).(E and F) EC1.2 with C- or N-terminal PolyR tag could not be purified. (G) EC1.2 with C-terminal StrepII tag could not be purified. (H) EC1.2 with N-terminal StrepII tag was purified and was verified via western blot analysis (E4 (α-EC1.2)). An additional band appeared at an apparent MW of 14-17 kDa (green bracket), which was not detected in the immunoblot. Degradation products appeared at an apparent MW of 10 kDa (black arrow).

antibody (Figure 4.17, B, red arrow). In comparison, a much higher amount of EC1.2-myc-HIS (14.0 kDa), with the shorter linker (18 aa), was purified from the same amount of crude culture volume using identical conditions (Figure 4.17, C, red arrow). Nevertheless, additional diffuse bands appeared at an apparent MW of ~15-25 kDa (green bracket). By immunodetection using the anti-EC1.2 antibody both bands were detected. Additionally, a band at an apparent MW of 12 kDa was visible on the silver stained Tris/Tricine SDS-PAGE that was very likely a degradation product (black arrow). A diffuse band with a higher MW was also visible on silver stained Tris/Tricine SDS-PAGEs of purified EC1.1-myc-HIS (Figure 4.17, D, green bracket). It is very difficult to distinguish between the diffuse band at an apparent MW of ~20-30 kDa and the band at the

apparent MW of ~18 kDa (red arrow; calculated MW of EC1.1-myc-HIS is 17.8 kDa). Additionally, diffuse bands of degradation products were visible at an apparent MW of ~12-14 kDa (black arrow) and three bands at apparent MWs of 45, 55 and 70 kDa (orange arrows) were visible on the silver stained Tris/Tricine SDS-PAGE. A large diffuse band at an apparent MW of ~18-30 kDa and a band at 45 kDa were also detected on a western blot using the anti-myc antibody, indicating that both bands derive from the EC1.1-myc-HIS fusion protein. The purification of PolyR tagged EC1.2 was not successful regardless whether the tag was fused to the N- or C-terminus (Figure 4.17, E and F). The results shown in Figure 4.17, G and H illustrate that it was possible to purify EC1.2 with an N-terminal Strep II tag, but not with a C-terminal Strep II tag. The purified StrepII-(-2)-EC1.2 appeared on the silver stained Tris/Tricine SDS-PAGE at the calculated MW of 12.8 kDa (red arrow) and could be verified via immunodetection on a western blot using the anti-EC1.2 antibody (Figure 4.17, H). Additionally, a degradation product was visible at a MW of ~9 kDa. As in all the other purifications of EC1 fusion proteins, an additional diffuse band at a higher MW appeared on the Tris/Tricine SDS-PAGE. Here, it migrated at an apparent MW of ~14-17 kDa (green bracket). The appearance of the broad diffuse band for all EC1 fusion proteins suggests posttranslational modifications such as glycosylation due to the expression in the eukaryotic *Pichia pastoris*.

4.4.3 Glycosylation of recombinant EC1 proteins

4.4.3.1 Glycosylation

The sequences of all recombinant fusion proteins were screened for *N*- and *O*-glycosylation recognition sites (Table 4.2) with the NetNGlyc 1.0 and the NetOGlyc 4.0 Server from the Center for Biological Sequence Analysis (CBS).

Table 4.2 Predicted glycosylation sites of EC1 fusion proteins.

Fusion protein	**Glycosylation site predictions with NetNGlyc 1.0 (http://www.cbs.dtu.dk/services/NetNGlyc) and NetOGlyc 4.0 Server (http://www.cbs.dtu.dk/services/NetOGlyc)**	
	N-glycosylation site positions (≥0.5 confidence score)	O-glycosylation site positions (≥0.5 confidence score)
StrepII-E-(-2)EC1.2		6; 24; 25; 103; 106; 109; 110; 114
StrepII-E-EC1.2		6; 23; 26; 27;105; 108; 111; 112; 116
PolyR-E-(-2)EC1.2		21; 22; 100; 103; 106; 107; 111
HIS-E-EC1.2		17; 24; 25; 103; 106; 109; 110; 114
EC1.2		5; 9; 12; 13; 91; 94; 98; 102
EC1.2-T-StrepII		10; 11; 89; 92; 96; 100
EC1.2-Tn-PolyR		10; 11; 89; 92; 95; 96; 100; 101; 110
EC1.2-T-myc-HIS		5; 12; 13; 91; 94; 97; 98; 102
EC1.2-P-myc-HIS		5; 12; 13; 91; 94; 98; 102
EC1.2-linker-myc-HIS		10; 11; 89; 92; 95; 96; 100; 101
EC1.2-myc-HIS		5; 12; 13; 91; 94; 97; 98; 102; 103
EC1.1-myc-HIS	102	10; 13; 14; 15; 17; 18; 19; 127; 128; 130

Table 4.1 shows the potential glycosylation site positions with a prediction confidence score higher than 0.5. According to the predictions, only the EC1.1-myc-HIS fusion protein seems to be N-glycosylated. This is supported by the fact that the EC1.1 fusion protein shows the most pronounced diffuse protein band above the calculated MW of 17.8 kDa on the Tris/Tricine SDS-PAGE (Figure 4.17, D). All tested EC1 fusion proteins have at least six predicted O-glycosylation sites and EC1.1-myc-HIS has with ten sites the most predicted O-glycosylation.

To investigate the glycosylation of recombinant expressed EC1.2, the DIG glycan differentiation kit from Roche was applied. The kit uses the specific binding of lectins to carbohydrate moieties. GNA (*Galanthus nivalis* agglutinin) recognizes terminal (1-3), (1-6) or (1-2) linked mannose, SNA (*Sambuccus nigra* agglutinin) recognizes sialic acid linked (2-6) to galactose, MAA (*Maackia amurensis* agglutinin) recognizes sialic acid linked (2-3) to galactose and PNA (Peanut agglutinin) recognizes the core disaccharide galactose (1-3) N-acetylgalactosamine. Finally, DSA (*Datura stramonium* agglutinin) recognizes Gal-(1-4)GlcNAc in complex and hybrid N-glycans, in O-glycans and GlcNAc in O-glycans. The glycoproteins can either be transferred onto nitrocellulose after gel electrophoretic separation or being identified on tissue sections in histochemistry (Chan *et al.,* 2010). For this study, five times 4 μg of EC1.2-myc-HIS (according to Bradford analysis) were separated on a Tris/Tricine SDS-PAGE by electrophoresis together with control glycoproteins and blotted onto a nitrocellulose membrane. The membrane was lengthwise cut in five pieces, each with EC1.1-myc-HIS and a control protein. These were incubated with the respective lectins that are conjugated with the steroid hapten digoxigenin, which enables immunological detection of the bound lectins (Figure 4.18, A). All control glycoproteins were visible and validated the function of the kit. EC1.2-myc-HIS was only recognized by the lectin GNA, which confirms the presence of *O*-glycosidically-linked mannoses or N-glycosidically-linked "high mannose" in EC1.2-myc-HIS. However, only the upper band of the EC1.2 fusion protein with an apparent MW of ~15-18 kDa was detected by the lectin (green bracket), while the lower band with an apparent MW of 14 kDa was not (red arrow). The third band (black arrow) at the apparent MW of 12 kDa is very likely a degradation product.

4.4.3.2 Expression of EC1.2 in the glyco-engineered Pichia pastoris *strain SuperMan*$_5$

To investigate the glycosylation of heterologously expressed EC1.2 in *Pichia pastoris* in detail, two different EC1.2 fusion proteins, HIS-EC1.2 and StrepII-EC1.2, were transferred into the *Pichia pastoris* strain SuperMan$_5$. This strain has an disruption of an endogenous glycosyltransferase gene (*OCH1*) and has significantly reduced ability to modify glycoproteins with hyperglycosyl N-glycans (Jacobs *et al.,* 2009). The proteins were expressed and purified as described before according to their affinity tags and separated by Tris/Tricine SDS-PAGE (Figure 4.18, B). The

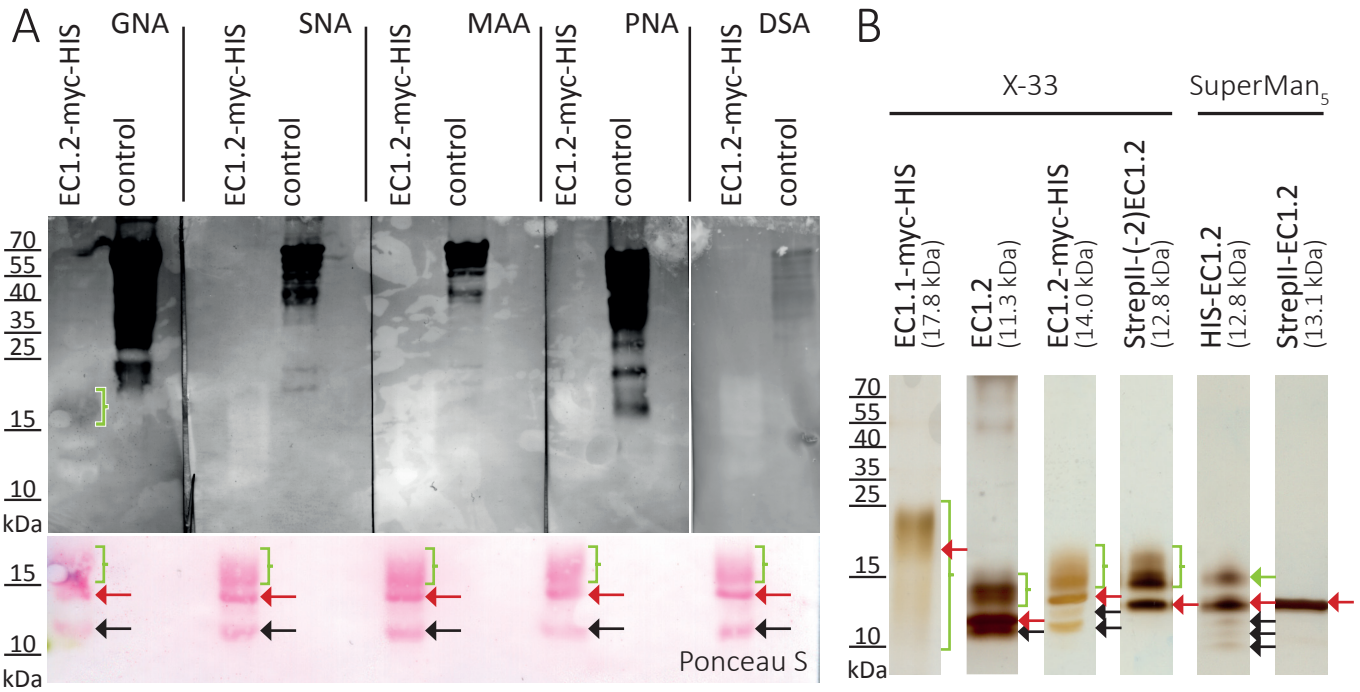

Figure 4.18 Glycosylation of EC1 proteins expressed in different *Pichia pastoris* strains.
(A) The glycosylation of EC1.2-myc-HIS (14.0 kDa) expressed in *Pichia pastoris* was analysed with the DIG Glycan Differentiation Kit (Roche) with different lectins (GNA, SNA, MAA, PNA and DSA) binding specifically to carbohydrate moieties. 4 µg EC1.2-myc-HIS each and the respective control glycoproteins were separated on a Tris/Tricine gel and blotted on a nitrocellulose membrane. After immunological detection with the respective lectins labelled with digoxigenin, the membranes were stained with NBT/BCIP. The diffuse upper band (green bracket) appearing at a MW of ~14-18 kDa was only recognized by GNA, while the lower band (red arrow) at an apparent MW of 14 kDa was not recognized by any lectin. Ponceau S staining showed the double band of EC1.2-myc-HIS and a putative degradation product with apparent MW of 12 kDa (black arrow). (B) Silver stain of tagged and untagged EC1.1 and EC1.2, expressed in the *Pichia pastoris* wild type strain X-33 and the GlycoSwitch® strain SuperMan$_5$. Red arrow, expected MW matches with apparent MW; black arrow, putative degradation product; green bracket/arrow, diffuse protein band with higher MW than expected. Abbreviations: GNA, *Galanthus nivalis* agglutinin; SNA, *Sambuccus nigra* agglutinin; MAA, *Maackia amurensis* agglutinin; PNA, Peanut agglutinin; DSA, *Datura stramonium* agglutinin; NBT, nitro-blue tetrazolium; BCIP, 5-bromo-4-chloro-3'-indolyphosphate.

HIS-EC1.2 protein shows a similar appearance as the proteins expressed in *Pichia pastoris* wild type (X-33) cells, despite that the upper band at an apparent MW of 14 kDa appears as a more distinct line (green arrow) compared to the diffuse bands of the fusion proteins purified from the wild type cells (green brackets). However, the StrepII-EC1.2 fusion protein appears as a single band at the expected size of 13.1 kDa. The StrepII-EC1.2 fusion protein expressed in *Pichia pastoris* SuperMan$_5$ cells therefore seems not to be glycosylated. In summary, the expression and purification of EC1.2, N-terminally tagged with Strep II, shows the best results regarding yield and purity.

4.5 EC1.2 protein characterization

4.5.1 Oligomerization of EC1.2

4.5.1.1 Size exclusion chromatography

In order to further characterize the EC1.2 protein, a final polishing step in the protein purification process was necessary, because biophysical analyses such as nuclear magnetic resonance (NMR) spectroscopy and crystallographic x-ray analysis require the removal of impurities such as aggregates to gain high quality results. EC1.2 fusion proteins were isolated using a size exclusion chromatography with the Superdex200 (Increase) 10/300 GL column. The column was calibrated with proteins from the low molecular weight (LMW) kit (GE healthcare; Figure 4.19). Strep II tagged EC1.2 was purified from *Pichia pastoris* X-33 cells via affinity chromatography with StrepTactin®, the buffer was exchanged to 500 µl 25 mM Tris/HCl, pH 7.5, 200 mM NaCl and the protein was loaded to the column using the automated chromatography system ÄKTA™ pure

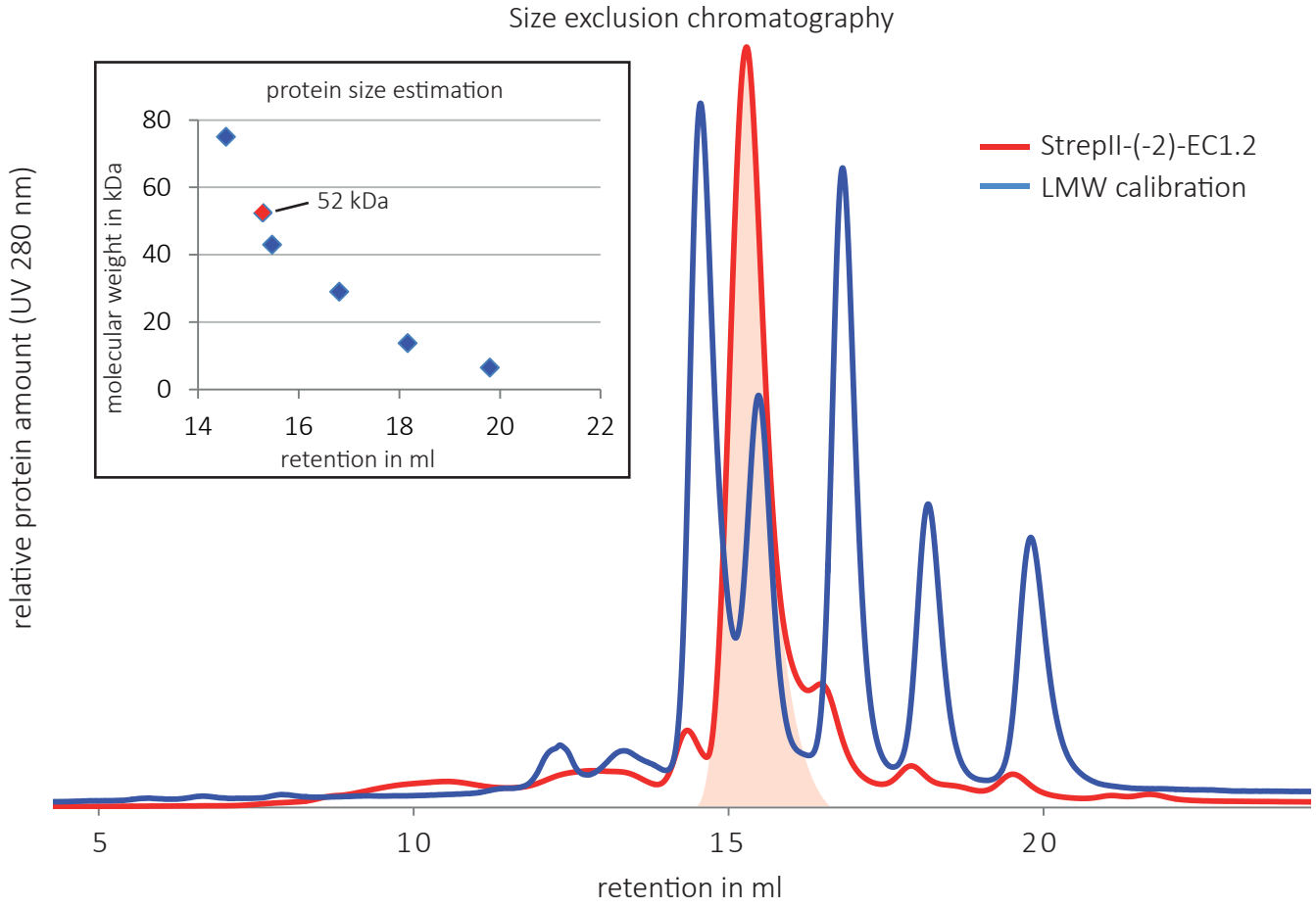

Figure 4.19 Size exclusion chromatography of StrepII-tagged EC1.2.
StrepII-(-2)-EC1.2 expressed in the *Pichia pastoris* wild type strain X-33 was purified via an affinity column with StrepTactin® (Qiagen) and concentrated with an Amicon® ultra centrifugal filter in 200 mM NaCl, 25 mM Tris/HCl, pH 7.5. Size exclusion chromatography was performed with a Superdex200 Increase 10/300 GL column on the ÄKTA pure system (GE Healthcare). The protein amount was detected via UV light at 280 nm and shown in milli absorbance units (mAU). The column was calibrated with the LMW calibration kit (blue chromatogram; GE Healthcare) prior to sample purification (red chromatogram). Overlay of both chromatograms allowed a protein size estimation of StrepII-(-2)-EC1.2 (12.8 kDa) in the filled red peak of about 52 kDa, indicating a tetramer (stoichiometry = 4.1).

(GE healthcare). The protein amount eluting from the column was continuously monitored as UV absorbance at 280 nm and displayed as a chromatogram (Figure 4.19). An overlay with the LMW calibration sample, allowed a size estimation of the StrepII-(-2)-EC1.2 fusion protein of 52 kDa. The calculated MW of monomeric StrepII-(-2)-EC1.2 is 12.8 kDa. This suggests that the fusion protein forms a tetramer under the selected buffer conditions with an estimated stoichiometry of 1:4.10. Similar results were obtained in sodium phosphate buffer pH 7.5 instead of Tris/HCl buffer (data not shown). Notably, the 52 kDa peak fraction of StrepII-(-2)-EC1.2 appeared as a double band when separated by Tris/Tricine SDS-PAGE. So, the glycosylated protein derivates of StrepII-(-2)-EC1.2 could not be separated by size exclusion chromatography. The EC1.2 fusion protein peak at 15.3 ml was wider compared to the peaks of the protein standards included in the LMW calibration.

This suggests that StrepII-(-2)-EC1.2 forms tetramers under the selected conditions. Furthermore, the tetramers contain different ratios of glycosylated and unglycosylated fusion proteins and may therefore appear in a broadened peak in the size exclusion chromatography. These tetramers are of limited suitability for further approaches like crystallisation and NMR.

4.5.1.2 Diffusion-ordered spectroscopy (DOSY)

NMR spectroscopy is a very powerful and widely used technique for determining molecular structure models (Li *et al.,* 2008). In this study, DOSY was used to determine the MW of EC1.2 and estimate the stoichiometry at different buffer conditions.

For all NMR spectra shown, C-terminal HIS tagged EC1.2 was analysed in 200 mM NaCl in 25 mM sodium phosphate buffer, because measurements in Tris/HCl buffer showed massive background signals. The spectra were recorded at pH 6.0 and 4.5, because in more acidic conditions, the pK_a values of the side chains allow more protonated amino acids and therefore more signals in the spectra. As an internal standard 4,4-dimethyl-4-silapentane-1-sulfonic acid (DSS; 196.34 Da) was used. The 1D-^{1}H spectra of EC1.2-myc-HIS mark the signals of EC1 and DSS that were used for DOSY measurements (Figure 4.20). Based on DOSY measurements, the calculated MW for EC1 at pH 6.0 is 71.23 kDa with a relative error of 21%, suggesting a tetramer (stoichiometry 1:5.1 ±1.1). In contrast, the calculated MW for EC1.2 at pH 4.5 varied from 106.7 kDa to 119.2 kDa with relative errors of 22% and 28% and the calculated stoichiometry varies from 1:7.6 to 8.5 (±2.1). However, at pH 4.5 the sample started to precipitate and therefore, the higher and more variable oligomerization level at the more acidic pH is an indication of aggregation of the fusion protein. Additionally, it was observed that the signal of the His residues was only visible at pH 4.5 due to high deprotonation rates at pH 6.0 (pK_a [histidine] = 6.04).

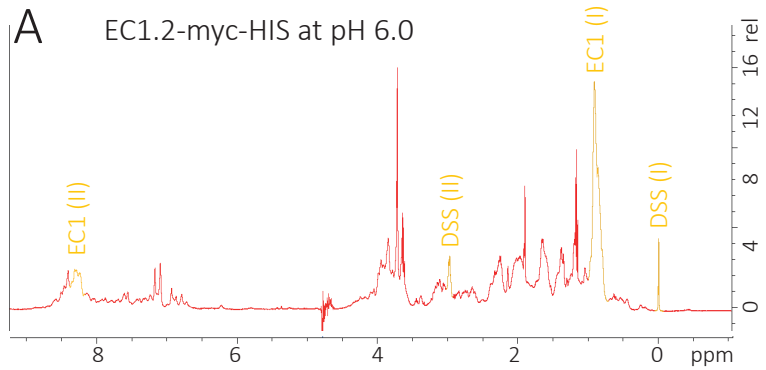

B

Results of DOSY measurements (pH 6.0)

signal pH 6.0	calculated M [kDa]	relative error	stoichio-metry
DSS (I)			
DSS (II)			
EC1 (I)	71.23	21%	5.1
EC1 (II)	71.23	21%	5.1

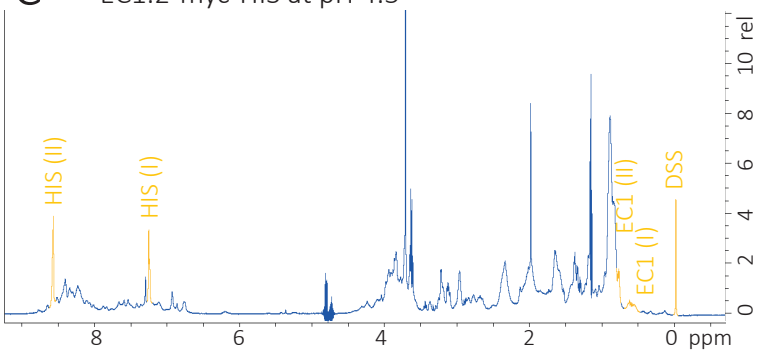

D

Results of DOSY measurements (pH 4.5)

signal pH 4.5	calculated M [kDa]	relative error	stoichio-metry
DSS			
EC1 (I)	119.2	22%	8.5
EC1 (II)	106.7	28%	7.6
HIS (I)	44.9	33%	2.6
HIS (II)	50.4	33%	2.9

Figure 4.20 The stoichiometry of EC1.2-myc-HIS changes pH-dependent.
Diffusion-Ordered Spectroscopy (DOSY) of EC1.2-myc-HIS in 200 mM NaCl, 25 mM Tris/HCl at pH 6.0 and 4.5. (A) 1H spectrum of EC1.2-HIS at pH 6.0 with the signals for DOSY measurements marked in orange. (B) Results of DOSY measurements for EC1.2-HIS at pH 6.0 show an aproximate oligomerisation grade of 5.1. (C) 1H spectrum of EC1.2-HIS at pH 4.5 with the signals for DOSY measurements marked in orange. (D) Results of DOSY measurements for EC1.2-HIS at pH 4.5 show an aproximate oligomerisation grade of 7.6-8.5. Signals of histidin (HIS) residues were only detectable at pH 4.5.

Taken together, the DOSY measurements and the observations in size exclusion chromatography suggest that EC1.2 is likely present as a tetramer at pH 6.0 and 7.5.

4.5.2 Secondary structure of EC1.2

4.5.2.1 Secondary structure predictions

To compare the sequences of all five EC1 proteins from *A. thaliana*, a multiple sequence alignment was performed with the CLC Main Workbench. In Figure 4.21 the sequence and structure information of the EC1 proteins are highlighted. According to UniProt, all of them have an N-terminal signal sequence of 22-32 amino acids that is very likely cleaved in the mature protein. Moreover, the proteins share two highly conserved regions that are termed EC1 signature motifs S1 and S2 (Sprunck *et al.*, 2012). In Sprunck *et al.* (2014), a distinct cysteine pattern was suggested, which was draw into the multiple sequence alignment (Figure 4.21). A secondary structure prediction was calculated separately for all five EC1 proteins by PSIRED (http://bioinf.cs.ucl.ac.uk/psipred). The results of all five EC1 proteins suggest four to six α-helices at variable length with four of them at conserved positions.

Figure 4.21 Secondary structure predictions of EC1 proteins from *Arabidopsis thaliana*.
Multiple sequence alignment of AtEC1 proteins was performed with CLC Main Workbench (Version 7.6.1) with consensus sequence logo colouring according to amino acid properties (red, negative charge; blue, positive charge; green, polar; black, hydrophobic) and matching residues as dots. N-terminal secretion signals are marked with a blue box according to UniProt (http://www.uniprot.org). Secondary structure predictions were calculated by PSIRED and α-helix predictions are marked with a red box. The conserved signal motifs S1 and S2 are labelled in red and the disulfide pattern is indicated in green, according to Sprunck *et al.* (2014).

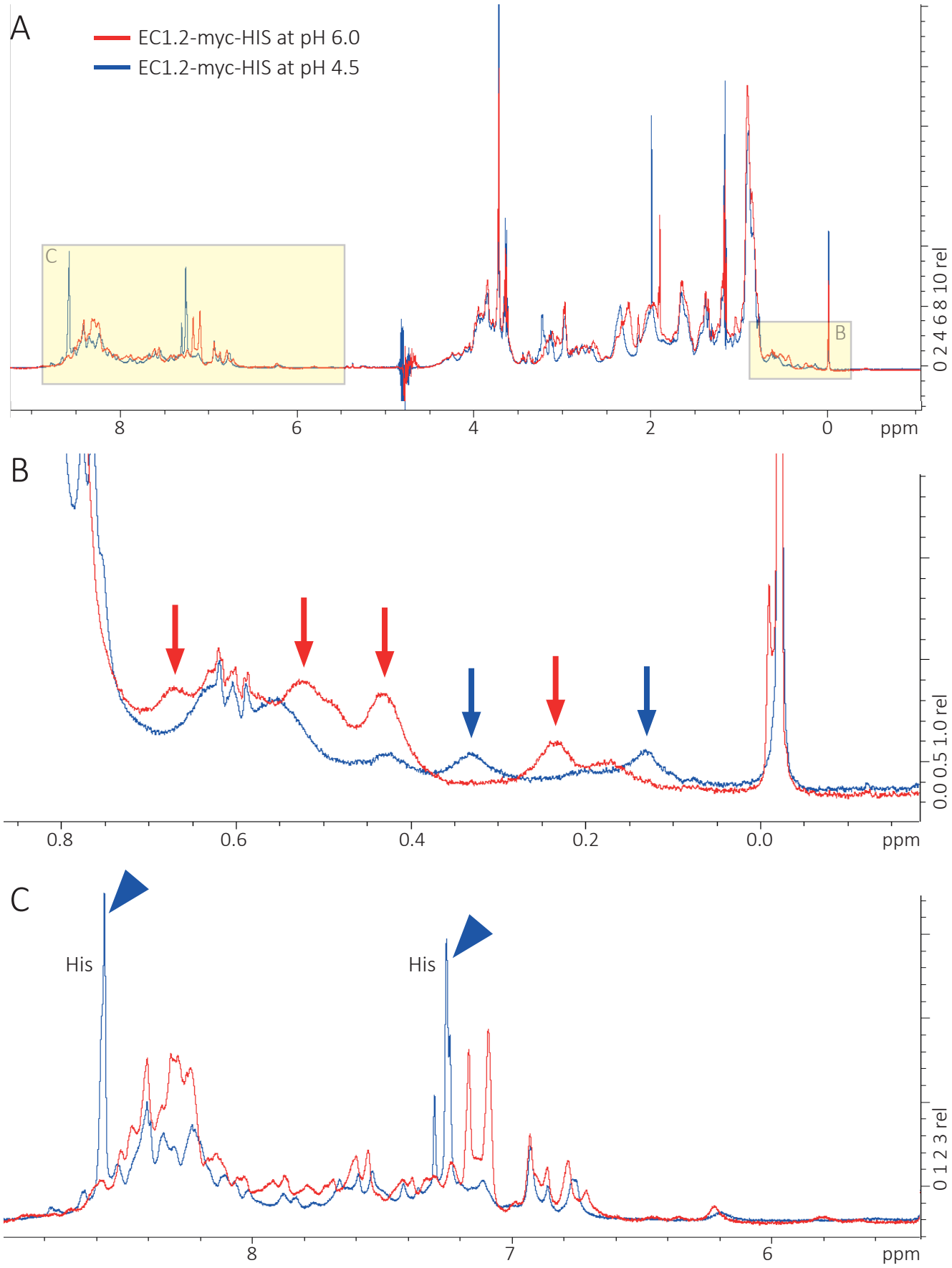

Figure 4.22 The structure of EC1.2-myc-HIS changes pH-dependent.
Comparison of 1D-^{1}H spectra of EC1.2-myc-HIS at pH 6.0 (red) and 4.5 (blue) in 200 mM NaCl in 25 mM sodium phosphate buffer. (A) Complete ^{1}H spectra. (B) Detail of the range with signals from methyl-groups of Val, Leu and Ille (arrows). (C) Detail of range with signals from His side chains (arrow heads).

4.5.2.2 1D-^{1}H NMR spectroscopy

To gain more information on the secondary structure, NMR spectroscopy of HIS tagged EC1.2 was performed. The interpretation of 1D-spectra from complex molecules, like proteins, is almost impossible due to the superimposition of signals. Nevertheless, direct comparison of spectra from the same molecule at different conditions allows some conclusions to structural changes. Therefore, the 1H-spectra of EC1.2-myc-HIS at pH 6.0 (red) and 4.5 (blue) were compared with a focus on conformational changes. The complete spectra (Figure 4.22, A) from 0.8 – 0 ppm (parts per million) shows that distinct peaks are visible and that most of the signals overlap. Thus, the protein sample was not denaturated at both conditions. In the region from 0.8 to 0 ppm (Figure 4.22, B) signals from methyl groups of the residues Val, Leu and Ile are typically visible. The methyl group peaks at pH 6.0 and 4.5 were marked with arrows and clearly show a difference at their distribution suggesting a conformational change of the secondary structure. In the range from 9 to 6 ppm (Figure 4.22, C) the imidazole proton of the His side chains is typically visible. The primary sequence of EC1.2 contains no His residues and thus, the peaks could be related to the HIS tag that was only visible at a pH of 4.5 (arrow heads). At standard conditions, the protons of the imidazole side chain of His have a pK_a value of 6.04. Hence, it is very likely that the HIS tags are deprotonated at pH 6.0 and therefore not visible in the spectrum. It is also possible that the HIS tags were masked with divalent ions at the higher pH. For further interpretations, an additional spectral dimension is needed, resulting in 2D-spectroscopy.

4.5.2.3 Total correlation spectroscopy (TOCSY)

In a correlation spectroscopy (COSY) experiment, the magnetic transfer occurs via scalar coupling (J-coupling). Protons connected via more than three bonds show no cross signal and so, the signals in a COSY-spectrum result only from protons connected via two or three bonds. Very important for structural determination are the J-couplings of H^N-protons with H^α-protons, due to a direct correlation between the size of the coupling constant $^3J(H^N\text{-}H^\alpha)$ and the angle of torsion of the protein backbone. In total correlation spectroscopy (TOCSY) the magnetisation is distributed over the complete spin system of an amino acid, correlating all protons of an amino acid. This results in characteristic signal patterns for each amino acid and allows their identification. (Berg *et al.,* 2002)

It was stated that TOCSY peaks are often stronger and hence easier to detect than the corresponding COSY peaks (Griesinger *et al.,* 1988). Consequently, TOCSY was chosen for further analysis. In a 2D-TOCSY spectrum, peaks in certain areas can be correlated to amino acids. An example for a typical 2D-TOCSY spectrum is depicted in chapter 6.6, where the relevant areas for secondary structure determination are highlighted in colour and can directly be transferred to other

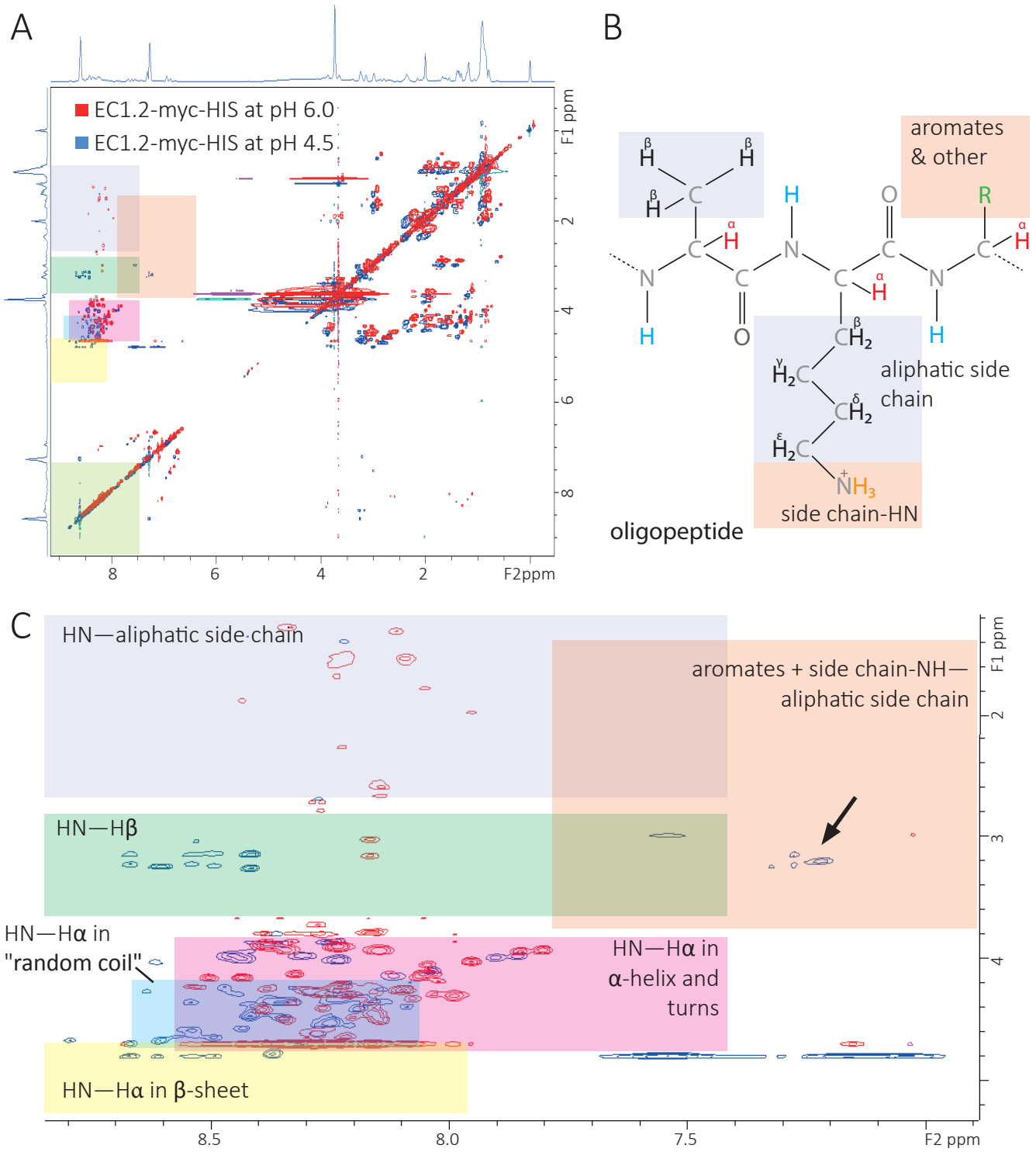

Figure 4.23 The secondary structure of EC1.2-myc-HIS consists of α-helices and turns.
Comparison of Total Correlation Spectroscopy (TOCSY) of EC1.2-His at pH 6.0 (red) and 4.5 (blue). The areas of typical expected signals are marked with rectangles. The expected signal positions for single amino acids are marked in the amino acid single letter code. (A) Complete 2D-TOCSY spectra of EC1.2-myc-HIS with areas for expected signals. (B) Oligopeptide with the aliphatic protons of the side chains marked from β to ε, the proton at the α-carbon in red and the proton at the nitrogen of the peptide bone in blue. Protons at the nitrogen of the side chain and at aromatic side chains are highlighted in orange. The aliphatic side chains are highlighted in violet. (C) Fingerprint region of the spectra in (A) allocating the signals to areas of expected J-coupling of proton pairs: HN backbone—aliphatic side chain (violet), HN backbone—Hβ (green), aromates and HN side chain—aliphatic side chain (orange), HN backbone—H α-carbon in α-helix and turns (magenta), HN backbone—H α-carbon in "random coil" (blue) and HN backbone—H α-carbon in β-sheet (yellow). The arrow points to possible histidine signals.

2D-TOCSY spectra for interpretation. The expected amino acids were marked in single letter code at their specific positions.

The same EC1.2 samples that were used for the 1H-spectroscopy were additionally used for 2D-TOCSY (Figure 4.23, A) at pH 6.0 (red) and 4.5 (blue). The coloured rectangles mark areas of expected signals that allow conclusions on the secondary structure. Figure 4.23, B shows an example of a random oligopeptide highlighting the different kinds of protons the 2D-TOCSY spectrum in panel C (Figure 4.23) refers to. The peaks highlighted in violet and green result from interactions of the proton at the nitrogen of the peptide bond in the backbone (HN) with protons at the β-carbon (Hβ) or the complete aliphatic side chain (Hβ-Hε). Interactions of protons from the aromatic side chains and from protons at the nitrogen on side chains (side chain-HN) with the aliphatic side chains are highlighted in orange.

The sequence of EC1.2-myc-His contains 7 aromatic amino acids (4xF, 1xY, 2xW) and 20 amino acids with side chain-HN (6xH, 8xN, 3xQ, 3xR), but only a few peaks appeared in the expected area. Furthermore, the peaks only appeared at pH 4.5, which, together with these signal positions, corresponds to histidine (arrow) and suggests that the HIS tag is masked at pH 6.0. The lack of other peaks in this area may be due to the oligomerization of the protein. Most of the peaks in the shown finger print area are located at the expected areas. These areas can be divided into partly overlapping areas for secondary structure determining positions. Almost no peaks were visible in the area for β-sheet and if, then only at pH 4.5. Moreover, the major part of pH 4.5 peaks is located to the "random coil" area, while most of the pH 6.0 peaks indicated α-helices and turns. This strongly suggests that the protein changes its conformation.

Again, there are much less signals detected than were expected for a protein with 130 residues, which could be due to oligomerization of the protein. However, the analysis of the TOCSY spectra leads to the conjecture that the secondary structure of the HIS tagged EC1.2 protein at pH 6.0 is mostly composed of α-helices and turns and is shifted to more "random coils" and β-sheet at pH 4.5, due to the appearance of HIS tag signals at lower pH. More detailed information on the secondary structure with NMR is obtained with an unglycosylated EC1.2 that guarantees a homooligomer instead of the heterooligomer that was used. Moreover, a monomer of EC1.2 would probably give the best results, because complex molecules lead to signal interferences and broadening of signals, but a condition in which EC1.2 is stable as a monomer was not found until now.

4.5.3 Tertiary structure of EC1.2

A tertiary structure of an EC1 protein from *A. thaliana* or from any other species is not available. To shed light in this aspect, homology modelling was performed. All models were visualised with the software UCSF Chimera (Martí-Renom *et al.,* 2000; Webb and Sali 2014).

4.5.3.1 The two main families of non-specific lipid transfer proteins

As described in chapter 3.6 the EC1, proteins are secreted small cysteine-rich peptides (CRPs) with similarity to the non-specific lipid-transfer proteins (nsLTPs). In the following, the disulfide patterns of two LTPs with known 3D-structure were compared to decide which pattern is more similar to EC1.2 (Figure 4.23; performed by Dr. Gregor Madej). As an example for a LTP-1 family protein, the Non-Specific Lipid Transfer Protein1 (LTP1; green with red residues) was compared with the putative lipid-transfer protein DIR1 (Defective Induced Resistance; ochre with black residues), which is a member of the LTP-2 family. The alternative disulfide bridges result from sequence-extension, since the helix bearing the –CXC- motif is longer by an odd number of turns in LTR-2. This leads to a different orientation of the cysteine with respect to the C- and N-terminal end of the protein (Samuel *et al.,* 2002). The cysteine positions are rotated by approximately 180° resulting in different disulfide bridges, but with only marginal impact on the structure (Figure 4.23, A and B). The predicted disulfide pattern of EC1.2 (Figure 4.23, C;

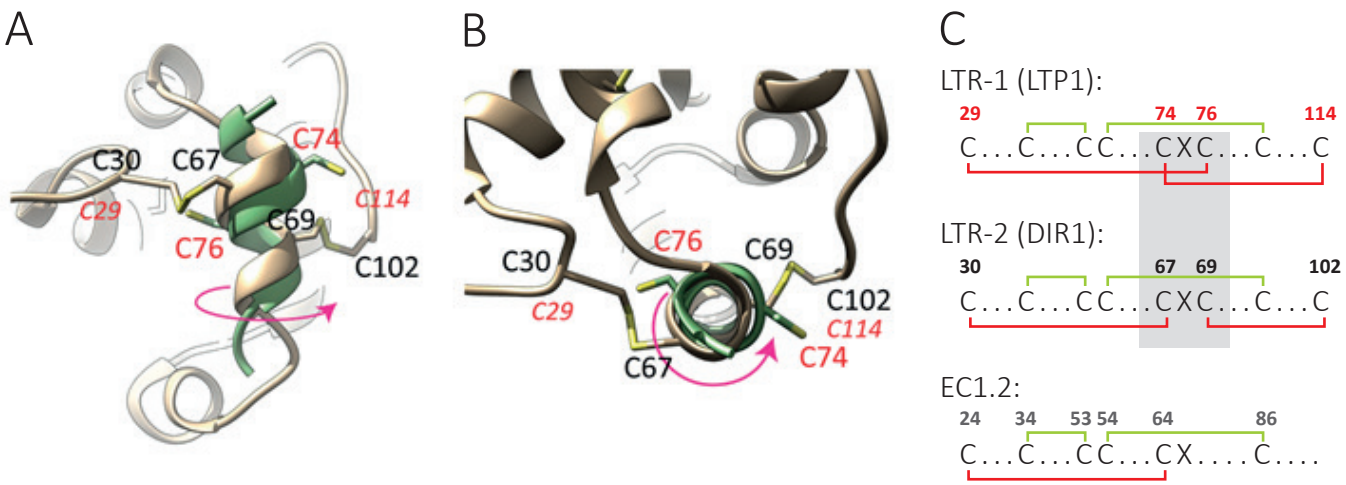

Figure 4.23 Comparison of disulfide patterns of two nsLTP proteins and EC1.2.
(A and B) Comparison of disulfide bridges in LTR-1 (Q42589; non-specific lipid-transfer protein1 (LTP1); green) and LTR-2 (Q8W453; putative lipid-transfer protein DIR1; ochre). Residue numbers participating in disulfides bonds of DIR1 are shown in black color and the corresponding residue numbers of LTP1 are indicated as red numbers. The arrow indicates the positional pseudo-rotation of the helix. (C) Disulfide pattern comparing LTR-1 with LTR-2 and EC1.2. Gray shaded area indicates the relevant position shown in A and B. EC1.2 has only 6 cysteines and shares the depicted disulfide pattern with DIR1. The comparison was performed by Dr. Gregor Madej.

Sprunck *et al.*, 2014) fits to the pattern of LTP-2 with C69 and C102 from DIR1 not being conserved in EC1.

With only very few structure models of LTP2 proteins available, the target protein was narrowed to DIR1, which shows a number of similarities to EC1.2. First, DIR1 has an acidic pI of 4.25 (EC1.2: theoretical pI 4.34), whereas most of the other LTPs are alkaline proteins (Lascombe *et al.*, 2008). Second, it was suggested that it promotes long distance signalling in *A. thaliana* (Maldonado *et al.*, 2002). Third, DIR1 has a proline rich domain as well as EC1, located at different positions in the respective sequence.

4.5.3.2 Homology modelling of EC1.2

To calculate a homology model, a sequence alignment of EC1.2 and DIR1 was generated using the CLC Main Workbench (Figure 4.24). The sequences aligned according to the cysteine pattern. EC1.2 (103 aa) is longer than DIR1 (77 aa) with a longer region at the N-terminus (19 aa) and a longer C-terminal tail (3 aa). The sequence identity of DIR1 and EC1.2 is 15.6%.

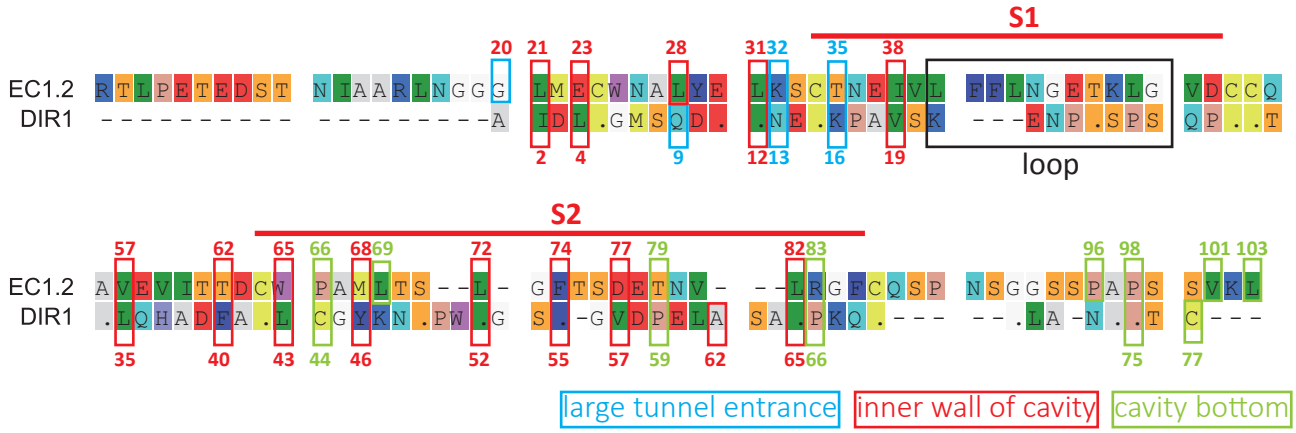

Figure 4.24 Multiple sequence alignment of the EC1.2 protein and the lipid transfer protein DIR1.
N-terminal secretion signals, according to UniProt (http://www.uniprot.org), were removed from sequences. Sequence alignment of EC1.2 with DIR1 was performed with CLC Main Workbench (Version 7.6.1). Identical residues are depicted as dots and gaps as dashes. Background in rasmol colours.

With DIR1 being a suitable target, EC1.2 (amino acids 20-103) was modelled against it by Dr. Gregor Madej with the software MODELLERv9.16 (Martí-Renom *et al.*, 2000, Webb and Sali 2014; Figure 4.25). To assess the homology model of EC1.2, a theoretical folding energy plot was generated that shows the discrete optimized protein energy (DOPE), which is a statistical potential. A DOPE score lower than -0.3 (red dotted line) counts for a resilient model. The plot clearly shows that the homology model of EC1.2 is robust and is only destabilised at the very C-terminus due to the lack of a fourth cysteine bridge, compared to the DIR1 protein.

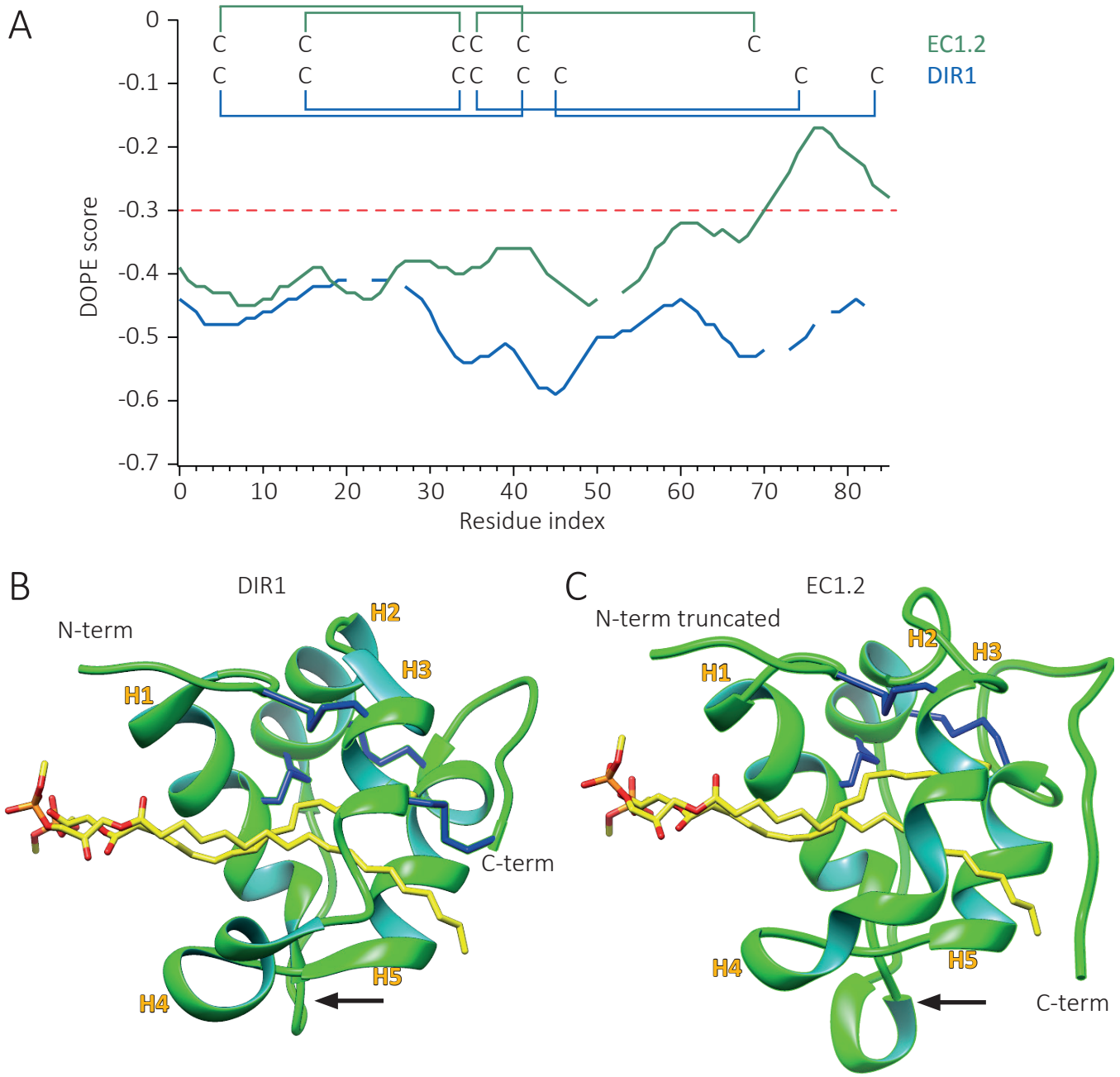

Figure 4.25 Homology modeling of DIR1 and EC1.2.
Comparison of the homology model of the EC1.2 protein to the crystal structure of the nsLTP protein DIR1, visualized with UCSF Chimera. (A) Theoretical folding engery plot of both proteins. A discrete optimized protein energy (DOPE) score lower than -0.3 (red dotted line) counts for a resilient model. The DOPE score of the EC1.2 homology model is lower than -0.3 over the main length of the protein. The lack of the fourth cystein bridge is clearly destabilizing the target protein, as the theoretical energy is rising above -0.3 at the C-terminus. (B and C) 3D models of DIR1 and EC1.2 are shown as cartoons with cysteines shown in blue and the lipid lysostearoylphosphatidyl choline (LP3) as sticks in yellow. (B) 3D structure of the putative liptid transfer protein DIR1 based on X-ray diffraction with two lipid molecules located inside the central cavity (Q8W453; Lascombe *et al.,* 2006). (C) Homology model of EC1.2 (residues 20-103) based on DIR1. The C-terminal prolongation (3 aa) of EC1.2 closes the internal cavity formed by 5 α-helices (H1-5). The big loop (arrow) in the S2 sequence motif of EC1.2 is longer than in DIR1. The energy plot and the homology model was calculated by Dr. Gregor Madej.

The x-ray diffraction based 3D structure of DIR1 shows five helices (H1-5) forming a central cavity at 45° for two molecules of the lipid lysostearoylphosphatidyl choline (LP3), which were co-crystallised by Lascombe *et al.* (2006) (Figure 4.25, B; Q8W453).

The homology based 3D-structure of EC1.2 excluding 19 amino acids at the N-terminus (Figure 4.25, C) has also five helices. However, helix 3 and 4 are shorter by at least one turn and the loop between helix 1 and 2 is longer by 3 residues (41-43). In EC1.2 the two lipids in the central cavity are orientated tail-to-tail and only the nonpolar ends (C18) are completely buried in the core of the protein. Similar to the DIR1 structure, the internal cavity is almost fully lined by hydrophobic residues: Leu21, Glu23, Leu28, Leu31, Ile38, Val57, Thr62, Trp65, Met68, leu72, Phe74, Asp77 and Leu82 (Figure 4.24). Furthermore, some polar residues are located around the large tunnel entrance (Gly20, Lys32 and Thr35) like in DIR1 (Gln9, Asn13, Lys16) for which it was suggested that the polar entry guides the two lipid heads towards the external solvent area (Lascombe *et al.*, 2008). Finally, the closure of the cavity at the end of the tunnel is different in EC1.2, as in DIR1 it is closed by three proline residues (Pro59, Pro66 and Pro75) and by a cysteine bridge (Cys44-Cys77). This cysteine bridge is missing in EC1.2 and the cavity is therefore closed by three proline residues from slightly different positions (Pro66, Pro96 and Pro98), an arginine (Arg83) and three hydrophobic residues (Leu69, Val101 and Leu103). Interestingly, the C-terminal prolongation of EC1.2 (residues 101-103) adopts the role of the cysteine bridge from DIR1 to close the cavity.

The N-terminal prolongation could not be modelled, as the nsLTPs lack this sequence, but several online tools (CFSSP, GOR, Scratch Protein Predictor and PSIRED) predicted a helix within these first 19 residues (Figure 4.21). This helix could serve as a removable lid to block access to the cavity.

4.5.4 EC1.2 is able to bind lipids

4.5.4.1 Hydrophobicity map of EC1.2

One of the major driving forces or protein folding in aqueous media is the hydrophobic/hydrophilic nature of amino acids (Berg *et al.*, 2002). Hydropathy scales are frequently used to map the hydrophobicity pattern of protein surfaces and rank amino acids on the basis of their free energies from nonpolar to aqueous phases (Jamadagni *et al.*, 2011). However, the accurate prediction of the binding modes of proteins with nonpolar molecules in a polar solvent is much more complex, but very useful to understand molecular recognition of ligands and receptors. A widely used approach to visualise hydrophobicity on the surface of proteins is coulombic surface colouring that makes use of the residues charges and was applied here.

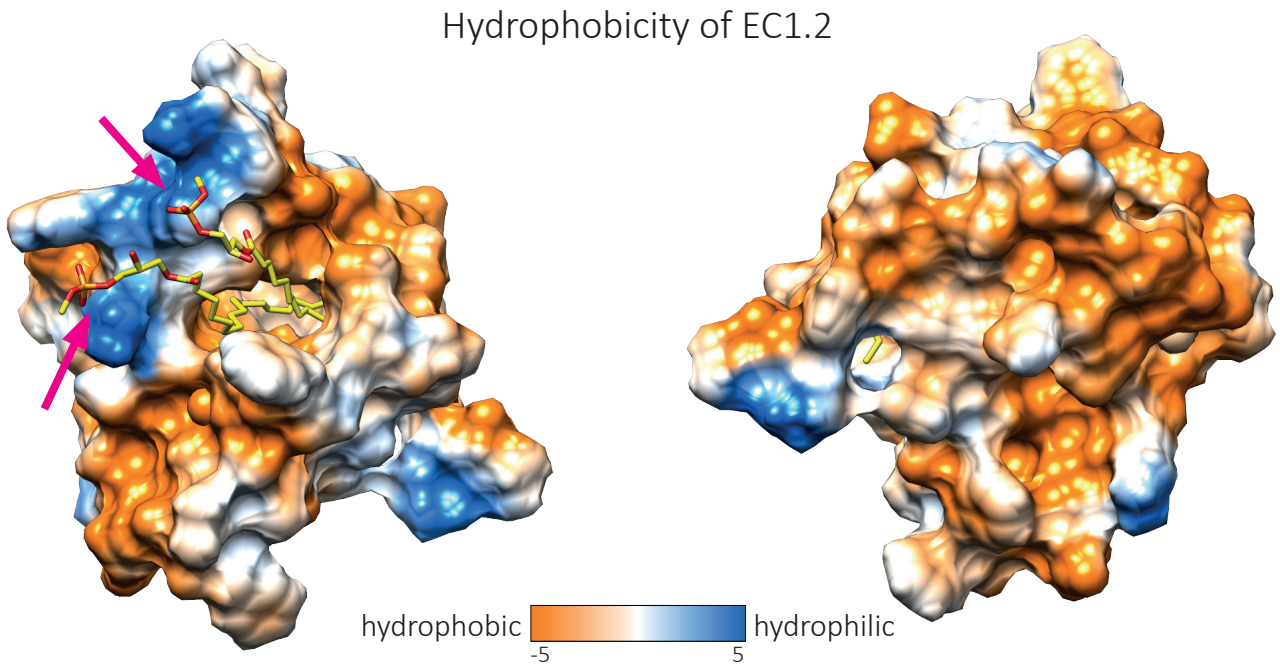

Figure 4.26 Electrostatic potential surface of EC1.2.
Electrostatic properties of EC1.2 as color-coded electrostatic surface in kcal/(mol*e) visualized with UCSF Chimera. The polar lipid heads are localised proximately to the polar cavity entry (arrows). The inner wall of the cavity is hydrophobic (orange), as well as the larger part of the protein surface.

The hydrophobicity of EC1.2 was calculated with a protein dielectric constant of 4 and a distance from surface of 1.4 with only the residues enclosed by a surface being used to calculate the potential on that surface (Figure 4.26). The molecular surface was coloured according to values from - 5 kcal/mol*e* in orange to + 5 kcal/mol*e* in blue. The polar choline heads of the lipids are located proximately to the negative charged cavity entry. Main parts of the inner cavity wall show a neutral electrostatic potential (white). Both features would ensure the binding of the two lipids in the core cavity of EC1.2.

4.5.4.2 The conserved signature motifs S1 and S2

Synthetic peptides of the conserved signature motifs S1 and S2 of EC1.1 were able to activate *A. thaliana* sperm cells. With the homology model of EC1.2 at hand it is possible to investigate the positions of the signature motifs in the 3D model in order to reveal their molecular function. The corresponding residues were highlighted on a surface model of EC1.2 (Figure 4.27, A). The surface areas of S1 (magenta) and S2 (cyan) are connected, but suggest different functions. While S1 covers mainly the outer surface, S2 lines a big part of the hydrophobic inner wall of the cavity. The longer S2 motif is part of 3 helices (H3-5) and encircles almost completely one of the two lipids in the cavity (Figure 4.27, B). However, the shorter S1 motif is not interacting with the lipids at all (Figure 4.27, B). It forms a long variable loop that turns into a helix on both ends (H1+2). This loop is much shorter in DIR1 and is folded in a β-turn followed by a 5-amino acid long

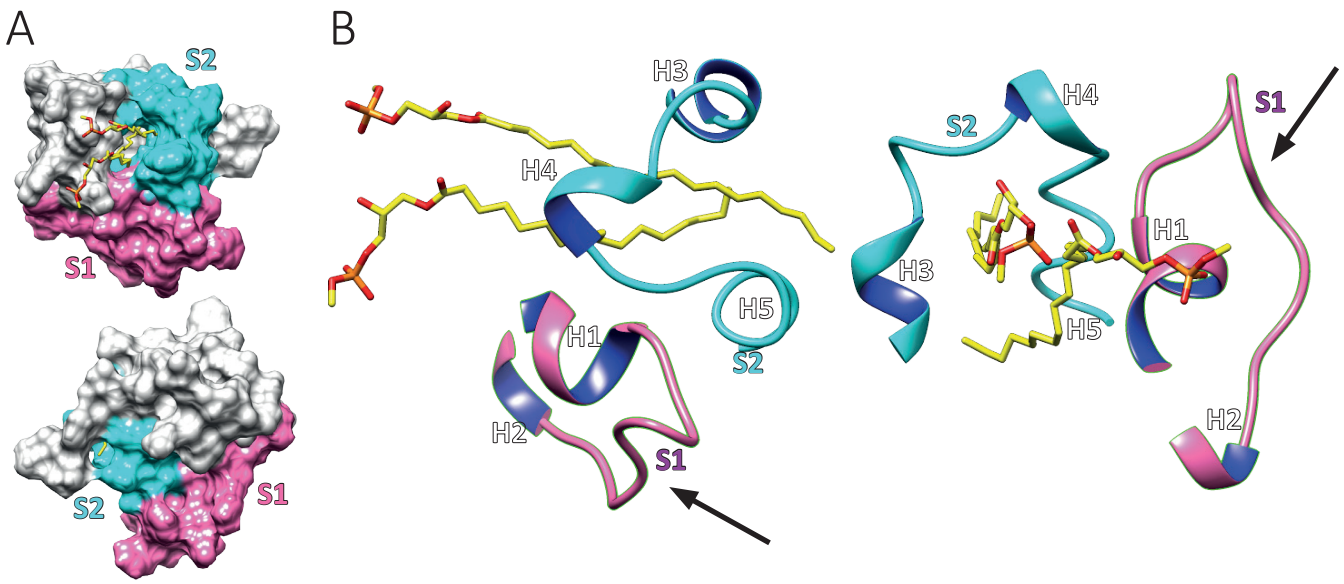

Figure 4.27 Conserved S1 and S2 signal motifs of EC1.2.
Homology model of EC1.2, visualized with UCSF Chimera. Sequence motifs S1 (magenta) and S2 (cyan) of EC1.2 with the lipid lysostearoylphosphatidyl choline (LP3) as sticks (yellow). (A) Surface of EC1.2 with highlighted conserved signal motifs S1 and S2. (B) Motif S1 is part of two helices (H1+2) connected via a variable loop (arrow) that is not part of the hydrophobic cavity. The sequence motif S2 is part of three helices (H3-5) and covers a big part of the hydrophopic inner wall of the cavity.

poly-proline type II (PPII) left-handed helix which was considered to as a putative candidate for the docking of a partner protein in signalling function (Lascombe *et al.*, 2008).

Therefore, the S1 motif may function in the binding to or the recognition of an interaction partner, while the S2 motif is more likely involved in lipid binding.

4.5.4.3 LysoPC binds to EC1.2

The nsLTP DIR1 was only crystalised as a (1:2) DIR1 lysostearoylphosphatidyl choline (LysoPC) complex and in the absence of the lipid, crystals have not been obtained (Lascombe *et al.*, 2008). The DIR1 protein was expressed in *Pichia pastoris,* purified and incubated with lysoPC followed by crystallisation using the vapour-diffusion technique in hanging drops.

In order to crystallise EC1.2 at very similar conditions, preliminary experiments were performed with the EC1.2-myc-HIS fusion protein. Important is in this regard that at the time point of the experiments only HIS-tagged EC1.2 expressed in the *Pichia pastoris* wild type strain X-33 was available. The fusion protein was incubated with LysoPC at an approximate molar ratio of 1:2000 at 4 °C overnight. To separate unbound protein and free lysoPC from EC1.2-myc-HIS/ LysoPC complexes the protein/lipid mixture was separated using size exclusion chromatography (Figure 4.28). The chromatogram of EC1.2-myc-HIS incubated with lysoPC (yellow) was superposed with chromatograms of pure EC1.2-myc-HIS (red) and a LMW calibration sample (blue). The

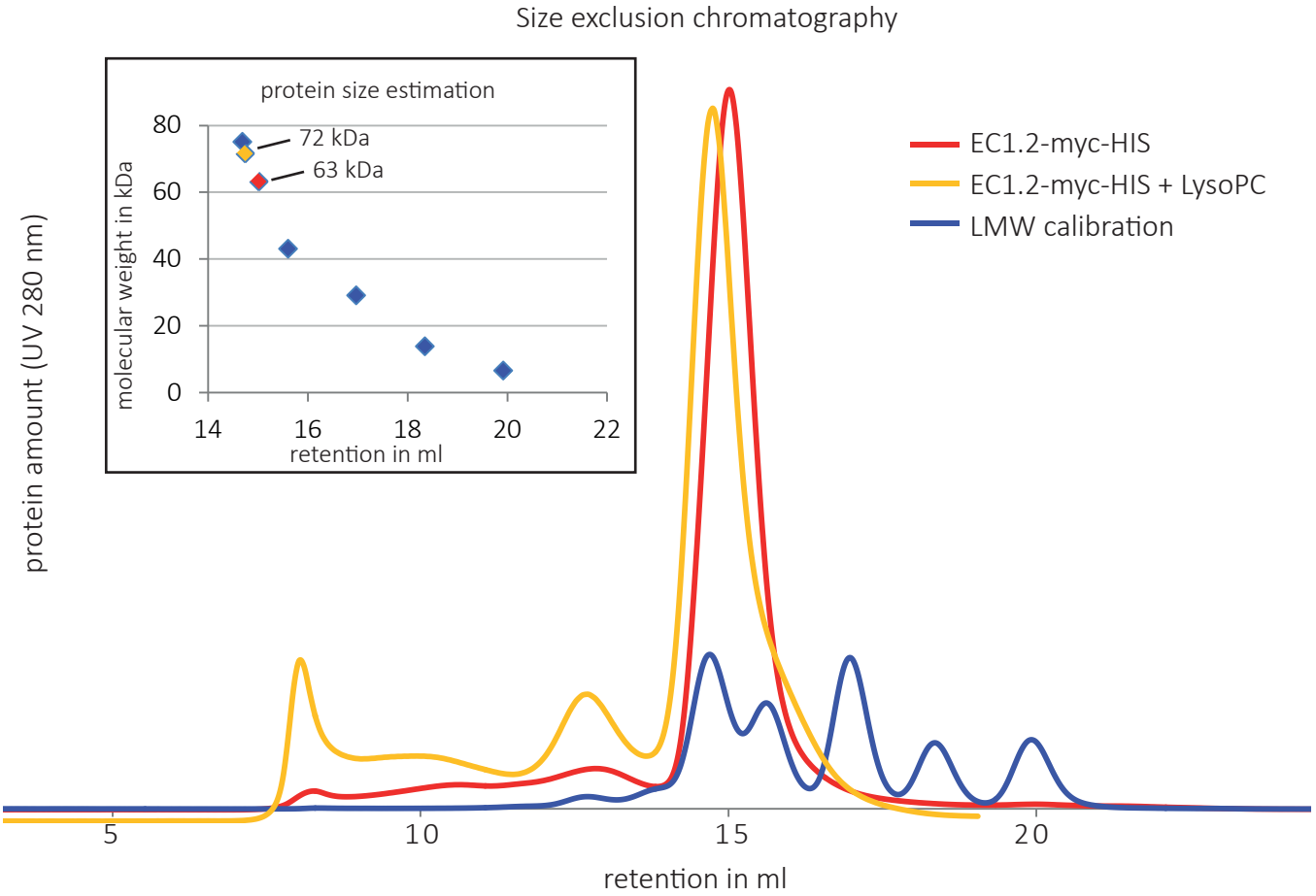

Figure 4.28 Purification of HIS-tagged EC1.2 with and without lysoPC for protein crystallization.
EC1.2-myc-HIS, expressed in the *Pichia pastoris* wild type strain X-33, was affinity purified via Ni-NTA-Agarose (Qiagen) and concentrated with an Amicon® ultra centrifugal filter in 200 mM NaCl, 50 mM sodium phosphate buffer, pH 7.5. EC1.2-myc-HIS (14.0 kDa) was incubated with lysoPC (525 Da) at an approx. molar ratio of 1:2000. Size exclusion chromatography of EC1.2-myc-HIS (red) or EC1.2-myc-HIS with LysoPC (yellow) was performed with a Superdex200 10/300 GL column on the ÄKTA pure system (GE Healthcare). The relative protein amount was detected via UV light at 280 nm. The column was calibrated with the LMW calibration kit (GE healthcare) prior to sample purification. Overlay of chromatograms allowed a protein size estimation of LysoPC-treated and untreated fusion protein. The MW of the EC1.2-myc-HIS sample incubated with lysoPC is about 8.4 kDa higher compared to the EC1.2-myc-HIS sample, theoretically corresponding to 16 molecules of lysoPC per tetramer of EC1.2-myc-HIS.

retention time of EC1.2-myc-HIS incubated with LysoPC is shifted shorter compared to EC1.2-myc-HIS, which demonstrated a higher mass.

Using the calibration curve, the molecular weights of both peaks were estimated. The MW of the putative tetramer of EC1.2-myc-HIS + lysoPC (71.6 kDa) was approximately 8 kDa higher than the tetramer of EC1.2-myc-HIS alone (63.2 kDa). This increase of mass equates to 16 molecules of lysoPC (525 kDa) theoretically indicating 4 lysoPC molecules per EC1.2 protein. For the fitting curve of the LMW calibration, proteins with MWs of 6.5 to 75 kDa were analysed and only one control protein has a longer retention time than EC1.2-myc-HIS. Therefore, the size estimation has to be treated with caution and the exact ratio of EC1.2 to lysoPC may be slightly different. Nevertheless, the shift of the peak clearly shows the binding of lysoPC to the EC1.2 protein.

The purified EC1.2-myc-HIS/LysoPC complex was used in a number of crystallisation trials performed with the Hampton Crystal Screen I and II, but no crystals could be detected so far. The HIS tagged EC1.2 fusion protein used for crystallisation was purified from the *Pichia pastoris* strain X-33, which showed glycosylation (Figure 4.18). As the StrepII tagged fusion protein from the glycosylation deficient strain SuperMan$_5$ showed higher purification efficiencies and no glycosylation, it should be used for future attempts to crystallise EC1.2 with lysoPC.

5. DISCUSSION

Independent from the species, the fertilisation processes during sexual reproduction are complex and highly regulated. This especially includes the activation, attachment and fusion of gametes. In *Arabidopsis thaliana* numerous mutants have been investigated to increase the knowledge on the double fertilisation process and the key players involved. The most important proteins known so far are GEX2 and HAP2 (also termed GCS1) that are sperm cell specific as well as the EC1 proteins that are egg cell specific. GEX2 was shown to be essential for gamete attachment (Mori *et al.*, 2014), while HAP2 mediates gamete fusion in various species and was shown to be genetically and structurally conserved amongst multiple kingdoms (von Besser *et al.*, 2006; Mori *et al.*, 2006; Liu *et al.*, 2008; Fédry *et al.*, 2017). The only known egg cell-specific key players are the EC1 proteins. They are small globular cysteine-rich proteins which were shown to be essential for fertilisation and to induce sperm cell plasma membrane modifications (Sprunck *et al.*, 2012). In this study, the membrane merger of male and female gametes and the molecular function of egg cell-specific EC1 proteins was analysed via cytological observations, physiological studies on gamete activation and biochemical studies on purified EC1 proteins.

5.1 The *Arabidopsis* sperm cell membrane is integrated into the membranes of the female gametes during double fertilisation

The gamete membrane merger is a capital step during fertilisation. The *in vivo* visualisation of this process in *Arabidopsis* is very challenging due to the fact that it takes place deeply embedded in the ovule. In previous studies (Igawa *et al.,* 2013) it was suggested that the sperm cell plasma membrane remains on the surface of the female gametes after plasmogamy, while the internal membrane components enter the female gametes. For these experiments pollen expressing the fusion protein HAP2-GFP was used, which mainly localises to the endomembrane system and only eventually to the plasma membrane of sperm cells (Wong and Johnson 2010; Sprunck *et al.*, 2012). Thus, it could not be distinguished whether the HAP2-GFP labelled membrane fragments, detected in the zygote, derived from the sperm cell plasma membrane or from sperm cell endosomes. Additionally, the fluorescence marker used to label the plasma membrane of the female gametes (RFP-PIP2a; *A. thaliana* Plasma membrane Intrinsic Protein 2A) was relatively weak and not only present in the plasma membrane but also in the endomembrane system of the egg cell and the central cell. Therefore and because most of the analyses were done with a non-confocal fluorescence microscope, further experiments were necessary to unravel the plasma membrane dynamics during fertilisation using a suitable marker for the plasma membrane of sperm cells and a strong marker for the egg cell plasma membrane. The fluorescence markers used in the present work were not only localised more specifically to the plasma membranes of the sperm cells and the egg cell, but showed fluorescence strong enough to visualise membranes deeply embedded in the ovule. It was therefore possible to investigate the membrane dynamics and, together with previous live-cell imaging of the fertilisation process (Hamamura *et al.,* 2011; Denninger *et al.*, 2014), to define six subsequent phases during egg cell fertilisation. It was clearly shown that the sperm cell plasma membrane is integrated into the egg cell plasma membrane upon gamete fusion and no GFP-derived fluorescence was detected inside the egg cell. Thus, the sperm cell plasma membrane is not internalised to the egg cell as it is the case in mammalian gamete fusion. A part of the sperm membrane together with a part of the egg membrane from the fusion site is internalised and becomes visible as a wedge-shaped vesicle inside the egg (Satouh *et al.,* 2012). Furthermore, the membrane dynamics of *Arabidopsis* gametes described by Igawa *et al.* (2013) were observed in *semi-in vitro* experiments as described by Palanivelu and Preuss (2006) and the experimental procedure could have had severe effects on the membranes of the gametes. The images of membrane dynamics shown in the present work were made from *in vivo* fertilisation events after hand pollination and should therefore have reduced extrinsic effects on the fertilisation process.

Interestingly, in this present work the fluorescence signal derived from TET9-GFP, initially localised to the sperm cell plasma membrane, was still visible at the fusion site of the egg cell during karyogamy. According to live-cell imaging by Hamamura *et al.* (2012), the karyogamy usually does not start until about 30 min after plasmogamy of the gametes. Together with the observation that the sperm-derived TET9-GFP signal is not homogenously incorporated into the fertilised egg cell but turns up in a patchy manner during karyogamy, it is suggested that the integrated sperm cell plasma membrane areas remain near to the fusion site within the first 30 to 45 minutes after plasmogamy instead of being rapidly distributed by mixing with the egg cell plasma membrane. However, the time frame for the sperm cell-derived plasma membrane accumulating near the fusion site and the sperm cell-derived membrane becoming distributed evenly to the surface of the zygote could be analysed in future live-cell imaging experiments.

Besides, the fertilised egg cell, as well as the fertilised central cell, integrates part of the sperm cell plasma membrane, as TET9-GFP derived fluorescence signals were detected at the border of the central cell. Interestingly, the TET9-GFP signal seemed to be weaker, located in a small area of the fertilised central cell membrane. Various reasons may be suggested: First, the fertilised central cell may have much higher lateral plasma membrane dynamics and thus the newly integrated sperm cell plasma membrane parts are rapidly distributed along the surface of the cell and therefore not detectable anymore. Second, much less sperm cell plasma membrane may be integrated in the fertilised central cell plasma membrane. Third, the TET9-GFP fusion protein that was used as a sperm cell plasma membrane marker is rapidly endocytosed and not recycled to the plasma membrane of the fertilised central cell. However, a quantitative analysis using other fluorescent membrane proteins expressed by the central cell and the sperm cells, as well as fluorescent dyes such as FM®4-64 or FM®1-43 binding to phospholipid bilayer membranes could shed more light on that.

5.2 Rearrangements of the male germ unit membranes

The analysis of confocal laser scanning microscopy images at timepoints after fusion of the male and female gametes, show that fluorescence signals derived from the sperm cell plasma membrane were also detected outside of the fertilised female gametes and it is likely that these signals are derived from the membrane extension that connects the leading sperm cell with the vegetative cell nucleus. But, as the vegetative nucleus was not labelled in these experiments, its localisation could not be determined on the images. However, in ultrastructural analyses of fertilisation in *Nicotiana tabacum* (Huang and Russell 1994) and in fluorescence labelled marker lines of *A. thaliana*

(Maruyama *et al.,* 2013), it was shown that the vegetative cell nucleus persists within the female gametophyte at the position of the degenerated synergid cell. After plasmogamy of a wild type egg cell, remnants of the sperm cell membrane extension were visible at the degenerating synergid, indicating that the extension is located outside of the fertilised gametes (Sprunck *et al.*, 2012). But due to the lack of plasma membrane markers of the female gametes, the fate of the membrane projection connecting the sperm cells with the vegetative nucleus could not be shown so far. It was shown in the present work that after fusion of the gametes *in vivo*, additional fluorescence signal derived from the sperm cell membrane projection was detected outside of the fertilised gametes.

Notably, the TET9-GFP derived signal shows the maximum fluorescence intensity in the region between the two sperm cells of a growing pollen tube. In sperm cells released from *semi-in vivo* grown pollen tubes, the localisation of TET9-GFP is more distributed towards the remaining plasma membranes of the sperm cells, but the intensity maximum is still detected between the sperm cell pair. Tetraspanins, such as TET9, are proteins with four transmembrane domains. Therefore, the high accumulation of TET9-GFP indicates a high accumulation of membrane components in the region that physically separates the two sperm cells. There are several possible explanations for that observation.

First, the sperm cells could be connected to each other only by adhesion at the region of the former cell division and the vegetative cell membrane enclosing the sperm cell pair ensures that the sperm cells stay together as a pair, connected with the vegetative cell nucleus to form the male germ unit. The high accumulation of ectopically expressed TET9-GFP between the sperm cell pair supports the idea that Tetraspanin-containing adhesion structures are involved in connecting the two sperm cells. In human cells it could be shown that the tetraspanins CD81 and CD82 play a role in cell-cell adhesion (Spring *et al.,* 2013; Stroe *et al.,* 2016). In *Arabidopsis,* TET11 and TET12 are expressed in sperm cells and TET11- and TET12-GFP fusion proteins were shown to be also enriched in the region between the two sperm cells (Boavida *et al.*, 2013). The authors termed the region as a tetraspanin-enriched microdomain and suggested that TET11/TET12 complexes perform specific functions in male gametes. In lab-on-a-chip experiments with pollen tubes growing through microgaps, the male germ unit was put under mechanical force and was observed to become temporally distorted, while squeezing through the microgap (Nezhad *et al.,* 2013). But, it has not been described that the male germ unit is disconnected in these experiments, which suggests that the connection is so strong that adhesion is not sufficient enough.

Therefore, as a second and more likely possibility, the sperm cells stay connected to each other as a result of incomplete cytokinesis. Golgi-derived and endosomal vesicles (carrying cell wall and cell membrane components) would accumulate at the plane of cell division but without a subsequent fusion of these vesicles within the cell plate. This would ensure that the sperm cells are tightly connected and do not get separated by the mechanical force applied to the male germ unit during

transportation along the growing pollen tube. A signal such as pollen tube burst and sperm cell release or the sperm cell adhesion to the female gametes could then act as a trigger for the sperm cell pair to complete cytokinesis. Electron microscopic images of cross sectioned pollen tubes from *A. thaliana* show the extracellular matrix between the sperm cells to form a jigsaw-like pattern (McCue *et al.*, 2011). This indicates fully separated sperm cells and excludes incomplete cytokinesis.

Finally, the strong TET9-GFP signal intensities could result from plasma membrane invaginations, which are formed in the previous cell division plane and which would increase the area of physical contact between the two sperm cells. This would also increase the attachment surface of both sperm cells and strengthen their physical connection. On the other hand, this surface enlargement would give the possibility of massive signalling between both sperm cells. Therefore, it is suggested that the high accumulation of TET9-GFP between the sperm cells results from multiple plasma membrane invaginations of both cells.

The styryl dye FM™ 4-64 is believed to insert into the outer leaflet of the surface membrane, where is becomes intensely fluorescent (FM™ 4-64 manual, Invitrogen). The dye is internalised upon endocytosis and labels vesicle trafficking. It was shown in this work that the FM™ 4-64 dye is visible in the endomembrane system of *A. thaliana* sperm cells, suggesting that the released sperm cells are active in endocytosis. Interestingly, the connection of the sperm cells was neither labelled by FM™ 4-64 nor by HAP2-YFP. Upon FM™ 4-64 staining, the gap between the sperm cells had a very similar appearance to the gap observed in TET9-GFP expressing sperm cells after EC1 S2 peptide treatment. This indicates that the membrane connection is neither accessible for FM™ 4-64 nor active in vesicle trafficking. Above all, the lack of HAP2-YFP at the sperm cell connection may be a protection to prevent the sperm cells from fusing with each other.

5.3 Attachment and unpairing of sperm cells

Sperm cells have a size of about 3-4 µm in diameter and the extended length of a sperm cell pair, according to Huang et al., (2015), is 9.57 µm (±1.2) in growing pollen tubes. The distance between egg cell and central cell at the fusion site needs to be smaller than the extended length of a sperm cell pair to enable successful fertilisation. Based on cell reconstructions, the computational modelling of the *effective area for sperm cell targeting* (EAST) defines the surface area on both female gametes where the sperm cells are able to attach to both gametes without being separated (Huang *et al.*, 2015). The authors predicted the EASTs for egg cells as 3.79 x 10^2 µm^2 and for central cells as 5.21 x 10^2 µm^2. Due to that small space and the sperm cells literally being squeezed between

the membranes of the female gametes, it is hard to distinguish between attached and non-attached sperm cells. Mori *et al.* (2014) established a method to plasmolyse the cells in the embryo sac with polysaccharide-digesting enzymes and as a result, the cells lose their typical shape and become round. The authors could furthermore show that the digestion procedure did not have a negative effect on the attachment of *hap2* sperm cells to female gametes before the degree of mutant *gex2* sperm cells attachment to the central cell and the egg cell was analysed using this method. Using this plasmolysation method in the present work, it could be shown that the majority (82%) of wild type sperm cells are not able to attach to the female gametes of *ec1-RNAi* mutant ovules, when plasmolysis was performed 14 to 20 hours after hand pollination. Only a low percentage of sperm cells was located very close to plasmolysed egg cells (6%) and central cells (12%) and may therefore be attached to either of the female gametes. However, it is possible that these sperm cells did not attach to the female gametes, but were by chance located in their close proximity. The introduction of fluorescent plasma membrane markers into the female gametes in the *ec1-RNAi* mutant background would help to precisely determine whether sperm cell attachment or fusion is affected when EC1 proteins are not present.

At the beginning of this work it was not known whether a sperm cell pair needs to break up its physical connection to be able to fuse with the egg cell and central cell, respectively. The maintenance of the physical connection might, for example, serve as a mechanistic element of double fertilisation, to ensure that each female gamete receives one of the sperm cells (Sprunck 2010) and to prevent polyspermy. It was described that during or after successful plasmogamy the sperm cell nuclei start to migrate in opposite directions (Hamamura *et al.*, 2011), a process referred to as 'unpairing' by Huang *et al.* (2015). The authors suggest that unpairing of sperm cells (ups) is the initial step leading to gamete fusion. They could show that the sperm cell nuclei, labelled by the photoconvertible fluorescent protein Kikume Green-Red (KikGR; Habuchi *et al.*, 2008) fused to HTR10, remain paired during a process they claimed as one-step rectification. According to Huang *et al.* (2015), this is the phase when a sperm cell pair that did not immediately manage to attach to both, the egg and the central cell, adjusts its position relatively to the female gametes and takes place before both sperm cells start to fuse. In live-cell imaging experiments monitoring the cytosolic Ca^{2+} in egg cells during the fertilisation process, the sperm cell nuclei start to move in opposite directions immediately after a second Ca^{2+} spike, while the first Ca^{2+} spike was observed upon sperm cell release (Denninger *et al.*, 2014). This suggests that the one-step rectification has to occur prior to the second Ca^{2+} spike in the egg cell.

In the plasmolysis experiments done in the present work, only 4% of all analysed sperm cell pairs were separated. If the sperm cells were not connected anymore, it is very likely that they would have been separated during the plasmolysis and were visible as two individual sperm cell nuclei. As this was not the case, it is suggested that two sperm cells are always present as a physically connected

pair in the *ec1-RNAi* mutant ovules. This suggests an important role of EC1 proteins for sperm cell unpairing, besides or in addition to the described sperm cell activation. In Mori *et al.* (2014), fertilisation arrested sperm cells of attachment deficiency *gex2* pollen appeared as single sperm cells at a much higher proportion (54%), which may be due to the presence of EC1 proteins, which are secreted by the egg cell. To quantify these differences, additional plasmolysis experiments have to be performed using wild type sperm cells with *ec1-RNAi* mutant ovules and wild type ovules and in parallel *hap2* and *gex2* sperm cells with wild type ovules.

Taken all this into account, it can be proposed that sperm cell attachment and sperm cell separation are distinct steps during double fertilisation and that EC1 is necessary for both processes.

5.4 Gamete activation mechanisms

Before gametes are able to fuse, they need to be activated. For that reason, a huge variety of mutual gamete activation mechanisms have developed during evolution of species. The single cell green algae *Chlamydomonas*, for example, does not have male and female gametes but mating-type plus and mating-type minus gametes that recognize and initially activate each other via their flagella. The activation signalling pathway is triggered by adhesion between the two sets of flagella (Liu et al., 2010). Interestingly, cAMP was shown to induce mating responses, while cGMP did not, and therefore cAMP was suggested to function as a primary sexual signal in gametes of *Chlamydomonas* (Pasquale and Goodenough 1987). The mating responses include the formation of local membrane protrusions, termed mating structures, which adhere tightly to each other. A single-pass transmembrane protein with domains related to the Ig-like domains of prokaryotic invasins and adhesins, FUS1, is plus gamete specific and essential for adhesion (Ferris et al., 1996; Liu et al., 2010). The minus gametes specifically express HAP2, which is required for the membrane merger after species-specific adhesion between both gamete membranes at the tip of the mating structures (Liu et al., 2008).

Compared to *Chlamydomonas*, the activation of mammalian gametes is much more complex regarding macroscopic and cell cyclic processes. The secondary oocyte arrests in the metaphase II of meiosis II until fertilisation. The oocyte activates spermatozoa by triggering their increased motility, chemoataxis, primary binding to the oozyte coat and the acrosome reaction when coming into contact with the oozyte's zona pellucida, summarized as capacitation. Fusion-induced oocyte activation results in electrical, morphological and metabolic modifications in the oocyte (Tosti and Ménézo 2016). Detailed knowledge of "oocyte activators" is still not available despite several hypotheses dominate the field. One model involves Ca^{2+}, a second model suggests receptor-

mediated activation and a third model is based on diffusible molecules entering the oocyte after fusion (Tosti and Ménézo 2010). In *Chlamydomonas,* the gametes activate each other simultaneously, while in mammals the oocyte continuously stimulates sperm activation until finally the successful fusion with the sperm happens. Sperm-egg fusion then activates the fertilised oocyte to complete meiosis and as it has already fused with the male gamete, the resulting cell is the zygote.

In flowering plants, all four gametes, the two sperm cells, one egg cell and one central cell, are mature prior to fertilisation and their mutual activation occurs prior to and probably also during fusion. In the following, the knowledge about egg cell activation is described.

5.4.1 The role of Ca^{2+} in egg cell activation in *Arabidopsis thaliana*

It was shown that EC1 activates sperm cells and is essential for successful fertilisation of egg cell and central cell (Sprunck *et al.*, 2012), but how is the egg cell activated in the first place? Or to ask more specifically: What is the trigger for the egg cell to secrete EC1? It was reported that cytoplasmic free calcium concentration ($[Ca^{2+}]_c$) dynamics play an important role during the entire double fertilisation process. Using Ca^{2+} sensors expressed in the egg cell, a first Ca^{2+} spike correlated with pollen tube rupture, while a second Ca^{2+} spike in the egg cell is associated with successful plasmogamy and it was suggested that Ca^{2+} signalling may be involved in egg cell activation (Denninger *et al.*, 2014, Hamamura *et al.*, 2014). Artificial elevation of $[Ca^{2+}]_c$ levels is feasible with a range of Ca^{2+} ionophores like the antibiotic A23187 or the more effective ionomycin (Liu and Hermann 1978, Monshausen *et al.,* 2008). Besides, it was shown that TCR-deficient Jurkat T cells could be stimulated pharmacologically with the combination of Ca^{2+} ionophores and phorbol esters (Weiss and Imboden 1987). In physiological studies using different Ca^{2+} ionophores, the secretion of EC1.1-GFP from the egg cell could not be triggered under the conditions tested. However, as the egg cells are deeply embedded in the ovules, it is possible that the ionophores did not reach the egg cells or were not internalised by the egg cells. Further, it is possible that the ionophores did trigger EC1.1-GFP secretion, but only at a very low amount. As there are five different EC1 proteins expressed in the egg cells, in addition to EC1.1-GFP driven by the endogenous *EC1.1* promoter, the proportion of secreted EC1.1-GFP may have been below the detection limit of the Leica SP8 HyD detectors. Therefore, the physiological experiments on triggered EC1 secretion were not further pursued. Another possibility is that at the time point of imaging, secreted EC1.1-GFP fusion protein is already degenerated.

To monitor whether the ionophores can indeed induce changes in the $[Ca^{2+}]_c$, the ionophores could also be tested using ovules expressing the Ca^{2+} sensor in the egg cells. Furthermore, it is possible that the elevation of $[Ca^{2+}]_c$ alone is not sufficient to trigger EC1 secretion and an external elicitor, provided by the pollen tube cytoplasm of the sperm cells, is necessary. One of the best studied cell is the

T cell of mammals, which play a central role in cell-mediated immunity. The activation of T cells is initiated by the Major Histocompatibility Complex (MHC)/T cell receptor (TCR) interaction and, amongst other downstream effects, leads to Ca^{2+} signalling (Smith-Garvin *et al.,* 2009). Similarly, a direct interaction of a sperm cell with the egg cell could be necessary for egg cell activation. In this case, only sperm cells at close proximity would be able to activate an egg cell and this would lead to the following phases of fertilisation, namely, sperm cell attachment, HAP2 relocalisation and gamete fusion. One aspect in disfavour of this theory is that at least one sperm cell would need to get into touch with the egg cell and this harbours the risk of being too inefficient to guarantee high double fertilisation rates. Notably, Huang *et al.* (2015) showed that sperm cells touching only the central cell rectified their position until both female gametes were in contact with one sperm cell before fusion was initiated. The rectification did also take place, when both sperm cells were only in contact with the egg cell at first. If the physical contact of sperm cells with an egg cell would be a sufficient trigger for EC1 protein secretion, the fertilisation of both female gametes is not assured. Considering the own results obtained from *ec1-RNAi* pollination experiments, it could therefore be speculated that EC1 proteins are secreted after the egg cell gets into physical contact with a sperm cell but before the attachment of the gametes.

Another possible egg cell activation mechanism is the physical contact of an egg cell with the pollen tube tip prior to pollen tube burst. In this case, triggered EC1 secretion would take place in the *feronia* mutant. In *feronia* mutant ovules, the pollen tube grows continuously inside the female gametophyte and does not burst (Huck *et al.,* 2003). But this potential EC1 protein secretion was not analysed so far.

Furthermore, the mechanical deformation of egg cells upon pollen tube burst, which was shown in several time lapses of *semi-in vivo* fertilisation assays (Denninger *et al.*, 2014), could be involved in egg cell activation. But as causing mechanical force on the egg cell without disrupting the egg cell is very challenging, it might be difficult to investigate this theory. It was shown by laser ablation technology that the disruption of a synergid cell causes intense Ca^{2+}-spiking in the egg cell, while the disruption of the central cell does not (Hamamura *et al.*, 2014). It may be that some cytoplasmic component of the synergid cell, which is released after synergid cell degeneration, triggers egg cell activation as well as EC1 protein secretion. Whether the laser ablation of a synergid cell triggers EC1 secretion by egg cells, was not analysed so far, but could shed some light on that theory. It is also possible that a cytoplasmic component of the pollen tube is the trigger for egg cell activation. To investigate this theory, *gex2* mutant sperm cells, for example, could be used that are deficient in sperm cell attachment. Egg cells expressing EC1.1-GFP should secrete this fusion protein upon pollen tube burst or upon laser ablation of a synergid cell, if a cytoplasmic component is the trigger for EC1 secretion.

Comparing all these possibilities, it is hypothesized that EC1 protein secretion is triggered either by direct physical contact of both sperm cells with both female gametes or by a cytoplasmic component of the pollen tube.

5.4.2 *Arabidopsis* sperm cell activation and putative downstream signalling events

Two EC1 peptides are able to induce changes in the endomembrane system of sperm cells (Sprunck *et al.*, 2012). In these experiments, freshly released sperm cells expressing HAP2-YFP were treated with synthetic peptides of the conserved signature motifs S1 and S2. As a consequence the fusion protein HAP2-YFP shifted its localisation from the endomembrane system towards the plasma membrane. However, it was not known whether the observed HAP2-YFP localisation at the plasma membrane of 22% and 33% of all sperm cells treated with control solutions was due to the experimental design. The experiments of the present work confirmed that the HAP2-YFP signal of sperm cells in *in vitro* growing pollen tubes is mainly detected in the endomembrane system in 28% (±4.1) of all sperm cells, which is significantly non-different to the controls from Sprunck *et al.* (2012) with scrambled peptides or DMSO ($p<0.005$). This suggests that HAP2-YFP is rarely present in the sperm cell plasma membranes but mainly in their endomembrane system and indeed relocalised when the sperm cells sense egg cell-secreted EC1. HAP2-YFP relocalisation was suggested to be a sign of sperm cell activation and thus, a gain of fusion competence (Sprunck *et al.*, 2012). Quite recently, the structural analysis of HAP2 from *Chlamydomonas* showed that it is similar to class II viral membrane fusion proteins and the developmental fusogen EFF-1 from *Caenorhabditis elegans* (Fédry *et al.*, 2017). Interestingly, also EFF-1-GFP is localised to the ER and becomes relocalised to membrane interfaces of fusing cells during embryo development (del Campo *et al.,* 2005).

Notably, the described shift of HAP2-YFP localisation to the plasma membrane could also be induced by treating the sperm cells with membrane permeable derivates of cGMP. The involvement of cGMP in plant hormone signalling was demonstrated by a phosphoproteomics analysis on *A. thaliana* root microsomal proteins. In the presence of membrane-permeable cGMP, several proteins, as e.g. the Ca^{2+}-dependent protein kinase CDPK19, showed rapid alterations in phosphorylation (Isner *et al.,* 2012). Further, it was shown that cGMP is involved in auxin signalling during *Arabidopsis* root growth and development (Nan *et al.,* 2014), regulates stomata opening (Joudoi *et al.,* 2013) and changes it's concentration levels during pollen germination (Takahashi *et al.,* 1978).

However, physiological effects in *in vitro* experiments, as they were done in the present work, do not necessarily imply a biological relevance. Cyclic nucleotide gated channels (CNGCs) are known downstream targets of cGMP and are only active when cyclic nucleotides are bound (Talke 2003).

Arabidopsis CNGC7, -8, -9, -10, -16 and -18 were shown to be Ca^{2+} channels, with CNGC18 being essential for pollen tube guidance (Gao *et al.,* 2016). As shown in the present work, the promoters of *CNGC9* and *CNGC10* are indeed active in *Arabidopsis* sperm cells, verifying microarray-based expression data of sperm cells (Borges *et al.,* 2008). Therefore, CNGC9 and CNGC10 could serve as direct targets for the cGMP derivates used for activation assays in the present work.

As the activation of CNGCs occurs intracellularly (Sanders *et al.,* 2002), cGMP needs to penetrate the sperm cell membrane to induce an effect. Due to the relatively low membrane permeability of cGMP, two different derivates with higher membrane permeabilities were used. Pilot experiments indicated that the strongest effect of 8-Br-cGMP on HAP2-YFP relocalisation to the sperm cell plasma membrane occurred at 50 mM compared with lower concentrations of 15 mM and 25 mM 8-Br-cGMP (data not shown). But as the concentration was far too high to be physiological, another cGMP derivate was tested. Notably, 8-pCPT-cGMP showed the strongest effect at a concentration of 100 µM and due to the lower effect at higher concentrations (1 mM) it is speculated that 8-pCPT-cGMP-induced sperm cell activation follows a dose dependent manner. The maximum effects may thus be at a lower and even more physiological concentration. Future experiments using 8-pCPT-cGMP in the nanomolar range should therefore be performed. Nevertheless, it is suggested that the activation of sperm cells by EC1.1 peptides is mediated by a signal transduction pathway involving cGMP and very likely CGNC9, CNGC10 and/or other cyclic nucleotide gated channels.

The shift of HAP2-YFP localisation in sperm cells is not the only effect of EC1.1 peptides, but the treatment of released sperm cells with TAMRA-labelled EC1.1 peptide S2 did induce a decrease of the strong TET9-GFP fluorescence signal, which is detectable in the tetraspanin-enriched area connecting a pair of sperm cells. The decrease of TET9-GFP signal intensity in this area proposes that TET9-GFP becomes endocytosed upon sperm cell activation. Other possibilities are that the proposed plasma membrane invaginations (see chapter 5.3) become flattened, resulting in a visible gap between the two sperm cells. The elimination of tetraspanin-containing adhesion structures or the loss of the sperm cell contact area would then facilitate the separation of the sperm cells during gamete fusion.

5.4.3 The sperm cell membranes are suitable targets for EC1

The synthetic TAMRA-labelled EC1.1 peptide S2 binds both to the vegetative cell membrane and to the membranes of released sperm cells and was detected at a very low amount on the surface of *in vitro* germinated pollen tubes. Additionally, it was shown that the majority of sperm cell pairs (82%) released from *in vitro* germinated pollen tubes either partially or completely stripped off the membrane of the vegetative cell. Therefore, it is assumed that the target membrane of EC1

is either the sperm cell plasma membrane itself or an interaction partner located at the sperm cell plasma membrane. However, it is not known which membranes of the male germ unit are accessible after *in vivo* pollen tube burst in the female gametophyte. To release sperm cells *in vitro,* pollen tubes grown through the upper part of a pistil were cut crosswise. Time lapse microscopy of pollen tube discharge in *semi-in vivo* experiments show that sperm cells are catapulted to the fusion site at a maximum velocity of 10 µm/s (Hamamura *et al.*, 2011). It is therefore possible that the burst of the pollen tube *in vivo* causes a much higher mechanical force on the male germ unit than the *in vitro* pollen tube cutting. Therefore, it could be that *in vivo* the vegetative membrane is removed or ruptured at even higher frequencies than *in vitro*. Microscopic studies of the fertilisation process using a double marker line expressing a strong fluorescent marker for the vegetative membrane and TET9-GFP for the sperm cell plasma membranes could show the localisation and fate of the vegetative membrane after pollen tube reception.

The fact that the recombinant fusion protein EC1.2-myc-HIS is able to bind lipids furthermore supports the hypothesis that the EC1 acts on membranes. Additionally, the homology model of EC1.2 shows that its central cavity is very hydrophobic and facilitates the binding of two phospholipids. Whether EC1 transports phospholipids from the egg cell to the sperm cell, binds to the sperm cell membrane or to a membrane-bound protein or whether EC1 modifies the sperm cell membrane composition remains to be investigated. Using small artificial vesicles, termed liposomes, the lipid binding and transport capability of purified EC1 proteins could be analysed. Liposomes were used to show the ability of various LTPs to transfer lipids as, for example, of Ups1 of yeast (Connerth *et al.,* 2012), extended synaptotagmins of mammals (Yu *et al.,* 2016) and DGD1 from *A. thaliana* (Kelly *et al.,* 2016).

5.5 Complementation of *ec1-RNAi* mutants

All cells from the female gametophyte were able to express the EC1.1-GFP fusion protein, while vegetative cells could not (Rademacher 2011). This may be due to various differences between reproductive and vegetative cells, e.g. regarding differentially expressed posttranscriptional regulatory modules and metabolic pathways (Wuest *et al.,* 2010). However, detection of fluorescence signals does not necessarily imply protein functionality. Functional complementation studies showed that EC1.1-GFP, ectopically expressed in antipodal cells, central cells or synergid cells cannot rescue the phenotype of the *ec1-RNAi* mutant. Functional complementation on the *ec1-RNAi* phenotype by EC1.1-GFP expressed in antipodal cells was not expected anyway, since it is not very

likely that EC1.1-GFP, secreted by the antipodal cells upon fertilisation, will reached the sperm cells due to the distance in the female gametophyte.

However, EC1.1-GFP expressed in synergid cells of *A. thaliana,* localises to their filiform apparatus. This protein localisation is similar to that of ectopic expressed ZmEA1 (Márton *et al.*, 2012), suggesting that EC1.1-GFP is secreted by the synergid cells but not stored in secretory vesicles. This was not unexpected, as the synergid cells are known to be highly active in secretion of various proteins (Higashiyama 2002). However, no EC1.1-GFP was detected along the cells of the inner and outer integuments forming the micropyle, suggesting that EC1.1-GFP accumulates at the filiform apparatus. Whether the molecular size of synergid-secreted EC1.1-GFP limits the diffusion to the micropyle or whether EC1.1-GFP locally accumulated inside the synergid cells and only becomes secreted upon fertilisation, should be analysed in future experiments.

As the central cell is the other female gamete next to the egg cell, a functional complementation by expressing EC1.1-GFP in the central cell seemed possible. However, no complementation of the ec1-RNAi phenotype of undeveloped seeds was observed. Notably, EC1.1-GFP is not only expressed by the central cell, but it was also detected extracellularly, even in the unfertilised ovule. EC1.1-GFP was also expressed by antipodal cells, despite the *DD65* promoter was reported to be central cell specific (Steffen *et al.*, 2007). Individual plant lines expressing EC1.1-GFP either in the synergid cell, the central cell or the antipodal cells, should be selected for future experiments analysing whether the EC1.1-GFP fusion protein is secreted by these cells upon fertilisation.

So far, the EC1.1-GFP fusion protein was not shown to be functional, despite it is secreted by the egg cell upon fertilisation in the wild type background. Complementation with egg cell-expressed EC1.1-GFP is not possible, as in the *ec1-RNAi* knockdown line, the *RNAi* construct also inhibits the expression of the fusion protein. A quintuple *ec1* mutant, for example, would allow complementation studies using either one of the five *Arabidopsis EC1* genes or *EC1* genes from various plant species to analyse the species-specificity or conserved action of EC1 proteins during double fertilisation.

5.6 The challenging task of EC1 purification

To verify the observations made in *in vivo* and in *semi-in vivo* experiments that EC1, or EC1 peptides, bind to and induce changes in the sperm cell membrane protein compositions, high amounts of purified EC1 proteins are needed for further biochemical and biophysical analyses. Using the endogenously expressed EC1 proteins from *A. thaliana,* egg cells would be the optimal source,

as any recombinant of ectopically expressed protein might have unfavourable alterations such as incorrect protein sequence due to alternative splicing effects, incorrect folding due to differing chaperones and additional or missing posttranslational modifications. Furthermore, there is no evidence that the EC1.1-GFP fusion protein expressed in egg cells is active.

However, the purification of the five EC1 proteins from flowers of *A. thaliana* was not performed for a number of reasons. First, the expected yield of EC1 proteins per plant is quite low, as only about 50-60 egg cells per flower express these proteins. Second, also the purification of untagged EC1 proteins without any affinity column at hand, such as an α-EC1 antibody coated column, is expected to result in very low yield. Third, the separation of the five EC1 proteins would be very challenging due to their similarities in sequence, size and theoretical isoelectric points (pIs).

As shown by Rademacher (2011), ectopic expression of EC1.1-GFP in vegetative tissues of *A. thaliana* was not possible and there is evidence that the misexpressed fusion protein is immediately degraded after translation. However, in the present work it was shown that all cells of the female gametophyte are able to express the EC1.1-GFP fusion protein. Notably, the fusion protein is differently localised in these cells, therefore, it is very likely that the purified fusion proteins would not be identical.

For recombinant EC1 protein expression, the *Pichia pastoris* expression system was chosen. *Pichia pastoris* is a yeast which is also known as *Komagataella phaffii* or *Komagataella pastoris* and is used in biotechnology since 1970 (Yamada *et al.,* 1995, Cereghino and Cregg 2000). One of the most important advantages of the *Pichia pastoris* expression system is not only the 10- to 100- fold higher expression levels compared to *Saccharomyces cerevisiae*, but the possibility to switch from intracellular to secretory protein expression. As *Pichia pastoris* secretes native proteins at very low levels, the secretion of heterologous proteins to the media serves as a first step in purification of the protein (EasySelect™ *Pichia* Expression Kit Manual, Invitrogen).

5.6.1 Orientation and properties of fused tags influence the expression and purification of EC1.2

The choice of an affinity tag depends on further experiments performed with the purified protein. Affinity tag comparisons showed that for experiments requiring large but partially purified material in high yields, the HIS (hexahistidine peptide, 6 aa) and GST (macromolecular glutathione *S*-transferase, 218 aa) tag seems to be the most attractive, while experiments requiring highest purity and small quantities may benefit most from using the FLAG (polypeptide, 8 aa) and HPC (heavy chain of protein C, 12 aa) tag (Lichty *et al.,* 2005). According to Lichty *et al.* (2005), the Strep II (polypeptide, 8 aa) tag is the best candidate for affinity purification due to its shortness and the high purity of the purified proteins. In search for other rather small tags, the PolyR (pentaarginine,

5 aa) was found to be used for protein purification for more than 30 years and furthermore, its sequence includes a cleavage site for the exoprotease carboxypeptidase B (CPB), which catalyses the sequential hydrolysis of peptide bonds of C-terminal basic residues (Fuchs and Raines 2005). The possibility of tag cleavage is a huge advantage, as especially large tags may interfere with biological functions or falsify biochemical analytics. But also small tags like the Strep II and the PolyR tag were reported to interfere e.g. with crystallisation in comparison with the HIS or FLAG tag (Bucher *et al.,* 2002).

The Strep II tag and the PolyR tag were introduced to EC1 fusion proteins together with cleavage sites. A broadly used protease is the enteropeptidase (Enterokinase), the physiological activator of trypsinogen with specificity for the sequence $(Asp)_4$-Lys/Ile (Berg *et al.*, 2002). It is especially convenient for N-terminal fusions, as the cleavage is terminated between the Lys and the Ile, leaving only one additional Ile residue at the protein of interest. The most frequently used protease is thrombin that cleaves peptide bonds on the carboxyl side of a basic amino acid residue, where the most common linker sequence is Leu-Val-Pro-Arg/Gly-Ser (Jenny *et al.,* 2003, Takagi and Doolittle 1974). The cleavage occurs at the Arg residue resulting in the protein of interest being extended at its N-terminus by two amino acids or at the C-terminus by four amino acids. Another very popular protease is the genetically engineered PreScission™ because of its unique specificity and high activity (Cowan-Jacob *et al.,* 2006). This protease is a genetically engineered fusion protein, consisting of human rhinovirus 3C protease and GST that cleaves between the Gln and Gly residues of the recognition sequence of Leu-Glu-Val-Leu-Phe-Gln/Gly-Pro.

The first tag tested for recombinant EC1 expression in the present work, was the C-terminal fused myc-HIS tag. Using the *Pichia pastoris* clone pPICZBαEC1.1-myc-HIS (generated by Svenja Rademacher), EC1.1-myc-HIS could be expressed and purified. However, the purified EC1.1 fusion protein was highly mannosylated, as could be shown later on. EC1.2 was therefore used for all further experiments, as it showed less glycosylation site predictions. EC1.2-myc-HIS protein, separated by Tris/Tricine SDS-PAGE, showed one distinct band of expected size (14.0 kDa) and one diffuse additional band (15-18 kDa). The protein expression thus improved, compared to one very diffuse band spreading from 10-25 kDa for EC1.1-myc-HIS. However, the yield of all purification approaches of EC1.2-myc-HIS was not satisfying, as most of the fusion protein did not bind to the affinity columns.

There are several possibilities why the binding efficiency was that low. One is that the HIS tag has been lost, which may be true for a part of the protein, as the strong band at an apparent MW of 11-12 kDa in the flow through and washing fractions did not appear in the eluate fractions, while the calculated size of the EC1.2-myc-HIS fusion protein is 14.0 kDa and the calculated size of the untagged EC1.2 is 11.0 kDa.

Another possibility is that the HIS tag has been insufficiently exposed to the matrix of the affinity column, which is supported by multiple observations. Two different EC1.2 fusion proteins with a C-terminally myc-HIS tag were expressed in *Pichia pastoris*. One had a short linker (EC1.2-myc-HIS; 18aa) and the other fusion protein had a long linker (EC1.2-linker-myc-HIS; 34aa), placed between the EC1.2 sequence and the HIS tag. Interestingly, the fusion protein with the longer linker could not be purified at all. This led to the conclusion that the extended C-terminal end might fold in a way that the accessibility of the His residues is even worse compared with EC1.2-myc-HIS. The results from the DOSY measurements, together with the results from the size exclusion chromatography, showed that EC1.2-myc-HIS was present as a tetramer at a pH of 6.0 and 7.5. It is therefore very likely that the HIS tags are positioned at the contact surface of the tetramer and therefore not accessible to the metal ions of the affinity matrix. The DOSY measurements at pH 4.5 furthermore show that the signals of the His residues became detectable at lower pH, which was possible due to pH-induced conformational changes. These changes were verified by the alterations in the 1D-^{1}H-spectra of EC1.2-myc-HIS at different pH values. Furthermore, the mannosylation of the EC1.2 fusion protein might also mask the HIS tag sterically and prevent binding to the affinity column.

Attempts to express N-terminal Poly-R tagged EC1.2 seemed to be successful, as a protein band of the expected size (12.5 kDa) appeared on the Tris/Tricine SDS-PAGE in the flow through and washing fractions. However, no fusion protein could be purified using the cation exchanger matrix with the described conditions, suggesting that the PolyR tag was either not accessible or that the purification conditions were not suitable. It is worth mentioning that C-terminal Poly-R tagged EC1.2 seemed not to be expressed at all by *Pichia pastoris*. Interestingly, also C-terminal StrepII tagged EC1.2 (12.7 kDa) could not be purified, despite a very strong protein band appearing at a MW of 12-13 kDa in the medium (Crude and flow through fractions). The most efficient purification of EC1.2 fusion proteins, considering yield and purity, was obtained with N-terminal StrepII-tagged EC1.2.

This suggests that an N-terminal StrepII tag fused to EC1.2 is more accessible to the affinity matrix than any of the C-terminal tags.

5.6.2 Glycosylation of EC1 proteins

When yeasts, such as *Saccharomyces cerevisiae* or *Pichia pastoris,* are chosen for protein expression, *N*- and *O*-linked glycosylation may become a problem as the protein glycosylation of microorganisms can be quite different from that in plant cells (Tanner 1986). *Pichia pastoris* is capable of adding both *O*- and *N*-linked carbohydrate moieties to secreted proteins (Goochee *et al.,* 1991). No

consensus primary amino acid sequence for *O*-glycosylation exists and different yeast hosts may add *O*-linked sugars on different residues in the same protein. *Pichia pastoris* is known to add *O*-oligosaccharides composed solely of mannose (Man) residues (Cereghino and Cregg 2000). However, *N*-glycosylation begins for all eukaryotes in the endoplasmic reticulum with the transfer of a lipid-linked oligosaccharide core unit, $Glc_3Man_9GlcNAc_2$, to Asn at the recognition sequence Asn-X-Ser/Thr. This core unit is always trimmed to $Man_8GlcNAc_2$ (M8), while the following glycosylation pattern is different in lower and higher eukaryotes (Goochee *et al.*, 1991). In yeast, *N*-glycans are further elongated by transfer of one α-1,6-mannose residue by the initiating α-mannosyltransferase (*Och1p*) in the Golgi apparatus and inactivation of OCH1 prevents elongation of the oligosaccharides to hypermannose structures (Vervecken *et al.,* 2004). By *N*-glycan engineering of *Pichia pastoris* strains, the α-1,2-mannosidase (*MDS1*) from *Trichoderma reesei* was introduced, which led to a strain with a shortened $Man_5GlcNAc_2$ (M5) core unit and is available from BioGrammatics as the GlycoSwitch® strain SuperMan$_5$ (Ahmad *et al.,* 2014). These SuperMan$_5$ cells show a highly reduced ability to modify glycoproteins with hyperglycosyl N-glycans (Jacobs *et al.*, 2009) and were also successfully used to express putative unglycosylated StrepII-EC1.2.

Notably, all recombinant expressed proteins (EC1.1-myc-HIS, EC1.2 without a tag, EC1.2-myc-HIS and StrepII-(-2)-EC1.2 expressed in X-33; HIS-EC1.2 and StrepII-EC1.2 expressed in SuperMan$_5$) appeared on the Tris/Tricine SDS-PAGE at the calculated MW, but expression in X-33 cells resulted in the appearance of a second band about 2 kDa (apparent MW) larger, which segued in a very diffuse band that was another 2-3 kDa larger. Although, HIS-EC1.2, expressed in SuperMan$_5$ cells, show a distinct upper band, it lacked the characteristic diffuse appearance, suggesting this to be caused by glycosylated EC1.2 variants.

StrepII-EC1.2, expressed in SuperMan$_5$ cells, did not show any additional bands to the band of the expected size (13.1 kDa) on the Tris/Tricine SDS-PAGE, neither degradation products nor additional diffuse bands at higher apparent MWs. Interestingly, the HIS-tagged EC1.2 protein purified from SuperMan$_5$ cells was not as monodisperse as the StrepII-tagged EC1.2. Whether the protein appearing as an upper band of approximately 14 kDa in the eluent of the affinity purification is glycosylated or otherwise posttranslationally modified, remains to be tested. However, the smear of this upper band is more reduced compared to the diffuse bands obtained with purified EC1.2 fusion proteins expressed in X-33 cells and this additional upper band could result from aggregated degradation products, as several degradation products were co-eluted from the affinity column together with the fusion protein.

The predictions on N- and O-glycosylation sites for all fusion proteins suggest that EC1.1-myc-HIS is the only protein with a N-glycosylation site, while all fusion proteins are suggested to have O-glycosylation sites at different amounts. EC1.1-myc-HIS showed a very strong and

diffuse higher molecular weight band on the Tris/Tricine SDS-PAGE, proposing that this extreme differences in appearance resulted from N-glycosylation. However, all EC1.2 fusion proteins showed diffuse higher molecular weight bands, too. For EC1.2-myc-HIS it was shown that the proteins appearing in this upper diffuse band are mannosylated. This characteristic diffuse upper band is not visible or at least dramatically reduced, in HIS-EC1.2 and StrepII-EC1.2 fusion proteins expressed in SuperMan$_5$ cells. Since the SuperMan$_5$ cells are only deficient in N-glycosylation, these diffuse bands were very likely the result of N-glycosylated proteins.

It has to be speculated whether the hyperglycosylation is only a result of the recombinant expression system *Pichia pastoris* or whether the EC1 proteins in the egg cell are glycosylated, too. Immunodetection of EC1.1-GFP, purified from *A. thaliana* pistils, showed a single distinct band at the calculated MW of 42.4 kDa and no diffuse additional bands (Sprunck *et al.*, 2012). Therefore, it is assumed that EC1.1, and very likely the other four EC1 proteins, too, are not glycosylated in the egg cell.

In summary, the StrepII tagged EC1.2 protein purified from SuperMan$_5$ cells is the most pure, appears as one distinct band on the silver-stained Tris/Tricine SDS-PAGE and is therefore suitable for forthcoming efforts of EC1.2 protein crystallisation, where high purity is absolutely necessary. Crystallisation attempts using purified EC1.2-myc-HIS with bound LysoPC have not been successful yet, which is very likely due to the fact that EC1.2-myc-HIS was not monodisperse but contained a varying degree of glycosylation. With the monodisperse StrepII-EC1.2 fusion protein secreted by SuperMan$_5$ cells at hand, further NMR and crystallisation studies are now feasible to unravel the 3D structure of EC1 proteins. Whether the StrepII tag is disturbing or even conducive in EC1.2 crystallisation, needs to be tested.

5.7 EC1 structure suggests activation of sperm cells via lipid binding

5.7.1 EC1.2 forms a tetramer at physiological pH

Diffusion-ordered spectroscopy (DOSY) seeks to separate the NMR signals of different species according to their diffusion coefficients, where a series of spin-echo spectra are measured with different pulse field gradient strength and the signal decays are analysed to extract a set of diffusion coefficients with which to synthesize the diffusion domain of a DOSY spectrum (Pelta *et al.*, 1998). Using internal calibration curves that are generated by a single DOSY measurement together with the NMR sample allows MW determination (Neufeld and Stalke 2015).

Using the DOSY spectra of EC1.2-myc-HIS, the stoichiometry of the fusion protein was calculated as 5.1 (±1.1) at a pH of 6.0 and according to the size exclusion chromatography data, the calculated stoichiometry of EC1.2-myc-HIS is 4.5, while it is 4.1 for Strep-(-2)-EC1.2. This discrepancy can have several reasons. First, the calculated relative error of the DOSY measurement was 21%. This allows a range of calculated stoichiometry from 4.0 to 6.2. Second, this DOSY measurement was made at pH 6.0 and another measurement at a pH of 4.5 showed even higher stoichiometry, while protein precipitation was observed in the NMR test tube. Therefore, the stoichiometry at pH values higher than 6.0 could be lower. Compared to the NMR measurements, the size exclusion chromatography was performed at a pH of 7.5. A different pH can cause tremendous conformational changes in proteins (Yang and Honig 1993) and may therefore be the main reason for the variance in stoichiometry. The stoichiometry is based on the calculated MW of the fusion proteins. All NMR spectra and each size exclusion chromatography in the present work were performed with EC1.2 fusion proteins expressed in the *Pichia pastoris* wild type strain X-33. The purified EC1.2 fusion proteins were shown to be partly glycosylated and should therefore have an increased effective MW. Therefore, the most likely stoichiometry of the measured fusion proteins is a tetramer. In future experiments, with the glycosylation deficiency strain SuperMan$_5$ at hand, StrepII-EC1.2 without high glycosylation should give more precise information about the exact stoichiometry and, hopefully, about the three-dimensional (3D) structure, too.

5.7.2 Challenges in protein modelling

A key question of protein analysis is the prediction of a 3D structure just from the primary sequence, the "protein folding problem". The "thermodynamic hypothesis" states that the 3D structure of a native protein in its normal physiological milieu (solvent, pH, ionic strength, presence of other components such as metal ions or prosthetic groups, temperature, etc.) is the one in which the Gibbs free energy of the whole system is the lowest; that is, because the native conformation is determined by the totality of interatomic interactions and hence by amino acid sequence, in a given environment (Anfinsen 1973). However, after more than 40 years of intensive research still no algorithm was found that can predict the 3D structure with any reasonable accuracy just from the primary sequence, with the exception of homologies to known structures (Lottspeich and Engels 2006). So, protein structure homology modelling has become a routine technique to generate 3D models for proteins when experimental structures are not available (Biasini *et al.,* 2014). It is by far the most widely used computational approach to predict the 3D structures of proteins and consists of four steps: (1) finding homologous template proteins of known structure, (2) selecting the best template, (3) optimizing the sequence alignment and (4) building the homology model for the query sequence that resembles as closely as possible the structures of the template (Meier and Söding 2015).

5.7.3 Is EC1 function similar to non-specific lipid transfer proteins?

As their name implies, non-specific lipid transfer proteins (nsLTPs) can transfer phospholipids across plasma membranes for various purposes. They are small, soluble, cysteine rich, have usually a MW smaller than 10 kDa, eight cysteine residues and an N-terminal signal peptide (Kader 1996). In total, there were 79 nsLTPs found in Arabidopsis thaliana (Edstam *et al.,* 2011), which were categorised into seven different classes including 12 LTP1, 13 LTP2, 12 LTPd proteins and 34 LTPg proteins (nsLTPs containing a GPI anchor; Salminen *et al.*, 2016). The authors classified DIR1 as an LTPd protein, which share their disulphide pattern with the LTP2 proteins and are important for systemic resistance signalling, cuticular wax accumulation and are involved in nodule development. While the nsLTPs are generally alkaline proteins, DIR1 is an exception as its theoretical isoelectric point is 4.25. Also all five EC1 proteins from *A. thaliana* have acidic isoelectric points (4.94, 4.34, 4.61, 4.44 and 4.46), while EC1.2 is the most acidic. The EC1 proteins belong to the family of ECA1 gametogenesis-related proteins, which were suggested to have evolved from the nsLTPs (Sprunck *et al.*, 2014). Taken all this into account, the nsLTP DIR1 was chosen as a template for homology modelling of EC1.2.

The theoretical folding energy plot for the homology model of EC1.2, using the nsLTP DIR1 as a template, assesses the model as resilient over the main part of the sequence. Interestingly, the missing disulphide bridge at the C-terminus of EC1.2 is destabilising the protein compared to DIR1, which contains four disulphide bridges. The disulphide bridge lacking in EC1.2 forms the bottom of the hydrophobic cavity in the DIR1 protein and this task is now fulfilled by the prolonged C-terminus of EC1.2. The three amino acids at the C-terminus (Val-Lys-Leu) are hydrophobic and close the cavity at the end. The possibility of two lipids binding to the hydrophobic cavity of EC1.2 suggests that EC1.2 proteins may facilitate phospholipid transfer between membranes, like reported for nsLTPs (DeBono *et al.,* 2009; Guo *et al.,* 2013).

Interestingly, the localisation of the EC1 signature motifs S1 and S2 in the 3D homology model of EC1.2 suggests that they may perform completely different tasks. While S2 covers a large part of the hydrophobic cavity, S1 is localised to a large loop at the edge of EC1.2, facing away from the large tunnel entrance. This loop of EC1.2 is three amino acids longer than the loop of DIR1 and shows considerable differences in amino acid composition. While the loop of DIR1 consists of eight amino acids and is relatively hydrophilic (KENPTSPS), the loop of EC1.2 is eleven amino acids long and relatively hydrophobic (LFFLNGETKLG). Considering the sequence conservation of S1 and assuming that the other EC1 proteins show a similar 3D structure, the loops of EC1.1 to EC1.4 are of the same length and nearly identical in sequence, while the loop of EC1.5 is eight amino acids longer. In summary, from 3D homology modelling it can be speculated that the loops of the S1 signature motifs are responsible for specific recognition of their interaction partner(s) and

the S2 signature motif is very likely important for lipid binding, as it is located to the core part of the hydrophobic cavity. This is supported by the fact that the TAMRA labelled S2 peptide does bind to the vegetative cell membrane and to membranes of released sperm cells.

In summary, it is not unlikely that EC1 proteins transport lipids from the egg cell to the sperm cell plasma membrane and/or interact with the sperm cell plasma membrane. In addition, it is hypothesized that the ECA1 gametogenesis-related proteins fulfil a similar variability of molecular functions, as shown for the nsLTP proteins.

5.8 Model of EC1 function

Despite the fact that EC1 promotes sperm cell activation, little was known about the activating mechanism or direct downstream effects of EC1 until now. In the present work, it could be shown that the EC1.1 signature peptide S2 can bind to sperm cell membranes and that the corresponding sequence covers a part of the hydrophobic cavity in the homology model. Furthermore, EC1.2-myc-HIS expressed in Pichia pastoris can bind the phospholipid lysoPC that is commonly used for binding assays of nsLTP from various species (Guerbette et al., 1999). The complex of lysoPC and EC1.2-myc-HIS was strong enough to allow a co-purification indicating a high binding constant. Additionally, the EC1.1 peptides induce exo- and endocytosis in sperm cells. More precisely, they induce a shift of HAP2-YFP from the endomembrane system to the plasma membrane of sperm cells and a decrease of membrane-localised TET9-GFP signal at the site where two sperm cells adhere to each other. These observations were characterised as sperm cell activation and could partially be mimicked by treatment with cGMP derivates, indicating that the signalling pathway leading to sperm cell activation is connected with cGMP signalling. Last but not least, it was shown that EC1 is required for sperm cell attachment. Sperm cells localise to the micropyle after fertilisation abortion in ovules of the quintuple *ec1-RNAi* mutant and were not attached to the female gametes.

The egg cell-secreted EC1 protein may have an interaction partner/receptor presented on the sperm cell surface or it may interact directly with the sperm cell plasma membrane. Possible mechanisms of EC1 action on sperm cells are represented schematically in Figure 5.1, which are supported by the research findings in the present work. It is possible that the EC1 proteins bind to a specific but unknown receptor in the sperm cell plasma membrane. The specificity may be given by the conserved S1 signature motif, which is not part of the hydrophobic pocket, or by a hydrophobic molecule that is transferred from the egg cell (I). As a second option, the EC1 interaction partner may also be a ligand-gated ion channel or transporter that allows ion to pass

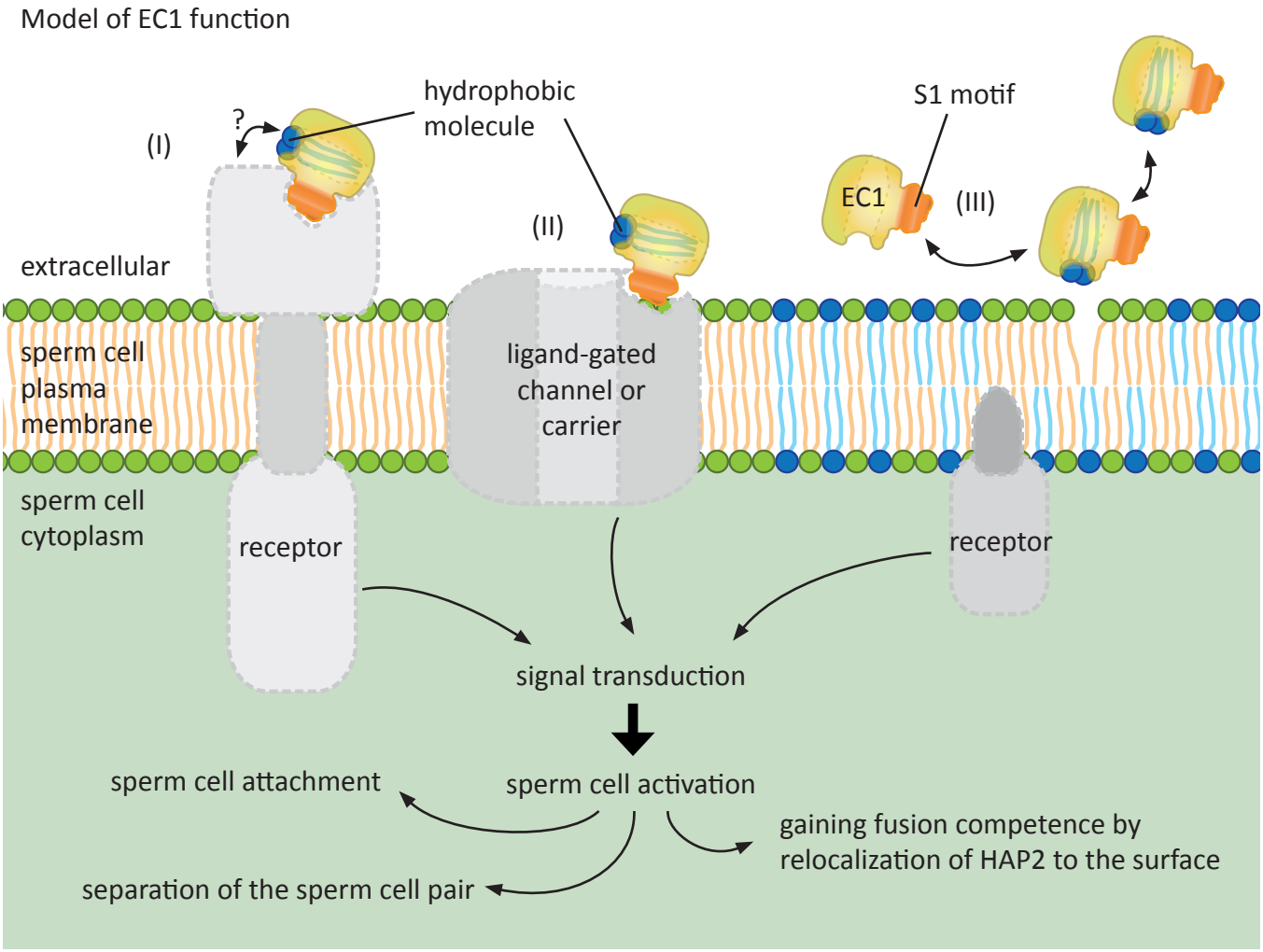

Figure 5.1 Model showing possible molecular functions of EC1 proteins.
EC1 proteins activate the sperm cells via a yet unknown mechanism. However, findings of this work suggest the following mechanisms: (I) With the conserved signal motif S1, which is not part of the hydrophobic pocket, a EC1 protein binds specifically to an unknown receptor located to the sperm cell plasma membrane. A lipid component, incorporated in the hydrophobic pocket of EC1 may play a role in interaction with the receptor. Afterwards, the activated receptor induces signal transduction resulting in sperm cell activation including sperm cell attachment, separation of the sperm cell pair and gain of fusion competence. (II) With the conserved signal motif S1, the EC1 protein binds specifically to a channel or transporter protein located to the sperm cell plasma membrane. Influx or efflux of ions induces signal transduction resulting in sperm cell activation. (III) The EC1 protein either shuffles phospholipids into or out of the plasma membrane. Local changes in membrane lipid composition are recognized by an unknown receptor. Signal transduction is induced by the receptor, which finally leads to sperm cell activation. During sperm cell activation exo- and endocytosis is induced, resulting in the relocalization of the fusion protein HAP2 from the endomembrane system to the plasma membrane and in the initiation of sperm cell separation.

through and thereby inducing sperm cell activation (II). Last but not least, it is also possible that EC1 proteins shuffle special lipids from or to the sperm cell plasma membrane and thus locally changes the membrane composition, generating fusogenic membrane patches (III). These alterations could be recognized by an unidentified receptor, which induces signal transduction in the sperm cells. No matter how the signal transduction is induced, it results in sperm cell activation, which includes sperm cell attachment, very likely to separation of sperm cells and to relocalisation of the fusogen HAP2 to the surface of the sperm cells. After the sperm cells are activated, they can fuse with both female gametes resulting in double fertilisation.

6. MATERIAL & METHODS

6.1 Instruments

6.1.1 Software

Software	Version/ usage date	References
Adobe Illustrator	CS6	Adobe Systems
Adobe InDesign	CS6	Adobe Systems
Adobe Photoshop	CS6	Adobe Systems
CFSSP	June 2017	Chou and Fasman 1974
Chimera	1.11.2	Pettersen *et al.,* 2004
CLC main workbench	6.9	CLC bio
GOR	June 2017	Garnier *et al.,* 1996
IBM SPSS Statistics	22	IBM
ImageJ	1.50h	Schneider *et al.,* 2012
Microsoft Excel	2010	Microsoft
Microsoft Word	2010	Microsoft
NetNGlyc	1.0	Blom *et al.,* 2004
NetOGlyc	4.0	Steentoft *et al.,* 2013
PSIRED	June 2017	Jones 1999
Scratch Protein Predictor	June 2017	http://scratch.proteomics.ics.uci.edu
Unicorn	7.1	GE Healthcare
UniProt	July 2017	Consortium 2017

6.1.2 Microscopes

Microscope	Stage	Objectives
Fluorescence microscope	Zeiss Axioskop	Plan-NEOFLUAR 10x/0.30 Ph2 Plan-NEOFLUAR 40x/0.75 EC- Plan-NEOFLUAR 40x/1.3 OIL DIC Plan-NEOFLUAR 63x/1.25 OIL Plan-NEOFLUAR 100x/1.30 OIL
Inverse fluorescence microscope	Nikon Eclipse TE200-S	Plan Fluor 4x/0.13 LWD 20x/0.40 Plan Fluor 20x/0.45 LWD 40x/0.55 Plan Fluor 40x/0.60
Inverse, confocal laser scanning microscope	Leica SP8	HC PL FLUOTAR 10x/0.30 DRY HC PL FLUOTAR L 20x/0.40 DRY HC PL APO CS2 20x/0.75 IMM HC PL APO CS2 40x/1.30 OIL HC PL APO CS2 63x/1.40 OIL HC PL APO CS2 63x 1.30 GLYC
Inverse, confocal spinning disc microscope	Leica DMi8 Visitron (SD)	HC PL APO 20x/0.80 HCX PL APO 20x/1.00 W HC PL APO 40x/1.10 W CORR CS2 HC PL APO63x/1.20 W CORR CS2 HC PL APO 63x/1.40-0.60 OIL

6.1.3 Other equipment

Equipment	Properties	Company
ÄKTA pure		GE Healthcare
Amicon® Ultra Centrifugal filters	3 kDa, 10 kDa	Millipore
Steritop sterile filter for *Pichia pastoris*	GV PVDF; 0.22 µm	Millipore
Stirred cell	8400	Millipore
Ultrafiltration discs	PLGC, 76 mm, 10 kDa	Millipore
Size exclusion chromatography column	Superdex 200 10/300 GL	GE Healthcare
Size exclusion chromatography column	Superdex 200 10/300 increase	GE Healthcare

6.2 Material

All chemicals and reagents used in this work had molecular grade or p.a. (pro analysis) grade purity.

6.2.1 Media, Chemicals, Enzymes and Antibodies

Material	Company
MS medium (M0255)	Duchefa Biochemie
PhytoAgar	Duchefa Biochemie
8-Br-cGMP	Sigma Aldrich
8-pCPT-cGMP	BIOLOG Life Science Institute
Cellulase	Worthington
Pectolyase Y23	Duchefa Biochemie
anti-myc (mouse)	Sigma Aldrich
anti-EC1.2 (rabbit)	Pineda Antikörper Service; Epitope: CWPAMLTSLGFTSDETNVLR
anti-mouse IgG-HRP	Sigma Aldrich
anti-rabbit IgG-HRP	Sigma Aldrich

6.2.2 Oligonucleotides

Oligo	Sequence
MEO_050	AATGCCTTCACCATGATTGG
MEO_095	TTGTTCTAGAAATTAAAGTTTCACAGAGGAAGGCGCCG
MEO_096	GCTGCAGGAATTCGCACCCTCCCGGAGACGGAAGATTCCACA
MEO_116	GCTGCAGGAATTCGCTGGAGTCATCCCCAATTTGAAAAGGACGATGACGATAAACTCCCGGAGACGGAAGAT
MEO_117	GCTGCAGGAATTCGCCGTAGAAGACGTAGAGACGATGACGATAAACTCCCGGAGACGGAAGAT
MEO_118	TTGTTCTAGAAATTACTTTTCAAATTGGGGATGACTCCAACTGCCACGGGGAACTAGAAGTTTCACAGAGGAAGGCG
MEO_119	TTGTTCTAGAAATTATCTACGTCTTCTACGACTGCCACGGGGAACTAGAAGTTTCACAGAGGAAGGCGCCG
MEO_120	GCTGCAGGAATTCTCCCGGAGACGGAAGATTCCACA
MEO_121	GATCCGAGACGGCCGGCTGGGCCAAGTTTCACAGAGGAAGGCG
MEO_122	GCTGCAGGAATTCGCTGGAGTCATCCCCAATTTGAAAAGGACGATGACGATAAACGCACCCTCCCGGAGAC
MEO_123	GCTGCAGGAATTCGCCATCATCATCATCATCATGACGATGACGATAAACGCACCCTCCCGGAGAC
DD31promfwd	GGATTACCATGTCGGACCGGAC
DD65p-118FW	CCACGACTTAGAATGTTCATGCATTG
CNGC9ap_FW	CACCTCCACTGTTTCCAGAGTCTTATGAACCG
CNGC9ap_REV	GCTTTTTCCTTGTGACTCAACTCATGAAT
CNGC10p_FW	CACCTGCAAAATTCAAGATTAGTATTAAGTCAATTTC
CNGC10p_REV	GCCAAACCCTTGTATATTTCAACTG

6.2.3 Plasmids

Plasmid	Provided by	Comment
pENTR-tagRFP-T-REM	F. Vogler	
pEC1.1-GW	T. Hackenberg	
pEC1.1p:tagRFP-T-REM	M. Kammerer	LR reaction of pENTR-tagRFP-T-REM and pEC1.1-GW
pHDD31p:EC1.1-GFP	M. Kammerer	
pHDD65p:EC1.1-GFP	M. Kammerer	
pBPUM14p-GW-GFP	M. Martón	
pHCNGC9ap:NLS3xGFP	M. Kammerer	
pHCNGC10p:NLS3xGFP	M. Kammerer	
pBEC1.1p:EC1.1-GFP_pAt2S3p:eGFP	T. Hackenberg	eGFP in seed coat
pBDD31p:EC1.1-GFP_pAt2S3p:eGFP		
pBDD65p:EC1.1-GFP_pAt2S3p:eGFP		
pBPUM14p:EC1.1-GFP_pAt2S3p:eGFP		
pPICZαB	Invitrogen™	secreted protein expression in *P. pastoris*
pPICZαB_StrepII-E-(-2)EC1.2		
pPICZαB_StrepII-E-EC1.2		
pPICZαB_PolyR-E-(-2)EC1.2		
pPICZαB_HIS-E-EC1.2		
pPICZαB_EC1.2-T-StrepII		
pPICZαB_EC1.2-T-PolyR		
pPICZαB_EC1.2-T-myc-HIS		
pPICZαB_EC1.2-P-myc-HIS		
pPICZαB_EC1.2-linker-myc-HIS		
pPICZαB_EC1.2-myc-HIS	I. Fuchs	
pPICZαB_EC1.1-myc-HIS	S. Alter	

6.2.4 Peptides

Peptide	Sequence	Company
TAMRA-S1	TAMRA-CSGELILFFLNGETYIGPG	Centic Biotec, Weimar
TAMRA-S2	TAMRA-CWPTMIGVLGFTAQEGDMLQGY	

6.2.5 Bacteria and yeast strains

Strain	Organism	Company
DH5α	*E. coli*	
DB3.1	*E. coli*	
C58	*A. tumefaciens*	
GV3101 (pMP90, pSOUP)	*A. tumefaciens*	
X-33	*P. pastoris* wild type	Invitrogen™
$SuperMan_5$	*P. pastoris*	BioGrammatics, Inc.

6.3 Plant work and cell biological methods

6.3.1 Plant growth conditions

Arabidopsis thaliana (ecotype *Columbia-0* [*Col-0*]) seeds were stratified for 2 days at 4 °C in the dark. Plants were grown on soil or on plates under a short-day photoperiod (8 h of light, 22 °C, 70% humidity) for 6–8 weeks, followed by a long-day photoperiod (16 h of light, 22 °C, 70% humidity).

6.3.2 Sterile seeds on plates

To select for transgenic plants, seeds were surface-sterilised by washing twice with 70% Ethanol, 0.1% Triton X-100 for 10 minutes, followed by washing twice with 96% Ethanol for 10 minutes and subsequent washing twice with water. Seeds were resuspended in sterile water and spilled on plates containing MES buffered half-strength MS medium, 2% sucrose, pH 5.7, a suitable antibiotic and solidified with 1% PhytoAgar. Plates were stratified for 2 days at 4 °C in the dark and seedlings were transferred to soil 10–14 days after sowing.

6.3.3 Emasculation of flowers

For emasculation an *A. thaliana* inflorescence, still connected to the plant, was fixed on a double sided sticky tape on an objective glass slide under a stereomicroscope. All siliques, open flowers and buds that show white petals were removed. The 2–3 oldest buds were opened and anthers, sepals and petals were cut off. The plants were put back into growth chambers for 2–3 days for the pistils to maturate.

6.3.4 Sperm cell release

To release sperm cells from pollen tubes emasculated pistils were put on a sticky tape under a stereomicroscope and hand-pollinated with pollen from freshly opened anthers. The pollinated pistils were cut approx. 100 µm under the style and placed upright on a plate containing solid pollen germination media (PGM; 10 µM 24-epibrassinolide, 18% sucrose, 0.01% boric acid, 1 mM $MgSO_4$, 1 mM $CaCl_2$, 1 mM $Ca(NO_3)_2$ and 0.5% low melting point agarose) for 60–90 min until the pollen germinated. To let the pollen tubes grow through the tissue, the pistils were transferred

to the surface of a drop of liquid PGM on a cavity slide until the pollen tubes grow out of the cut surface and into the PGM in 60–90 minutes. To release the sperm cells the pistils were one by one transferred into a drop of solution of interest on an objective glass slide and the pollen tubes were cut off with a razor blade. The pistils were removed that only sperm cells and pollen tube tips remain in the solution. A cover slip was mounted and the sperm cells were analysed at a confocal laser scanning microscope or a spinning disc microscope.

6.3.5 Hand-pollination

To cross plants or observe fertilisation at the microscope, mature emasculated pistils were hand-pollinated with pollen from freshly opened anthers by dabbing the anthers on the stigma under a stereomicroscope with the help of forceps.

6.3.6 Preparation of ovules

To prepare ovules a flower or flower bud was put on an objective glass slide under a stereomicroscope. The petals, sepals and anthers were removed and the pistil was cut longitudinally along both sides of the septum using a hypodermic needle. The pistil was turned by 180 ° and cut again longitudinally along both sides of the septum. For microscopy of ovules the pistil was then transferred into a drop of buffer (100 mM sodium phosphate buffer, pH 7.5). The stigma and pedicel was cut off and the carpels were removed. The septum with the attached ovules was teared longitudinally in two pieces.

6.4 Molecular biology methods

Standard methods of molecular biology were performed as described in Sambrook *et al.,* 1989 using molecular grade reagents.

6.4.1 Purification of genomic DNA from *Arabidopsis thaliana*

The protocol was modified after Richards *et al.,* 2001. 1 g leaf tissue was grinded in a precooled mortar with liquid N2 and added to 5 ml CTAB buffer (2% CTAB, 1% polyvinyl pyrrolidone, 1.4 mM NaCl, 20 mM EDTA, 100 mM Tris, pH 8.0) preheated to 60 °C. The plant tissue was incubated for 30 min at 60 °C with regular mixing followed by addition of 1 volume phenol:chlorophorm:isoamylalcohol (25:24:1). After centrifugation for 10 min at 5,000 x g at 4 °C, the supernatant was transferred to 5 µl RNase A (10 mg/ml) and incubated for 30 min at 37 °C and 5 min at 4 °C. The DNA was precipitated with 0.6 volumes of ice cold (-20 °C) isopropanol, incubated at -20 °C overnight and centrifuged for 10 min at 12 x g at 4 °C. The DNA pellet was washed twice with 70% ethanol, air dried and dissolved in 200 µl TE, pH 8.0.

6.4.2 Polymerase chain reaction (PCR)

Reaction mix		
2.5	µl	10X Taq buffer + KCl
1.5	µl	$MgCl_2$ (25 mM)
0.5	µl	dNTPs (10 mM)
0.5	µl	Primer forward (10 µM)
0.5	µl	Primer reverse (10 µM)
0.5	µl	Taq DNA Polymerase (1U/µl)
10 pg - 1 µg		Template
ad 25	µl	H_2O

Steps	Temp. ° C	Time	Cycles
Initial denaturation	95	5 min	1
Denaturation	95	30 s	
Annealing	T_m –5	30 s	25–35
Extension	72	1 min/kb	
Final Extension	72	10 min	1

The number of cycles varied depending on the amount of template.

6.4.3 Restriction endonuclease digestion

Digestions were performed according to manufacturer's instructions (NEB; Fermentas) using the following typical reaction conditions.

Reaction mix		
1	µg	DNA
5	µl	10X buffer
1	µl	Restriction enzyme
ad 50	µl	H_2O

Incubation	
Time	1 hour
Temperature	Enzyme dependent

6.4.4 Ligation with Rapid DNA Dephos & Ligation Kit

Ligation was performed according to manufacturer's instructions (Roche).

6.4.5 Cloning with Gateway® technology

Cloning was performed according to manufacturer's instructions (Invitrogen). This included creation of entry vectors using the pENTR/D-TOPO® cloning kit and creation of expression vectors using the LR Clonase® enzyme mix.

6.5 Microbiology methods

6.5.1 Generation of transgenic *Arabidopsis thaliana*

6.5.1.1 Media recipes

	LB	$LB_{lowsalt}$	YEP
Yeast extract	0.5%	0.5%	1%
Peptone			1%
Tryptone	1%	1%	
NaCl	1%	0.5%	1%
Agar	± 2%		

6.5.1.2 Transformation of E. coli

100 µl of chemically competent cells were thawed on ice and added to 1 µg of Plasmid DNA. The cells were transformed by incubation on ice for 60 min, in a 42 °C water bath for 2 min and on ice for 2 more minutes. After addition of 800 µl LB media, the cells were horizontally shaken for 45 min at 300 rpm at 37 °C and spread on plates containing solid LB media with suitable antibiotics.

6.5.1.3 Transformation of Agrobacterium tumefaciens

100 µl of chemically competent cells were thawed on ice and added to 1 µg of Plasmid DNA. The cells were transformed by incubation on ice for 30 min followed by 1 min in liquid N_2 and thawed in a 37 °C water bath for several minutes. After addition of 800 µl YEP media, the cells were horizontally shaken for 2–3 h at 300 rpm at 28 °C and spread on plates containing solid YEP media with suitable antibiotics.

6.5.1.4 Transformation of Arabidopsis thaliana

The floral dipping method was modified after Clough and Bent 1998.

Agrobacteria were grown overnight at 28 °C in 5 ml YEP media preculture followed by 500 ml YEP media culture, containing suitable antibiotics. The cells were harvested for 15 min at 5,000 x g at room temperature and resuspended carefully in 500 ml H_2O with 3% sucrose and 0.07% Silwet L-77. For transformation the inflorescences, containing numerous unopened floral buds, of an *A. thaliana* plant were dipped into the Agrobacteria solution for 2 min. To create a humid atmosphere for the Agrobacteria to grow, the plant was covered with a transparent plastic bag for two days. After 2–3 weeks, the seeds were dried and harvested.

6.5.2 Expression of recombinant proteins in *Pichia pastoris*

The method was modified after the EasySelect™ *Pichia* Expression Kit (Invitrogen).

6.5.2.1 Media recipes

	YPD	YPDS	MGY	MM	BMG	BMM	BMGY	BMMY
Yeast extract	1%	1%					1%	1%
Peptone	2%	2%						
Dextrose	2%	2%						
Sorbitol		1 M						
YNB			1.34%	1.34%	1.34%	1.34%	1.34%	1.34%
Glycerol			1%		1%		1%	
Biotin			0.04 ‰	0.04 ‰	0.04 ‰	0.04 ‰	0.04 ‰	0.04 ‰
Methanol				0.5%		0.5%		0.5%
K phosphate, pH 6.0					0.1 M	0.1 M	0.1 M	0.1 M
Zeocin®	± 2%							
Agar	± 2%							

6.5.2.2 Transformation of Pichia pastoris by electroporation

To prepare *Pichia* for electroporation, the yeast was grown in 5 ml of YPD in a 50 ml conical flask at 30 °C overnight. 500 ml of fresh medium in a 2 litre flask were inoculated with 0.1–0.5 ml of the overnight culture and grown overnight to an OD600 = 1.3–1.5. The cells were washed multiple times by centrifugation for 5 min at 1,500 x g at 4 °C followed by resuspension in 500 ml and 250 ml of ice-cold, sterile H2O as well as 20 ml and 1.5 ml of ice-cold 1 M sorbitol respectively. The cells were kept on ice and used the same day.

For transformation 80 µl of cells were mixed with 5–10 µg of linearized DNA (in 5–10 µl sterile water), transferred to an ice-cold 0.2 cm electroporation cuvette and incubated on ice for 5 min. The cells were pulsed with the GenePulser™ (1.25 V; 200 Ω; 25 µFD) and diluted immediately with 1 ml of ice-cold 1 M sorbitol. The cells were transferred to a sterile 15-ml tube and incubated for 1–2 h at 30 °C without shaking. The cells (10, 25, 50, 100 and 200 µl each) were spread on YPDS plates containing 100 µg/ml Zeocin®. After 3–10 days of incubation at 30 °C, 10–15 colonies were tested.

6.5.2.3 Cultivation of Pichia

A single colony was used to inoculate 25 ml (or 250 ml) of MGY (Minimal Glycerol Medium), BMG (Buffered Minimal Glycerol) or BMGY (Buffered Glycerol-complex Medium) medium in a 250 ml baffled flask. The cells were grown overnight at 30 °C at 200 rpm until the culture reached an OD600 = 2–6 and the cells were in log-phase growth. The cells were harvested by centrifugation at 2,000 x g for 5 min at room temperature. The cells were resuspended to an OD600 = 0.9 in 100 ml in a 1 litre baffled flask (or 1,000 ml in a 5 litre baffled flask) MM (Minimal Methanol Medium), BMM (Buffered Minimal Methanol) or BMMY (Buffered Methanol-complex Medium) medium to induce expression. The cells were grown overnight (22–24 h) at 30 °C at 200 rpm.

6.5.3 Purification of recombinant proteins expressed in *Pichia pastoris*

6.5.3.1 Preparation and concentration

The cells were centrifuged at 3,500 x g and the supernatant, containing the secreted recombinant proteins, was filter sterilised at room temperature. The proteins were concentrated in the cold-room at 4 °C using a stirred cell and ultrafiltration membrane discs with a nominal molecular weight limit (NMWL) of 3, 10 or 100 kDa, respectively.

6.5.3.2 Isolation via affinity tags

Proteins with a HIS tag, a StrepII tag or a PolyR tag were purified via affinity chromatography using batch and gravity flow columns, respectively. Different chromatography media were used according to manufacturer's instructions. However, a standard procedure and buffer compositions for each tested media are described in the following.

1 litre sterile protein supernatant (sample crude) was concentrated to 100 ml (sample conc) as described above, while the flow through of the ultrafiltration was collected, too (sample FT conc). A gravity flow column with a volume of 100 ml was packed with 2 ml chromatography media of choice and equilibrated with the corresponding buffer. The protein was loaded onto the column and emptied by gravity flow (sample FT). The column was washed 3 times with 5 ml wash buffer and emptied by gravity flow (sample Wash). The protein was eluted 6 times with 1.5 ml elution buffer each (samples E1–E6). The column was regenerated according to manufacturer's instructions.

Wash buffer (W) Elution buffer (E) Concentrations in mM	Ni-NTA agarose (Qiagen)		HIS-Select® HF (Sigma Aldrich)		TALON® (Clontech)		Ni-Sepharose (GE Healthcare)		Streptactin Sepharose HP (GE Healthcare)		Strep-Tactin Superflow Plus (Qiagen)		SP Sepharose HP (GE Healthcare)	
	W	E	W	E	W	E	W	E	W	E	W	E	W	E
NaCl	300		300		300		500		150		300			500
Imidazole	15	250	10	250	10	100	20	500						
Sodium phosphate buffer	50		50		50		20				50			
Tris-HCl									100				50	
EDTA									1					
Desthiobiotin										2.5		2.5		
pH	8.0		8.0		7.0		7.4		8.0		8.0			

6.5.3.3 Polishing via size exclusion chromatography

The ÄKTA pure (GE Healthcare) system was handled according to manufacturer's instructions. All liquids were filter sterilised and vented shortly before usage. The system and the column "Superdex 200 10/300 GL" was first equilibrated in H_2O and then in 200 mM NaCl, 25 mM Tris/HCl, pH 7.5 at room temperature. The protein sample was filtered using Corning® Costar® Spin-X® centrifuge tube filters and loaded manually in a 500 µl sample loop with a 1 ml syringe. The separation of proteins was performed at a flow rate of 0.5 ml/min and monitored at a wavelength of 280 nm. The eluate was collected in 500 µl fractions. Afterwards the column was equilibrated in H_2O and stored in 20% EtOH.

6.5.4 Gel electrophoresis and Western blotting

6.5.4.1 Protein precipitation with DOC/TCA

18 µl of 2% DOC was added to 1.8 ml protein sample and incubated on ice for 30 min. For precipitation 200 µl trichloroacetic acid was added, vortexed immediately for 30 sec and the sample was freezed at –20 °C for at least 1 h. The precipitated proteins were pelleted by centrifugation at 14,000 x g for 15 min at 4 °C. The pellet was washed twice with 1 ml acetone, dried and resolved in 1X sample buffer (2% SDS, 5% glycerol, 5% β-mercaptoethanol, 0.01% bromophenol blue, 0.8% DTT and 63 mM Tris-HCl, pH 6.8).

6.5.4.2 Tris/Tricine SDS-PAGE

Protein samples were separated by Tris/Tricine SDS-PAGE, modified after Schägger and von Jagow 1987.

	Separating gel	**Stacking gel**
acrylamide/bisacrylamide	12%	18.5%
Tris-HCl, pH 8.45	1 M	0.75 M
SDS	0.1%	0.075%
Glycerol	9.3%	
APS	0.1%	0.1%
TEMED	0.4 ‰	0.4 ‰

Tris/Tricine SDS running buffer	
Tris	100 mM
Tricine	100 mM
SDS	0.1%

6.5.4.3 Silver stain

Silver stain method was modified after Switzer III *et al.,* 1979.

Step 1: Gel was fixed in 40% ethanol, 12% acetic acid and 0.02% formaldehyde for at least 20 min. *Step 2*: Gel was washed twice with 50% ethanol and once with 30% ethanol for 10 min each. *Step 3*: Gel was pretreated with 0.02% sodium thiosulfate for 1 min and rinsed three times with water. *Step 4*: Gel was impregnated with 0.2% silver nitrate and 0.03% formaldehyde for 20 min and rinsed three times with water. *Step 5*: Gel was developed with 6% sodium carbonate, 0.02% formaldehyde and 0,4 ‰ sodium thiosulfate for 1 sec to 10 min until staining was sufficient. Staining was stopped by addition of citric acid in powder form until development of gas stopped. *Step 6*: Gel was washed in water three times for 10 min each.

6.5.4.4 Western blotting

Western blotting was performed after Burnette 1981.

The membrane with proteins was incubated in blocking solution (3% milk powder in TBST) for at least 60 min. Afterwards the membrane was incubated with the primary antibody at a typical dilution of 1:3000 in blocking solution for at least 4 hours. After three washing steps in TBST, the membrane was incubated with the secondary antibody fused to horse radish peroxidase at a dilution of 1:500 in blocking solution for 2 hours followed by three more washing steps in TBST. The detection of the secondary antibody was performed via chemoluminescence signals from the ECL Western Blotting Substrate (Pierce) on the FluorChem®FC2 MultiImage®II (Alpha Innotech).

6.5.5 NMR spectroscopy

NMR spectroscopy was performed by Prof. Dr. Werner Kremer at the Institute of Biophysics and physical Biochemistry at the University of Regensburg.

Figure 6.1 shows an example of a 2D-TOCSY spectra, where the areas of typical expected signals are marked with rectangles. This scheme was used as a reference for the 2D-TOCSY spectra that were analysed in the present work.

7. BIBLIOGRAPHY

Ahmad, M., Hirz, M., Pichler, H. & Schwab, H., (2014). Protein Expression in Pichia pastoris: Recent Achievements and Perspectives for Heterologous Protein Production. *Applied microbiology and biotechnology* **98**, 5301-5317

An, L.-H. & You, R.-L., (2004). Studies on Nuclear Degeneration During Programmed Cell Death of Synergid and Antipodal Cells in Triticum aestivum. *Sexual plant reproduction* **17**, 195-201

Anfinsen, C. B., (1973). Principles That Govern the Folding of Protein Chains. *Science* **181**, 223-230

Beale, K. M., Leydon, A. R. & Johnson, M. A., (2012). Gamete Fusion Is Required to Block Multiple Pollen Tubes from Entering an Arabidopsis Ovule. *Current Biology* **22**, 1090-1094

Bedinger, P., (1992). The Remarkable Biology of Pollen. *The Plant cell* **4**, 879

Berg, J., Tymoczko, J. & Stryer, L. *Biochemistry*. Vol. 5th edition (2002).

Biasini, M., Bienert, S., Waterhouse, A., Arnold, K., Studer, G., Schmidt, T., Kiefer, F., Cassarino, T. G., Bertoni, M., Bordoli, L. & Schwede, T., (2014). Swiss-Model: Modelling Protein Tertiary and Quaternary Structure Using Evolutionary Information. *Nucleic acids research* **42**, W252-W258

Blom, N., Sicheritz-Pontén, T., Gupta, R., Gammeltoft, S. & Brunak, S., (2004). Prediction of Post-Translational Glycosylation and Phosphorylation of Proteins from the Amino Acid Sequence. *Proteomics* **4**, 1633-1649

Boavida, L. C., Qin, P., Broz, M., Becker, J. D. & McCormick, S., (2013). Arabidopsis Tetraspanins Are Confined to Discrete Expression Domains and Cell Types in Reproductive Tissues and Form Homo- and Heterodimers When Expressed in Yeast. *Plant physiology* **163**, 696-712

Borg, M., Rutley, N., Kagale, S., Hamamura, Y., Gherghinoiu, M., Kumar, S., Sari, U., Esparza-Franco, M. A., Sakamoto, W. & Rozwadowski, K., (2014). An Ear-Dependent Regulatory Module Promotes Male Germ Cell Division and Sperm Fertility in Arabidopsis. *The Plant cell* **26**, 2098-2113

Borges, F., Gomes, G., Gardner, R., Moreno, N., McCormick, S., Feijó, J. A. & Becker, J. D., (2008). Comparative Transcriptomics of Arabidopsis Sperm Cells. *Plant physiology* **148**, 1168-1181

Brewbaker, J. L., (1967). The Distribution and Phylogenetic Significance of Binucleate and Trinucleate Pollen Grains in the Angiosperms. *American journal of botany*, 1069-1083

Bucher, M. H., Evdokimov, A. G. & Waugh, D. S., (2002). Differential Effects of Short Affinity Tags on the Crystallization of Pyrococcus Furiosus Maltodextrin-Binding Protein. *Acta Crystallographica Section D* **58**, 392-397

Burnette, W. N., (1981). "Western Blotting": Electrophoretic Transfer of Proteins from Sodium Dodecyl Sulfate-Polyacrylamide Gels to Unmodified Nitrocellulose and Radiographic Detection with Antibody and Radioiodinated Protein A. *Analytical biochemistry* **112**, 195-203

Cass, D., Peteya, D. & Robertson, B., (1986). Megagametophyte Development in Hordeum vulgare. 2. Later Stages of Wall Development and Morphological Aspects of Megagametophyte Cell Differentiation. *Canadian journal of botany* **64**, 2327-2336

Cereghino, J. L. & Cregg, J. M., (2000). Heterologous Protein Expression in the Methylotrophic Yeast Pichia pastoris. *FEMS Microbiology Reviews* **24**, 45-66

Chae, K., Gonong, B. J., Kim, S.-C., Kieslich, C. A., Morikis, D., Balasubramanian, S. & Lord, E. M., (2010). A Multifaceted Study of Stigma/Style Cysteine-Rich Adhesin (SCA)-Like Arabidopsis Lipid Transfer Proteins (LTPs) Suggests Diversified Roles for These LTPs in Plant Growth and Reproduction. *Journal of experimental botany* **61**, 4277-4290

Chan, M. C. W., Chan, R. W. Y., Yu, W. C. L., Ho, C. C. C., Yuen, K. M., Fong, J. H. M., Tang, L. L. S., Lai, W. W., Lo, A. C. Y., Chui, W. H., Sihoe, A. D. L., Kwong, D. L. W., Wong, D. S. H., Tsao, G. S. W., Poon, L. L. M., Guan, Y., Nicholls, J. M. & Peiris, J. S. M., (2010). Tropism and Innate Host Responses of the 2009 Pandemic H1N1 Influenza Virus in Ex Vivo and In Vitro Cultures of Human Conjunctiva and Respiratory Tract. *The American Journal of Pathology* **176**, 1828-1840

Chen, Y.-H., Li, H.-J., Shi, D.-Q., Yuan, L., Liu, J., Sreenivasan, R., Baskar, R., Grossniklaus, U. & Yang, W.-C., (2007). The Central Cell Plays a Critical Role in Pollen Tube Guidance in Arabidopsis. *The Plant cell* **19**, 3563-3577

Chernomordik, L. V. & Kozlov, M. M., (2005). Membrane Hemifusion: Crossing a Chasm in Two Leaps. *Cell* **123**, 375-382

Cheung, A. Y. & Wu, H.-M., (2016). LURE Is Bait for Multiple Receptors. *Nature* **531**, 178-181

Chou, P. Y. & Fasman, G. D., (1974). Prediction of Protein Conformation. *Biochemistry* **13**, 222-245

Christensen, C. A., King, E. J., Jordan, J. R. & Drews, G. N., (1997). Megagametogenesis in Arabidopsis Wild Type and the Gf Mutant. *Sexual plant reproduction* **10**, 49-64

Clough, S. J. & Bent, A. F., (1998). Floral Dip: A Simplified Method for Agrobacterium-Mediated Transformation of Arabidopsis thaliana. *The Plant journal for cell and molecular biology* **16**, 735-743

Connerth, M., Tatsuta, T., Haag, M., Klecker, T., Westermann, B. & Langer, T., (2012). Intramitochondrial Transport of Phosphatidic Acid in Yeast by a Lipid Transfer Protein. *Science* **338**, 815-818

Consortium, U., (2017). Uniprot: The Universal Protein Knowledgebase. *Nucleic acids research* **45**, D158-D169

Cowan-Jacob, S. W., Ramage, P., Stark, W., Fendrich, G. & Jahnke, W. In *Protein Tyrosine Kinases: From Inhibitors to Useful Drugs* (eds Doriano Fabbro & Frank McCormick) 187-230

DeBono, A., Yeats, T. H., Rose, J. K., Bird, D., Jetter, R., Kunst, L. & Samuels, L., (2009). Arabidopsis LTPG is a Glycosylphosphatidylinositol-Anchored Lipid Transfer Protein Required for Export of Lipids to the Plant Surface. *The Plant cell* **21**, 1230-1238

Deeken, R., Saupe, S., Klinkenberg, J., Riedel, M., Leide, J., Hedrich, R. & Mueller, T., (2016). The NsLTP AtLTP1-4 is Involved in Suberin Formation of Arabidopsis thaliana Crown Galls. *Plant physiology*, pp. 01486.02016

DeFalco, T. A., Moeder, W. & Yoshioka, K., (2016). Opening the Gates: Insights into Cyclic Nucleotide-Gated Channel-Mediated Signaling. *Trends in Plant Science* **21**, 903-906

del Campo, J. J., Opoku-Serebuoh, E., Isaacson, A. B., Scranton, V. L., Tucker, M., Han, M. & Mohler, W. A., (2005). Fusogenic Activity of EFF-1 Is Regulated Via Dynamic Localization in Fusing Somatic Cells of C. elegans. *Current biology* **15**, 413-423

Denninger, P., Bleckmann, A., Lausser, A., Vogler, F., Ott, T., Ehrhardt, D. W., Frommer, W. B., Sprunck, S., Dresselhaus, T. & Grossmann, G., (2014). Male–Female Communication Triggers Calcium Signatures During Fertilization in Arabidopsis. *Nature communications* **5**, 4645

Diboll, A. G. & Larson, D. A., (1966). An Electron Microscopic Study of the Mature Megagametophyte in Zea mays. *American Journal of Botany* **53**, 391-402

Drews, G. N. & Koltunow, A. M., (2011). The Female Gametophyte. *The Arabidopsis book* **62**, e0155

Edstam, M. M., Viitanen, L., Salminen, T. A. & Edqvist, J., (2011). Evolutionary History of the Non-Specific Lipid Transfer Proteins. *Molecular plant* **4**, 947-964

Edstam, M. M., Blomqvist, K., Eklöf, A., Wennergren, U. & Edqvist, J., (2013). Coexpression Patterns Indicate That GPI-Anchored Non-Specific Lipid Transfer Proteins Are Involved in Accumulation of Cuticular Wax, Suberin and Sporopollenin. *Plant molecular biology* **83**, 625-649

Englhart, M., (2012) *Die Rolle Der Gruppe III Pumilios bei der Reproduktion von Arabidopsis thaliana* Master of Science Thesis, Regensburg.

Escobar-Restrepo, J.-M., Huck, N., Kessler, S., Gagliardini, V., Gheyselinck, J., Yang, W.-C. & Grossniklaus, U., (2007). The Feronia Receptor-Like Kinase Mediates Male-Female Interactions During Pollen Tube Reception. *Science* **317**, 656-660

Fédry, J., Liu, Y., Péhau-Arnaudet, G., Pei, J., Li, W., Tortorici, M. A., Traincard, F., Meola, A., Bricogne, G., Grishin, N. V., Snell, W. J., Rey, F. A. & Krey, T., (2017). The Ancient Gamete Fusogen HAP2 is a Eukaryotic Class II Fusion Protein. *Cell* **168**, 904-915.e910

Ferris, P., Woessner, J. & Goodenough, U., (1996). A Sex Recognition Glycoprotein Is Encoded by the Plus Mating-Type Gene FUS1 of Chlamydomonas reinhardtii. *Molecular biology of the cell* **7**, 1235-1248

Fuchs, S. M. & Raines, R. T., (2005). Polyarginine as a Multifunctional Fusion Tag. *Protein Science* **14**, 1538-1544

Gao, Q.-F., Gu, L.-L., Wang, H.-Q., Fei, C.-F., Fang, X., Hussain, J., Sun, S.-J., Dong, J.-Y., Liu, H. & Wang, Y.-F., (2016). Cyclic Nucleotide-Gated Channel 18 Is an Essential Ca^{2+} Channel in Pollen Tube Tips for Pollen Tube Guidance to Ovules in Arabidopsis. *Proceedings of the National Academy of Sciences* **113**, 3096-3101

Garnier, J., Gibrat, J.-F. & Robson, B., (1996). [32] GOR Method for Predicting Protein Secondary Structure from Amino Acid Sequence. *Methods in enzymology* **266**, 540-553

Goochee, C. F., Gramer, M. J., Andersen, D. C., Bahr, J. B. & Rasmussen, J. R., (1991). The Oligosaccharides of Glycoproteins: Bioprocess Factors Affecting Oligosaccharide Structure and Their Effect on Glycoprotein Properties. *Nat Biotech* **9**, 1347-1355

Griesinger, C., Otting, G., Wüthrich, K. & Ernst, R. R., (1988). Clean TOCSY for Proton Spin System Identification in Macromolecules. *Journal of the American Chemical Society* **110**, 7870-7872

Groß-Hardt, R., Kägi, C., Baumann, N., Moore, J. M., Baskar, R., Gagliano, W. B., Jürgens, G. & Grossniklaus, U., (2007). LACHESIS Restricts Gametic Cell Fate in the Female Gametophyte of Arabidopsis. *PLoS biology* **5**, e47

Grossniklaus, U., Vielle-Calzada, J.-P., Hoeppner, M. A. & Gagliano, W. B., (1998). Maternal Control of Embryogenesis by MEDEA, a Polycomb Group Gene in Arabidopsis. *Science* **280**, 446-450

Guerbette, F., Grosbois, M., Jolliot-Croquin, A., Kader, J.-C. & Zachowski, A., (1999). Lipid-Transfer Proteins from Plants: Structure and Binding Properties. *Molecular and Cellular Biochemistry* **192**, 157-161

Guo, L., Yang, H., Zhang, X. & Yang, S., (2013). Lipid Transfer Protein 3 as a Target of MYB96 Mediates Freezing and Drought Stress in Arabidopsis. *Journal of experimental botany* **64**, 1755-1767

Habuchi, S., Tsutsui, H., Kochaniak, A. B., Miyawaki, A. & Van Oijen, A. M., (2008). mKikGR, a Monomeric Photoswitchable Fluorescent Protein. *PloS one* **3**, e3944

Hamamura, Y., Saito, C., Awai, C., Kurihara, D., Miyawaki, A., Nakagawa, T., Kanaoka, M. M., Sasaki, N., Nakano, A., Berger, F. & Higashiyama, T., (2011). Live-Cell Imaging Reveals the Dynamics of Two Sperm Cells During Double Fertilization in Arabidopsis thaliana. *Current biology CB* **21**, 497-502

Hamamura, Y., Nishimaki, M., Takeuchi, H., Geitmann, A., Kurihara, D. & Higashiyama, T., (2014). Live Imaging of Calcium Spikes During Double Fertilization in Arabidopsis. *Nature communications* **5**, 4722

Han, Y.-Z., Huang, B.-Q., Zee, S.-Y. & Yuan, M., (2000). Symplastic Communication between the Central Cell and the Egg Apparatus Cells in the Embryo Sac of Torenia fournieri Lind. Before and During Fertilization. *Planta* **211**, 158-162

Hedhly, A., Vogler, H., Schmid, M. W., Pazmino, D., Gagliardini, V., Santelia, D. & Grossniklaus, U., (2016). Starch Turnover and Metabolism During Flower and Early Embryo Development. *Plant physiology* **172**, pp. 00916

Heinemann, B., Andersen, K. V., Nielsen, P. R., Bech, L. M. & Poulsen, F. M., (1996). Structure in Solution of a Four-Helix Lipid Binding Protein. *Protein Science* **5**, 13-23

Higashiyama, T., Kuroiwa, H., Kawano, S. & Kuroiwa, T., (2000). Explosive Discharge of Pollen Tube Contents in Torenia Fournieri. *Plant physiology* **122**, 11-14

Higashiyama, T., Yabe, S., Sasaki, N., Nishimura, Y., Miyagishima, S., Kuroiwa, H. & Kuroiwa, T., (2001). Pollen Tube Attraction by the Synergid Cell. *Science* **293**, 1480-1483

Higashiyama, T., (2002). The Synergid Cell: Attractor and Acceptor of the Pollen Tube for Double Fertilization. *Journal of Plant Research* **115**, 0149-0160

Higashiyama, T. & Yang, W.-C., (2017). Gametophytic Pollen Tube Guidance: Attractant Peptides, Gametic Controls, and Receptors. *Plant physiology* **173**, 112-121

Hou, Y., Guo, X., Cyprys, P., Zhang, Y., Bleckmann, A., Cai, L., Huang, Q., Luo, Y., Gu, H. & Dresselhaus, T., (2016). Maternal ENODLS Are Required for Pollen Tube Reception in Arabidopsis. *Current Biology* **26**, 2343-2350

Huang, B.-Q. & Russell, S. D., (1992). Female Germ Unit: Organization, Isolation, and Function. *International Review of Cytology* **140**, 233-293

Huang, B.-Q. & Russell, S. D., (1994). Fertilization Innicotiana tabacum: Cytoskeletal Modifications in the Embryo Sac During Synergid Degeneration. *Planta* **194**, 200-214

Huang, J., Ju, Y., Wang, X., Zhang, Q. & Sodmergen. (2015). A One-Step Rectification of Sperm Cell Targeting Ensures the Success of Double Fertilization. *Journal of Integrative Plant Biology* **57**, 496-503

Huang, Q., Dresselhaus, T., Gu, H. & Qu, L. J., (2015). Active Role of Small Peptides in Arabidopsis Reproduction: Expression Evidence. *Journal of Integrative Plant Biology* **57**, 518-521

Huck, N., Moore, J. M., Federer, M. & Grossniklaus, U., (2003). The Arabidopsis Mutant feronia Disrupts the Female Gametophytic Control of Pollen Tube Reception. *Development* **130**, 2149-2159

Igawa, T., Yanagawa, Y., Miyagishima, S.-y. & Mori, T., (2013). Analysis of Gamete Membrane Dynamics During Double Fertilization of Arabidopsis. *Journal of Plant Research* **126**, 387-394

Isner, J. C., Nuhse, T. & Maathuis, F. J., (2012). The Cyclic Nucleotide cGMP is Involved in Plant Hormone Signalling and Alters Phosphorylation of Arabidopsis thaliana Root Proteins. *Journal of experimental botany* **63**, 3199-3205

Jacobs, P. P., Geysens, S., Vervecken, W., Contreras, R. & Callewaert, N., (2009). Engineering Complex-Type N-Glycosylation in Pichia pastoris Using Glycoswitch Technology. *Nature protocols* **4**, 58-70

Jamadagni, S. N., Godawat, R. & Garde, S., (2011). Hydrophobicity of Proteins and Interfaces: Insights from Density Fluctuations. *Annual Review of Chemical and Biomolecular Engineering* **2**, 147-171

Jenny, R. J., Mann, K. G. & Lundblad, R. L., (2003). A Critical Review of the Methods for Cleavage of Fusion Proteins with Thrombin and Factor Xa. *Protein expression and purification* **31**, 1-11

Jensen, W. A., (1964). Observations on the Fusion of Nuclei in Plants. *The Journal of cell biology* **23**, 669

Jones, D. T., (1999). Protein Secondary Structure Prediction Based on Position-Specific Scoring Matrices. *Journal of molecular biology* **292**, 195-202

Joudoi, T., Shichiri, Y., Kamizono, N., Akaike, T., Sawa, T., Yoshitake, J., Yamada, N. & Iwai, S., (2013). Nitrated Cyclic GMP Modulates Guard Cell Signaling in Arabidopsis. *The Plant cell* **25**, 558-571

Kader, J.-C., (1996). Lipid-Transfer Proteins in Plants. *Annual review of plant biology* **47**, 627-654

Kader, J. C., Julienne, M. & Vergnolle, C., (1984). Purification and Characterization of a Spinach-Leaf Protein Capable of Transferring Phospholipids from Liposomes to Mitochondria or Chloroplasts. *The FEBS Journal* **139**, 411-416

Kägi, C., Baumann, N., Nielsen, N., Stierhof, Y.-D. & Groß-Hardt, R., (2010). The Gametic Central Cell of Arabidopsis Determines the Lifespan of Adjacent Accessory Cells. *Proceedings of the National Academy of Sciences* **107**, 22350-22355

Kasahara, R. D., Portereiko, M. F., Sandaklie-Nikolova, L., Rabiger, D. S. & Drews, G. N., (2005). MYB98 Is Required for Pollen Tube Guidance and Synergid Cell Differentiation in Arabidopsis. *The Plant cell* **17**, 2981-2992

Kasahara, R. D., Maruyama, D., Hamamura, Y., Sakakibara, T., Twell, D. & Higashiyama, T., (2012). Fertilization Recovery after Defective Sperm Cell Release in Arabidopsis. *Current Biology* **22**, 1084-1089

Kelly, A. A., Kalisch, B., Hölzl, G., Schulze, S., Thiele, J., Melzer, M., Roston, R. L., Benning, C. & Dörmann, P., (2016). Synthesis and Transfer of Galactolipids in the Chloroplast Envelope Membranes of Arabidopsis thaliana. *Proceedings of the National Academy of Sciences* **113**, 10714-10719

Kessler, S. A., Shimosato-Asano, H., Keinath, N. F., Wuest, S. E., Ingram, G., Panstruga, R. & Grossniklaus, U., (2010). Conserved Molecular Components for Pollen Tube Reception and Fungal Invasion. *Science* **330**, 968-971

Kiyosue, T., Ohad, N., Yadegari, R., Hannon, M., Dinneny, J., Wells, D., Katz, A., Margossian, L., Harada, J. J. & Goldberg, R. B., (1999). Control of Fertilization-Independent Endosperm Development by the MEDEA Polycomb Gene in Arabidopsis. *Proceedings of the National Academy of Sciences* **96**, 4186-4191

Kőszegi, D., Johnston, A. J., Rutten, T., Czihal, A., Altschmied, L., Kumlehn, J., Wüst, S. E., Kirioukhova, O., Gheyselinck, J. & Grossniklaus, U., (2011). Members of the RKD Transcription Factor Family Induce an Egg Cell-Like Gene Expression Program. *The Plant Journal* **67**, 280-291

Kraus, M., (2015) *Subcellular Localization of EC1.1 and its Interacting Phosphatase Subunit PP2ab'ϑ in Arabidopsis thaliana* Bachelor of Science thesis, University of Regensburg.

Krohn, N. G., Lausser, A., Juranić, M. & Dresselhaus, T., (2012). Egg Cell Signaling by the Secreted Peptide ZmEAl1 Controls Antipodal Cell Fate. *Developmental cell* **23**, 219-225

Lalanne, E. & Twell, D., (2002). Genetic Control of Male Germ Unit Organization in Arabidopsis. *Plant physiology* **129**, 865-875

Lascombe, M. B., Buhot, N., Bakan, B., Marion, D., Blein, J. P., Lamb, C. J. & Prange, T., (2006). Crystallization of DIR1, a LTP2-Like Resistance Signalling Protein from Arabidopsis thaliana. *Acta crystallographica. Section F, Structural biology and crystallization communications* **62**, 702-704

Lascombe, M. B., Bakan, B., Buhot, N., Marion, D., Blein, J. P., Larue, V., Lamb, C. & Prange, T., (2008). The Structure of "Defective in Induced Resistance" Protein of Arabidopsis thaliana, DIR1, Reveals a New Type of Lipid Transfer Protein. *Protein science a publication of the Protein Society* **17**, 1522-1530

Lefebvre, B., Timmers, T., Mbengue, M., Moreau, S., Hervé, C., Tóth, K., Bittencourt-Silvestre, J., Klaus, D., Deslandes, L., Godiard, L., Murray, J. D., Udvardi, M. K., Raffaele, S., Mongrand, S., Cullimore, J., Gamas, P., Niebel, A. & Ott, T., (2010). A Remorin Protein Interacts with Symbiotic Receptors and Regulates Bacterial Infection. *Proceedings of the National Academy of Sciences* **107**, 2343-2348

Leshem, Y., Johnson, C., Wuest, S. E., Song, X., Ngo, Q. A., Grossniklaus, U. & Sundaresan, V., (2012). Molecular Characterization of the Glauce Mutant: A Central Cell-Specific Function Is Required for Double Fertilization in Arabidopsis. *The Plant cell* **24**, 3264-3277

Leshem, Y., Johnson, C. & Sundaresan, V., (2013). Pollen Tube Entry into the Synergid Cell of Arabidopsis Is Observed at a Site Distinct from the Filiform Apparatus. *Plant reproduction* **26**, 93-99

Li, D., Keresztes, I., Hopson, R. & Williard, P. G., (2008). Characterization of Reactive Intermediates by Multinuclear Diffusion-Ordered NMR Spectroscopy (DOSY). *Accounts of chemical research* **42**, 270-280

Li, H.-J., Zhu, S.-S., Zhang, M.-X., Wang, T., Liang, L., Xue, Y., Shi, D.-Q., Liu, J. & Yang, W.-C., (2015). Arabidopsis CBP1 Is a Novel Regulator of Transcription Initiation in Central Cell-Mediated Pollen Tube Guidance. *The Plant cell* **27**, 2880-2893

Li, J. & Berger, F., (2012). Endosperm: Food for Humankind and Fodder for Scientific Discoveries. *New Phytologist* **195**, 290-305

Lichty, J. J., Malecki, J. L., Agnew, H. D., Michelson-Horowitz, D. J. & Tan, S., (2005). Comparison of Affinity Tags for Protein Purification. *Protein expression and purification* **41**, 98-105

Lin, H. & Goodenough, U. W., (2007). Gametogenesis in the Chlamydomonas reinhardtii Minus Mating Type Is Controlled by Two Genes, MID and MTD1. *Genetics* **176**, 913-925

Liu, C. & Hermann, T. E., (1978). Characterization of Ionomycin as a Calcium Ionophore. *Journal of Biological Chemistry* **253**, 5892-5894

Liu, F., Zhang, X., Lu, C., Zeng, X., Li, Y., Fu, D. & Wu, G., (2015). Non-Specific Lipid Transfer Proteins in Plants: Presenting New Advances and an Integrated Functional Analysis. *Journal of experimental botany* **66**, 5663-5681

Liu, Y., Tewari, R., Ning, J., Blagborough, A. M., Garbom, S., Pei, J., Grishin, N. V., Steele, R. E., Sinden, R. E. & Snell, W. J., (2008). The Conserved Plant Sterility Gene HAP2 Functions after Attachment of Fusogenic Membranes in Chlamydomonas and Plasmodium Gametes. *Genes & development* **22**, 1051-1068

Liu, Y., Misamore, M. J. & Snell, W. J., (2010). Membrane Fusion Triggers Rapid Degradation of Two Gamete-Specific, Fusion-Essential Proteins in a Membrane Block to Polygamy in Chlamydomonas. *Development* **137**, 1473-1481

Lockhart, J., (2014). Uncovering Male Germline Development in Arabidopsis: The Gametophyte Revealed. **26**

Lockhart, J., (2016). Sticking the Landing: Probing the Roles of LORELEI in Pollen Tube Reception. **28**, 995-996

Lottspeich, F. & Engels, J. W. *Bioanalytik* (Spektrum Akademischer Verlag, 2006).

Mable, B. K. & Otto, S. P., (1998). The Evolution of Life Cycles with Haploid and Diploid Phases. *BioEssays* **20**, 453-462

Maldonado, A. M., Doerner, P., Dixon, R. A., Lamb, C. J. & Cameron, R. K., (2002). A Putative Lipid Transfer Protein Involved in Systemic Resistance Signalling in Arabidopsis. *Nature* **419**, 399-403

Mansfield, S., Briarty, L. & Erni, S., (1991). Early Embryogenesis in Arabidopsis thaliana. I. The Mature Embryo Sac. *Canadian Journal of Botany* **69**, 447-460

Marondedze, C., Groen, Arnoud J., Thomas, L., Lilley, Kathryn S. & Gehring, C., (2016). A Quantitative Phosphoproteome Analysis of cGMP-Dependent Cellular Responses in Arabidopsis thaliana. *Molecular plant* **9**, 621-623

Martí-Renom, M. A., Stuart, A. C., Fiser, A., Sánchez, R., Melo, F. & Šali, A., (2000). Comparative Protein Structure Modeling of Genes and Genomes. *Annual review of biophysics and biomolecular structure* **29**, 291-325

Marton, M. L., Cordts, S., Broadhvest, J. & Dresselhaus, T., (2005). Micropylar Pollen Tube Guidance by EGG APPARATUS 1 of Maize. *Science* **307**, 573-576

Márton, M. L., Fastner, A., Uebler, S. & Dresselhaus, T., (2012). Overcoming Hybridization Barriers by the Secretion of the Maize Pollen Tube Attractant ZmEA1 from Arabidopsis Ovules. *Current Biology* **22**, 1194-1198

Maruyama, D., Hamamura, Y., Takeuchi, H., Susaki, D., Nishimaki, M., Kurihara, D., Kasahara, R. D. & Higashiyama, T., (2013). Independent Control by Each Female Gamete Prevents the Attraction of Multiple Pollen Tubes. *Developmental cell* **25**, 317-323

Maruyama, D., Volz, R., Takeuchi, H., Mori, T., Igawa, T., Kurihara, D., Kawashima, T., Ueda, M., Ito, M., Umeda, M., Nishikawa, S., Gross-Hardt, R. & Higashiyama, T., (2015). Rapid Elimination of the Persistent Synergid through a Cell Fusion Mechanism. *Cell* **161**, 907-918

McCormick, S., (1993). Male Gametophyte Development. *The Plant cell* **5**, 1265

McCue, A. D., Cresti, M., Feijo, J. A. & Slotkin, R. K., (2011). Cytoplasmic Connection of Sperm Cells to the Pollen Vegetative Cell Nucleus: Potential Roles of the Male Germ Unit Revisited. *Journal of experimental botany* **62**, 1621-1631

Meier, A. & Söding, J., (2015). Automatic Prediction of Protein 3D Structures by Probabilistic Multi-Template Homology Modeling. *PLoS computational biology* **11**, e1004343

Moll, C., Von Lyncker, L., Zimmermann, S., Kägi, C., Baumann, N., Twell, D., Grossniklaus, U. & Groß-Hardt, R., (2008). CLO/GFA1 and ATO Are Novel Regulators of Gametic Cell Fate in Plants. *The Plant Journal* **56**, 913-921

Monshausen, G. B., Messerli, M. A. & Gilroy, S., (2008). Imaging of the Yellow Cameleon 3.6 Indicator Reveals That Elevations in Cytosolic Ca^{2+} Follow Oscillating Increases in Growth in Root Hairs of Arabidopsis. *Plant physiology* **147**, 1690-1698

Mori, T., Kuroiwa, H., Higashiyama, T. & Kuroiwa, T., (2006). GENERATIVE CELL SPECIFIC 1 Is Essential for Angiosperm Fertilization. *Nature cell biology* **8**, 64-71

Mori, T., Igawa, T., Tamiya, G., Miyagishima, S. Y. & Berger, F., (2014). Gamete Attachment Requires GEX2 for Successful Fertilization in Arabidopsis. *Current biology CB* **24**, 170-175

Nakamura, M. & Hashimoto, T., (2009). A Mutation in the Arabidopsis γ-Tubulin-Containing Complex Causes Helical Growth and Abnormal Microtubule Branching. *Journal of Cell Science* **122**, 2208-2217

Nan, W., Wang, X., Yang, L., Hu, Y., Wei, Y., Liang, X., Mao, L. & Bi, Y., (2014). Cyclic GMP Is Involved in Auxin Signalling During Arabidopsis Root Growth and Development. *Journal of experimental botany* **65**, 1571-1583

Nelson, B. K., Cai, X. & Nebenführ, A., (2007). A Multicolored Set of in vivo Organelle Markers for Co-Localization Studies in Arabidopsis and Other Plants. *The Plant Journal* **51**, 1126-1136

Neufeld, R. & Stalke, D., (2015). Accurate Molecular Weight Determination of Small Molecules Via DOSY-NMR by Using External Calibration Curves with Normalized Diffusion Coefficients. *Chemical Science* **6**, 3354-3364

Nezhad, A. S., Naghavi, M., Packirisamy, M., Bhat, R. & Geitmann, A., (2013). Quantification of Cellular Penetrative Forces Using Lab-on-a-Chip Technology and Finite Element Modeling. *Proceedings of the National Academy of Sciences* **110**, 8093-8098

Okuda, S. *et al.*, (2009). Defensin-Like Polypeptide LURES Are Pollen Tube Attractants Secreted from Synergid Cells. *Nature* **458**, 357-361

Olsen, O.-A., (2004). Nuclear Endosperm Development in Cereals and Arabidopsis thaliana. *The Plant cell* **16**, S214-S227

Pagnussat, G. C., Yu, H.-J. & Sundaresan, V., (2007). Cell-Fate Switch of Synergid to Egg Cell in Arabidopsis eostre Mutant Embryo Sacs Arises from Misexpression of the Bel1-Like Homeodomain Gene BLH1. *The Plant cell* **19**, 3578-3592

Palanivelu, R. & Preuss, D., (2006). Distinct Short-Range Ovule Signals Attract or Repel Arabidopsis thaliana Pollen Tubes in vitro. *BMC plant biology* **6**, 7

Park, S.-Y., Jauh, G.-Y., Mollet, J.-C., Eckard, K. J., Nothnagel, E. A., Walling, L. L. & Lord, E. M., (2000). A Lipid Transfer–Like Protein Is Necessary for Lily Pollen Tube Adhesion to an in Vitro Stylar Matrix. *The Plant cell* **12**, 151-163

Pasquale, S. M. & Goodenough, U. W., (1987). Cyclic Amp Functions as a Primary Sexual Signal in Gametes of Chlamydomonas reinhardtii. *The Journal of Cell Biology* **105**, 2279-2292

Pastuglia, M., Azimzadeh, J., Goussot, M., Camilleri, C., Belcram, K., Evrard, J.-L., Schmit, A.-C., Guerche, P. & Bouchez, D., (2006). γ-Tubulin Is Essential for Microtubule Organization and Development in Arabidopsis. *The Plant cell* **18**, 1412-1425

Pelta, M. D., Barjat, H., Morris, G. A., Davis, A. L. & Hammond, S. J., (1998). Pulse Sequences for High-Resolution Diffusion-Ordered Spectroscopy (HR-DOSY). *Magnetic resonance in chemistry* **36**, 706-714

Pettersen, E. F., Goddard, T. D., Huang, C. C., Couch, G. S., Greenblatt, D. M., Meng, E. C. & Ferrin, T. E., (2004). UCSF Chimera - a Visualization System for Exploratory Research and Analysis. *Journal of computational chemistry* **25**, 1605-1612

Pii, Y., Astegno, A., Peroni, E., Zaccardelli, M., Pandolfini, T. & Crimi, M., (2009). The Medicago truncatula N5 Gene Encoding a Root-Specific Lipid Transfer Protein Is Required for the Symbiotic Interaction with Sinorhizobium meliloti. *Molecular plant-microbe interactions MPMI* **22**, 1577-1587

Pii, Y., Pandolfini, T. & Crimi, M., (2010). Signaling Ltps: A New Plant LTPs Sub-Family? *Plant signaling & behavior* **5**, 594-597

Poliakova, T., (1964). Development of the Male and Female Gametophytes of Arabidopsis thaliana (L) Heynh. *Issled. Genet. USSR* **2**, 125-133

Preuss, D., Rhee, S. Y. & Davis, R. W., (1994). Tetrad Analysis Possible in Arabidopsis with Mutation of the QUARTET (QRT) Genes. *Science-AAAS-Weekly Paper Edition-including Guide to Scientific Information* **264**, 1458-1459

Rademacher, S., (2011) *EGG CELL 1 Function and Stability During Double Fertilization in Arabidopsis thaliana* PhD Thesis.

Rademacher, S. & Sprunck, S., (2013). Downregulation of Egg Cell-Secreted EC1 Is Accompanied with Delayed Gamete Fusion and Polytubey. *Plant signaling & behavior* **8**, e27377

Reski, R. & Cove, D. J., (2004). Physcomitrella patens. *Current Biology* **14**, R261-R262

Richards, E., Reichardt, M. & Rogers, S. in *Current Protocols in Molecular Biology* (John Wiley & Sons, Inc., 2001).

Rövekamp, M., Bowman, John L. & Grossniklaus, U., (2016). Marchantia MpRKD Regulates the Gametophyte-Sporophyte Transition by Keeping Egg Cells Quiescent in the Absence of Fertilization. *Current Biology* **26**, 1782-1789

Russell, S. in *Encyclopedia of Applied Plant Sciences* Vol. 2 Ch. Reproduction and Biodiversity, 262-268 (2017).

Russell, S. D., (1983). Fertilization in Plumbago zeylanica: Gametic Fusion and Fate of the Male Cytoplasm. *American journal of botany* **70**, 416-434

Russell, S. D., (1987). Quantitative Cytology of the Egg and Central Cell of Plumbago zeylanica and Its Impact on Cytoplasmic Inheritance Patterns. *Theoretical and Applied Genetics* **74**, 693-699

Russell, S. D., Strout, G. W., Stramski, A. K., Mislan, T. W., Thompson, R. A. & Schoemann, L. M., (1996). Microgametogenesis in Plumbago zeylanica (Plumbaginaceae). Descriptive Cytology and Three-Dimensional Organization. *American journal of botany* **83**, 1435-1453

Salminen, T. A., Blomqvist, K. & Edqvist, J., (2016). Lipid Transfer Proteins: Classification, Nomenclature, Structure, and Function. *Planta* **244**, 971-997

Sambrook, J., Fritsch, E. F. & Maniatis, T. *Molecular Cloning: A Laboratory Manual*. (Cold Spring Harbor Laboratory Press, 1989).

Samuel, D., Liu, Y. J., Cheng, C. S. & Lyu, P. C., (2002). Solution Structure of Plant Nonspecific Lipid Transfer Protein-2 from Rice (Oryza Sativa). *The Journal of biological chemistry* **277**, 35267-35273

Sanders, D., Pelloux, J., Brownlee, C. & Harper, J. F., (2002). Calcium at the Crossroads of Signaling. *The Plant cell* **14**, S401-S417

Satouh, Y., Inoue, N., Ikawa, M. & Okabe, M., (2012). Visualization of the Moment of Mouse Sperm–Egg Fusion and Dynamic Localization of IZUMO1. *J Cell Sci* **125**, 4985-4990

Schacht, H., (1857). *Jahrbücher Wissenschaftliche Botanik* **1**, 193-232

Schägger, H. & von Jagow, G., (1987). Tricine-Sodium Dodecyl Sulfate-Polyacrylamide Gel Electrophoresis for the Separation of Proteins in the Range from 1 to 100 kDa. *Analytical biochemistry* **166**, 368-379

Schneider, C. A., Rasband, W. S. & Eliceiri, K. W., (2012). NIH Image to ImageJ: 25 Years of Image Analysis. *Nature methods* **9**, 671-675

Schneitz, K., Hulskamp, M. & Pruitt, R. E., (1995). Wild-Type Ovule Development in Arabidopsis thaliana: A Light Microscope Study of Cleared Whole-Mount Tissue. *Plant Journal* **7**, 731-749

Smith-Garvin, J. E., Koretzky, G. A. & Jordan, M. S., (2009). T-Cell Activation. *Annual review of immunology* **27**, 591-619

Smyth, D. R., Bowman, John L. and Meyerowitz, Elliot M. (1990). Early Flower Development in Arabidopsis. *The Plant cell* **2**, 755-767

Šoljić, L., (2012) *Microarray Analysis of Single Isolated Cells of the Female Gametophyte Reveals Potential Regulators of Female Germline Development in Arabidopsis thaliana* PhD Thesis, Regensburg.

Song, X., Yuan, L. & Sundaresan, V., (2014). Antipodal Cells Persist through Fertilization in the Female Gametophyte of Arabidopsis. *Plant reproduction* **27**, 197-203

Spring, F. A., Griffiths, R. E., Mankelow, T. J., Agnew, C., Parsons, S. F., Chasis, J. A. & Anstee, D. J., (2013). Tetraspanins CD81 and CD82 Facilitate A4β1-Mediated Adhesion of Human Erythroblasts to Vascular Cell Adhesion Molecule-1. *PloS one* **8**, e62654

Sprunck, S., Baumann, U., Edwards, K., Langridge, P. & Dresselhaus, T., (2005). The Transcript Composition of Egg Cells Changes Significantly Following Fertilization in Wheat (Triticum aestivum L.). *The Plant Journal* **41**, 660-672

Sprunck, S., (2010). Let's get physical: gamete interaction in flowering plants. *Biochem. Soc. Trans.* **38**, 635-640

Sprunck, S. & Gross-Hardt, R., (2011). Nuclear Behavior, Cell Polarity, and Cell Specification in the Female Gametophyte. *Sexual plant reproduction* **24**, 123-136

Sprunck, S., Rademacher, S., Vogler, F., Gheyselinck, J., Grossniklaus, U. & Dresselhaus, T., (2012). Egg Cell-Secreted EC1 Triggers Sperm Cell Activation During Double Fertilization. *Science* **338**, 1093-1097

Sprunck, S., Hackenberg, T., Englhart, M. & Vogler, F., (2014). Same Same but Different: Sperm-Activating EC1 and Eca1 Gametogenesis-Related Family Proteins. *Biochemical Society transactions* **42**, 401-407

Steentoft, C., Vakhrushev, S. Y., Joshi, H. J., Kong, Y., Vester-Christensen, M. B., Katrine, T., Schjoldager, B., Lavrsen, K., Dabelsteen, S. & Pedersen, N. B., (2013). Precision Mapping of the Human O-GalNaC Glycoproteome through SimpleCell Technology. *The EMBO journal* **32**, 1478-1488

Steffen, J. G., Kang, I. H., Macfarlane, J. & Drews, G. N., (2007). Identification of Genes Expressed in the Arabidopsis Female Gametophyte. *The Plant Journal* **51**, 281-292

Strasburger, E., (1894). The Periodic Reduction of the Number of the Chromosomes in the Life-History of Living Organisms. *Annals of Botany* **8**, 281-316

Stroe, P., Claridge, E. & Odintsova, E., (2016). Cell Boundary Detection for Quantitative Studies of the Role of Tetraspanin CD82 in Cell-Cell Adhesion. *Procedia Computer Science* **90**, 107-112

Switzer III, R. C., Merril, C. R. & Shifrin, S., (1979). A Highly Sensitive Silver Stain for Detecting Proteins and Peptides in Polyacrylamide Gels. *Analytical biochemistry* **98**, 231-237

Takagi, T. & Doolittle, R. F., (1974). Amino Acid Sequence Studies on Factor XIII and the Peptide Released During Its Activation by Thrombin. *Biochemistry* **13**, 750-756

Takahashi, N., Eijri, S.-i. & Katsumata, T., (1978). Changes of Cyclic AMP and Cyclic GMP Levels During Germination of Pine Pollen. *Agricultural and Biological Chemistry* **42**, 1605-1606

Takeuchi, H. & Higashiyama, T., (2012). A Species-Specific Cluster of Defensin-Like Genes Encodes Diffusible Pollen Tube Attractants in Arabidopsis. *PLoS Biology* **10**, e1001449

Takeuchi, H. & Higashiyama, T., (2016). Tip-Localised Receptors Control Pollen Tube Growth and Lure Sensing in Arabidopsis. *Nature* **531**, 245-261

Talke, I., (2003). CNGCs: Prime Targets of Plant Cyclic Nucleotide Signalling? *Trends in Plant Science* **8**, 286-293

Tanaka, H., Ishikawa, M., Kitamura, S., Takahashi, Y., Soyano, T., Machida, C. & Machida, Y., (2004). The AtNACK1/HINKEL and STUD/TETRASPORE/AtNACK2 Genes, Which Encode Functionally Redundant Kinesins, Are Essential for Cytokinesis in Arabidopsis. *Genes to Cells* **9**, 1199-1211

Tanner, W., (1986). Glykoproteine: Struktur, Biosynthese, Funktion. *Berichte der Deutschen Botanischen Gesellschaft* **99**, 237-249

Thomas, B., Murphy, D. J. & Murray, B. G. *Encyclopedia of Applied Plant Sciences*. (Academic Press, 2016).

Tosti, E. & Ménézo, Y., (2010). Sperm Induced Oocyte Activation. *Human Spermatozoa: Maturation, Capacitation and Abnormalities. New York: Nova Biomedical Books*, 379-397

Tosti, E. & Ménézo, Y., (2016). Gamete Activation: Basic Knowledge and Clinical Applications. *Human Reproduction Update* **22**, 420-439

Tsukamoto, T., Qin, Y., Huang, Y., Dunatunga, D. & Palanivelu, R., (2010). A Role for LORELEI, a Putative Glycosylphosphatidylinositol-Anchored Protein, in Arabidopsis thaliana Double Fertilization and Early Seed Development. *The Plant Journal* **62**, 571-588

Valansi, C., Moi, D., Leikina, E., Matveev, E., Graña, M., Chernomordik, L. V., Romero, H., Aguilar, P. S. & Podbilewicz, B., (2017). Arabidopsis HAP2/GCS1 is a Gamete Fusion Protein Homologous to Somatic and Viral Fusogens. *The Journal of Cell Biology* **216**, 571-581

Van Aelst, A., Pierson, E., Van Went, J. & Cresti, M., (1993). Ultrastructural Changes of Arabidopsis thaliana Pollen During Final Maturation and Rehydration. *Zygote* **1**, 173-179

Vervecken, W., Kaigorodov, V., Callewaert, N., Geysens, S., De Vusser, K. & Contreras, R., (2004). In Vivo Synthesis of Mammalian-Like, Hybrid-Type N-Glycans in Pichia pastoris. *Applied and Environmental Microbiology* **70**, 2639-2646

Vollbrecht, E. & Hake, S., (1995). Deficiency Analysis of Female Gametogenesis in Maize. *genesis* **16**, 44-63

von Besser, K., Frank, A. C., Johnson, M. A. & Preuss, D., (2006). Arabidopsis HAP2 (GCS1) Is a Sperm-Specific Gene Required for Pollen Tube Guidance and Fertilization. *Development* **133**, 4761-4769

Wang, J.-G., Feng, C., Liu, H.-H., Feng, Q.-N., Li, S. & Zhang, Y., (2017). AP1G Mediates Vacuolar Acidification During Synergid-Controlled Pollen Tube Reception. *Proceedings of the National Academy of Sciences* **114**, 201617967

Wang, T., Liang, L., Xue, Y., Jia, P. F., Chen, W., Zhang, M. X., Wang, Y. C., Li, H. J. & Yang, W. C., (2016). A Receptor Heteromer Mediates the Male Perception of Female Attractants in Plants. *Nature* **531**, 241-244

Webb, B. & Sali, A., (2014). Protein Structure Modeling with Modeller. *Protein Structure Prediction*, 1-15

Weiss, A. & Imboden, J. B., (1987). Cell Surface Molecules and Early Events Involved in Human T Lymphocyte Activation. *Advances in immunology* **41**, 1-38

Wong, J. L. & Johnson, M. A., (2010). Is HAP2-GCS1 an Ancestral Gamete Fusogen? *Trends in cell biology* **20**, 134-141

Wuest, S. E., Vijverberg, K., Schmidt, A., Weiss, M., Gheyselinck, J., Lohr, M., Wellmer, F., Rahnenführer, J., von Mering, C. & Grossniklaus, U., (2010). Arabidopsis Female Gametophyte Gene Expression Map Reveals Similarities between Plant and Animal Gametes. *Current Biology* **20**, 506-512

Yadegari, R. & Drews, G. N., (2004). Female Gametophyte Development. *The Plant cell* **16**, S133-S141

Yamada, Y., Matsuda, M., Maeda, K. & Mikata, K., (1995). The Phylogenetic Relationships of Methanol-Assimilating Yeasts Based on the Partial Sequences of 18S and 26S Ribosomal RNAs: The Proposal of Komagataella Gen. Nov. (Saccharomycetaceae). *Bioscience, biotechnology, and biochemistry* **59**, 439-444

Yamamoto, Y., Nishimura, M., Hara-Nishimura, I. & Noguchi, T., (2003). Behavior of Vacuoles During Microspore and Pollen Development in Arabidopsis thaliana. *Plant and Cell Physiology* **44**, 1192-1201

Yang, A.-S. & Honig, B., (1993). On the pH Dependence of Protein Stability. *Journal of Molecular Biology* **231**, 459-474

Yu, H., Hu, S. & Russell, S., (1992). Sperm Cells in Pollen Tubes of Nicotiana tabacum L.: Three-Dimensional Reconstruction, Cytoplasmic Diminution, and Quantitative Cytology. *Protoplasma* **168**, 172-183

Yu, H., Liu, Y., Gulbranson, D. R., Paine, A., Rathore, S. S. & Shen, J., (2016). Extended Synaptotagmins Are Ca^{2+}-Dependent Lipid Transfer Proteins at Membrane Contact Sites. *Proceedings of the National Academy of Sciences* **113**, 4362-4367

Yu, X., Luo, A. & Sun, M.-x., (2016). An Efficient Antipodal Cell Isolation Method for Screening of Cell Type-Specific Genes in Arabidopsis thaliana. *PloS one* **11**, e0166390

Yuan, L., Liu, Z., Song, X., Johnson, C., Yu, X. & Sundaresan, V., (2016). The CKI1 Histidine Kinase Specifies the Female Gametic Precursor of the Endosperm. *Developmental cell* **37**, 34-46

Zhang, D., (2009). Homology between DUF784, DUF1278 Domains and the Plant Prolamin Superfamily Typifies Evolutionary Changes of Disulfide Bonding Patterns. *Cell Cycle* **8**, 3428-3430

Zhou, P., Silverstein, K. A., Gao, L., Walton, J. D., Nallu, S., Guhlin, J. & Young, N. D., (2013). Detecting Small Plant Peptides Using SPADA (Small Peptide Alignment Discovery Application). *BMC bioinformatics* **14**, 335

8. LIST OF FIGURES

9. ABBREVIATIONS

2D	two dimensional
35S	*Cauliflower Mosaic Virus 35S*
3D	three dimensional
8-Br-cGMP	8-Bromo cyclic guanosine monophosphate
8-pCPT-cGMP	8- (4- Chlorophenylthio) cyclic guanosine monophosphate
APS	ammonium persulfate
cc	central cell
cGMP	cyclic guanosine monophosphate
CLSM	confocal laser scanning microscopy
COSY	correlation spectroscopy
CRP	cysteine-rich peptide
CTAB	cetyl trimethylammonium bromide
DIG	digoxigenin
DIR1	defective in induced resistance 1
DMSO	dimethyl sulfoxide
DNA	deoxyribonucleic acid

DOC	sodium deoxycholate
DOSY	diffusion-ordered spectroscopy
DSS	4,4-dimethyl-4-silapentane-1-sulfonic acid
DTT	dithiothreitol
EAST	effective area for sperm cell targeting
ec	egg cell
EC1	egg cell secreted protein 1
ER	endoplasmic reticulum
fa	filiform apparatus
GFP	green fluorescent protein
GST	glutathione S-transferase
hai	hours after induction
hap	hours after pollination
HAP2	hapless 2
HIS	hexahistidine
HPC	heavy chain of protein C
IMAC	immobilised metal affinity chromatography
LMW	low molecular weight
LTP	lipid transfer protein
lysoPC	lysostearoylphosphatidyl choline
MGU	male germ unit
MtSYMREM	*Medicago truncatula* symbiotic remorin 1
Ni-NTA	Ni^{2+}-nitrilotriacetate complex
NMR	nuclear magnetic resonance
nsLTP	non-specific lipid transfer protein
PIP2a	plasma membrane intrinsic protein 2A
PolyR	pentaarginine
pt	pollen tube
RFP	red fluorescent protein
RNA	ribonucleic acid
RNAi	RNA interference
sc	sperm cell
SD	Spinning disc
SDS	sodium dodecylsulfate
syn	synergid cell
TAMRA	tetramethylrhodamine
TEMED	tetramethylethylenediamine
TET9	tetraspanin 9
TOCSY	total correlation spectroscopy
YNB	yeast nitrogen base

10. ACKNOWLEDGEMENTS

First of all, I want to thank PD Dr. Stefanie Sprunck for introducing me to the world of *Arabidopsis* flowers. From the first time I prepared an ovule for microscopy I was captivated. Despite all the throwbacks, I still love to sit at the microscope. I am very thankful for this great research topic with such diverse scope, for all the ideas and support in developing my project and for the patience in improving my thesis.

I thank Prof. Dr. Thomas Dresselhaus for the opportunity to do my PhD at his department and I want to thank my mentoring team, Prof. Dr. Thomas Dresselhaus, Prof. Dr. Rüdiger Simon and Prof. Dr. Christine Ziegler, for all the constructive criticism throughout the last years. And my special thanks go to Christine Ziegler for her never ending enthusiasm for my project, her protein expertise and for the opportunity to use the equipment in her lab.

I very much thank Prof. Dr. Werner Kremer for performing the NMR studies and his help with their analysis. I am very grateful to Prof. Dr. Frank Sprenger for giving me the opportunity to use the Spinning Disc microscope at his department and for introducing me to the world of ImageJ macros. I very much thank Dr. Gregor Madej for the homology model and for critical reading my thesis.

I am indebted to Ingrid for sharing her expertise in protein purification and for making the best competent cells ever. I am likewise thankful to Monika for all her help in the lab. I am deeply thankful to Günther, Uschi, Armin and Noureddine for sowing, picking, watering and taking care of my plants and to Vroni for always having an answer in terms of administration.

I very much thank Barbara, Balu, Pia, Veronika and Steffi from the AG Ziegler for their patience in helping me with the ÄKTA. Thank you, Andrea for all the help with the microscopes. I further want to thank all my students, Michael, Christina, Peter, Martina, Marie, Maria and Andrea for their contribution to my project.

A very big "thank you" goes to Frank for his implicitness in helping and encouraging me and for all the creative energy in developing new ideas. You were a great inspiration.

I am deeply thankful to Frank, Ingrid, Marc, Mary, Monika, Phil, Tom, Steffi, Kinga and Sanna for the great atmosphere in the lab, in the office and outside the university. I am also very thankful for everyone who critically read my thesis, especially Steffi, Frank, Anne, Tom, Miriam and Sandra.

Das allergrößte Dankeschön geht an meine Familie. Allen voran, bin ich meinen Eltern unendlich dankbar, dass sie mir diesen Weg ermöglicht haben. Vielen Dank für die die Selbstverständlichkeit mit der sie mich mein Leben lang in Dingen jeglicher Art unterstützt haben. Mama und Papa, ihr seid die besten Eltern, die man sich wünschen kann. Von größtem Herzen danke ich Christian. Deine unendliche Geduld, dein Mitleiden bei Rückschlägen und deine positive Energie sind mein größter Antrieb. Ich freue mich auf ein Leben mit dir.

11. Eidesstattliche Erklärung

Ich erkläre hiermit an Eides statt, dass ich die vorliegende Arbeit ohne unzulässige Hilfe Dritter und ohne Benutzung anderer als der angegebenen Hilfsmittel angefertigt habe; die aus anderen Quellen direkt oder indirekt übernommenen Daten und Konzepte sind unter Angabe des Literaturzitats gekennzeichnet.

Die Arbeit wurde bisher weder im In- noch im Ausland in gleicher oder ähnlicher Form einer anderen Prüfungsbehörde vorgelegt.

Maria Englhart

Regensburg